2-14-2014

JEMEZ RIVER CASE STUDY: UTILIZING A FROUDE NUMBER SIMILITUDE PHYSICAL MODEL, 1-D MOBILE BED NUMERICAL MODEL, AND A 2-D FIXED BED NUMERICAL MODEL FOR WEIR DESIGN INSIGHT

Emile Kareem Saint-Lot

Emile Kareem Saint-Lôt
Candidate

Civil Engineering
Department

This thesis is approved, and it is acceptable in quality and form for publication:

Approved by the Thesis Committee:

Julie Coonrod PhD, P.E. , Chairperson

Mark Stone PhD, P.E.

Darrell Eidson P.E. D. WRE

JEMEZ RIVER CASE STUDY: UTILIZING A FROUDE NUMBER SIMILITUDE PHYSICAL MODEL, 1-D MOBILE BED NUMERICAL MODEL, AND A 2-D FIXED BED NUMERICAL MODEL FOR WEIR DESIGN INSIGHT

BY

EMILE KAREEM SAINT-LOT

BACHELOR OF SCIENCE
DEPARTMENT OF CIVIL ENGINEERING
UNIVERSITY OF NEW MEXICO, 2010

THESIS

Submitted in Partial Fulfillment of the
Requirements for the Degree of

Master of Science
Civil Engineering

The University of New Mexico
Albuquerque, New Mexico

December, 2013

ACKNOWLEDGMENTS

I would like to thank God for continuously blessing me and guiding me to perform His will. I would like to thank my family for their never ending support. Thanks, Mom and Dad, for always cooking a little extra so I could take it to school for lunch. Thanks, Shaina, Jameel, and Talal, for all the outside fun including tennis and biking. I'd like to thank Patricia for encouraging me throughout my graduate program and blessing me with a beautiful daughter, Jaeda.

I would like to thank my professors Julie Coonrod and Mark Stone for providing me with this opportunity, sharing their knowledge, and guiding my modeling and thesis work. Thanks for helping with the physical models, sharing laughs, and making graduate school fun Tyler, Robert, Jeffrey, Harris, and Dave.

"L'Union Fait la Force" – Haitian Flag

JEMEZ RIVER CASE STUDY: UTILIZING A FROUDE NUMBER SIMILITUDE PHYSICAL MODEL, 1-D MOBILE BED NUMERICAL MODEL, AND A 2-D FIXED BED NUMERICAL MODEL FOR WEIR DESIGN INSIGHT

By

Emile Kareem Saint-Lôt

B.S., Civil Engineering, University of New Mexico, 2010
M.S., Civil Engineering, University of New Mexico, 2013

ABSTRACT

Physical and numerical models have been widely used to describe flooding patterns and to gain further understanding of river hydraulics around complex structures. Located on the Jemez River in New Mexico, the Jemez Weir stops the upstream progression of stream degradation and supports healthy upstream riparian vegetation. Localized bed scour began to occur just downstream of the Jemez Weir following construction. The United States Army Corps of Engineers (USACE) built the structure in 2003 and developed a HEC-RAS model in 2010 to re-evaluate the long term bed degradation downstream of the weir to assess structure stability. Additionally, the USACE estimated downstream localized scour depths using scour equations developed by Bormann and Julien (1991), Laursen and Flick (1983), and Lim (1992). After noting the structure needed additional modifications to prevent structural failure the USACE funded the development of a physical mobile bed model based on Froude Similitude to model scour patterns downstream of the Jemez Weir. This research takes the investigation one step further through the development and testing of a two-dimensional fixed bed model using the Bureau of Reclamation's Sedimentation and River Hydraulics – Two Dimensional (SRH-2D) program. The two-dimensional fixed bed model was used

to gain further understanding of flow interactions between the main channel and floodplain. The model was also utilized to develop a weir discharge rating curve for the Jemez Weir, and evaluate velocity and shear stress distributions around the Jemez Weir. SRH-2D results show a lower main channel discharge when compared to the HEC-RAS results around the Jemez Weir. Shear stress and velocity distributions agree with physical model results, and show localized scour will continue to threaten the structure unless modified. The results of this study can inform hydraulic modeling studies in similar settings because of the three different modeling techniques employed to address specific questions. Therefore, future case studies can use this study's results to guide modeling technique and help formulate an approach to answer a specific research question.

Table of Contents

List of Figures

List of Tables

Introduction

Physical and numerical models have been widely used to describe flood patterns and gain further understanding of river hydraulics around complex structures. Savage and Johnson (2001) compared the results of a physical model, a two-dimensional, and a three dimensional numerical model, for flow over an ogee spillway to validate the numerical models. Savage and Johnson (2001) found the Flow 2-D and Flow 3-D numerical models of the ogee spillway provided accurate discharge and pressure data, while decreasing modeling time and costs. Lv, Zou, and Reeve (2011) used a newly developed numerical model to simulate flow over broad and sharp crested weirs in a rectangular channel. Lv et al. (2011) found the numerical model performed well when compared to experimental measurements, and stated the numerical model is also "capable of resolving the time evolution of very complex vertical motions, air entrainment and impact pressure variations due to violent collision downstream of the weir crest." The studies above exhibit the advancement of numerical modeling capabilities and provide alternatives to traditional modeling studies within the field of hydraulic engineering.

Piotrowski (2010) used a high resolution two-dimensional numerical model, Sedimentation and River Hydraulics – Two Dimensional (SRH-2D), to simulate a flood event along a reach of the Iowa River. Piotrowski (2010) found the numerical model results were accurate with a mean over prediction of 0.01 meters for water surface elevation. The United States Army Corps of Engineers (USACE) commissioned a physical model performed by the University of New Mexico (UNM) to simulate scour patterns around the Jemez Weir and test three preliminary counter measure designs (Coonrod, Saint-Lot, & Gillihan, 2012). Coonrod et al. (2012) successfully used the

physical model to document failure modes using photography and video, and were able to evaluate counter measure performance with depth gauge measurements. Hoffmans and Pilarczyk (1995) specifically describe how local scour at the downstream end of a hydraulic structure evolves and discuss scour depth equations. The focus of this research is to describe Jemez River hydraulics near the Jemez Weir using both a two-dimensional numerical fixed bed model and a physical model.

Site Location, Jemez River Details, and Jemez Weir Details

The Jemez River, located in north central New Mexico, serves as the primary drainage channel for the Jemez Mountains, and flows in the southeast direction before discharging into the Rio Grande, see **Figure 1**.

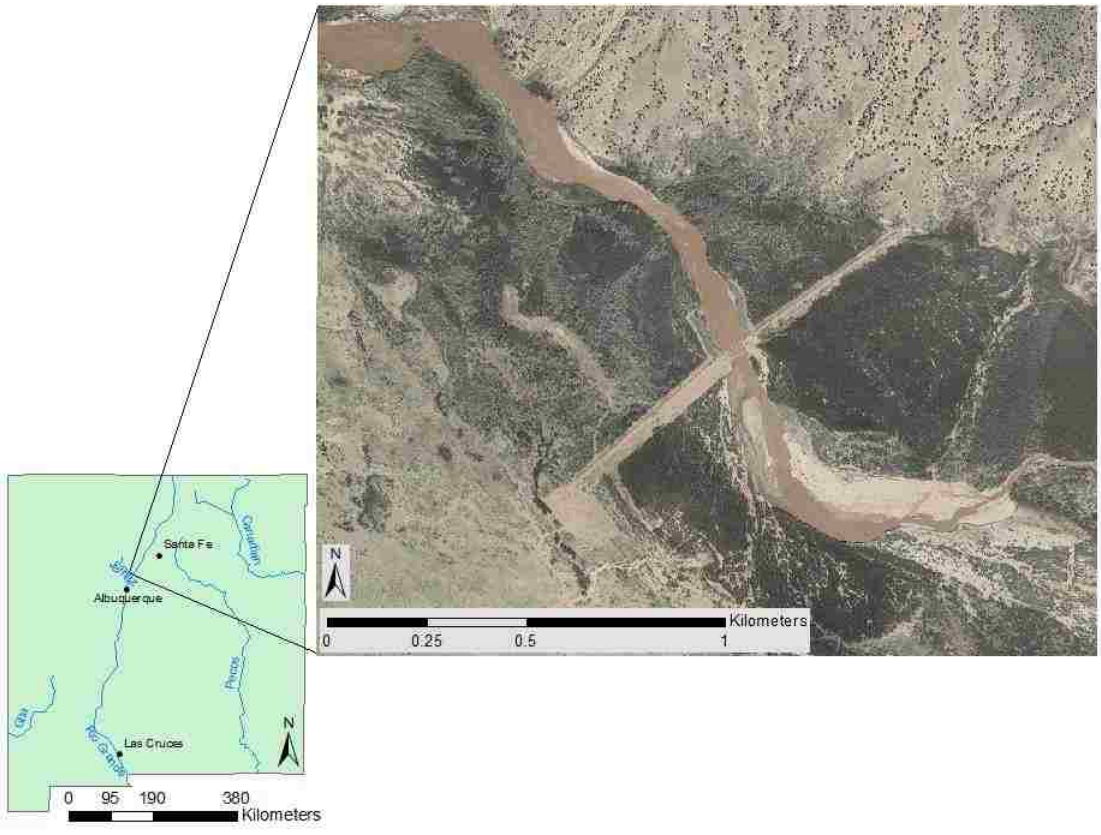

Figure 1: Jemez River and Jemez Weir location map

Draining approximately 1,217 square kilometers (470 square miles), the Jemez River daily discharge ranges from 0.06 to 89.48 m^3/s (2.1 to 3,160 ft^3/s) with an annual average discharge from 1954-2012 water years of 2.07 m^3/s (73.2 ft^3/s) (U.S. Geological Survey, 2013). Average annual rainfall in the Jemez Watershed varies with elevation, ranging from approximately 25.4 to 50.8 centimeters (10 to 20 inches) (Jemez Watershed Group, 2005). Jemez Canyon Dam is located approximately five kilometers upstream of the Jemez River's confluence with the Rio Grande. The site location, shown in the top right corner of **Figure 1**, is roughly five and a half kilometers upstream of the Jemez Canyon Dam.

Following operational changes to the Jemez Canyon Dam in 2001 the Jemez River began experiencing bed degradation. The Jemez Weir shown in **Figure 2** was built by the United States Army Corps of Engineers (USACE) in 2003 to prevent upstream progression of channel degradation. The Jemez Weir also promotes healthy riparian vegetation upstream of the structure by elevating upstream surface water profiles, thereby increasing inundation frequency (Coonrod et al., 2012).

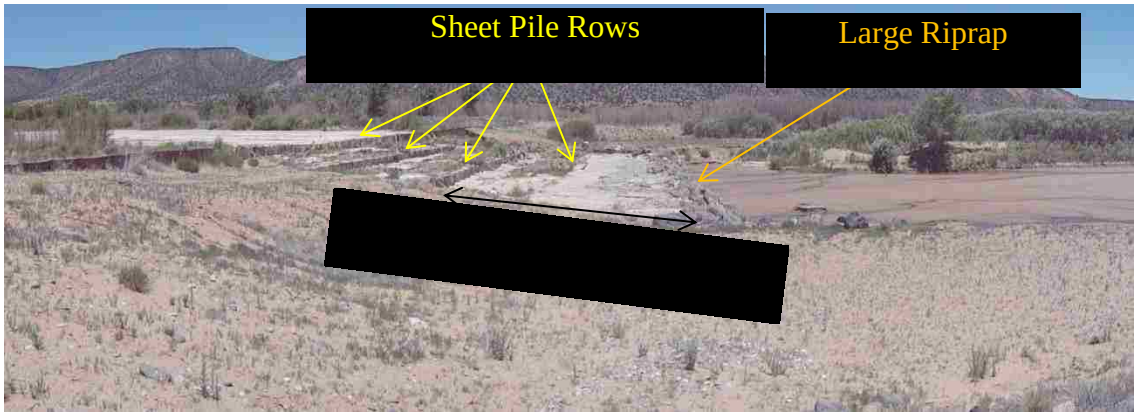

Figure 2: Jemez Weir prototype view from right overbank

Localized bed scour began to occur just downstream of the Jemez Weir structure's lowest bed armament sometime after operation began. In an attempt to stabilize the sheet piles, the USACE extended the weir structure 7.6 m (25 ft.) downstream of the last sheet pile with cobbles, confined by a row of large diameter riprap. The large riprap diameter is estimated to range between 0.9 and 1.8 m (3-6 ft.). Localized scour downstream of the large riprap developed to a depth of approximately 0.61 meters (two feet) over the span of five years. The USACE funded the development and analysis of a one-dimensional numerical model using HEC-RAS to estimate future bed change for the reach downstream of the Jemez Weir, and assess the potential risk to the structure (Maynord, Floyd, Heath, & Little, 2012). The USACE also funded the development and analysis of a physical model based on Froude Number similitude to evaluate scour patterns downstream of the Jemez Weir (Coonrod et al., 2012).

The aim of this research is to provide the United States Army Corps of Engineers with a better description of river hydraulics around the Jemez Weir Structure and to evaluate countermeasures. SRH-2D, a two-dimensional finite volume numerical model, is utilized to add further understanding of river hydraulics near the Jemez Weir. Objectives include:

1. Develop and test alternative mesh configurations to represent Jemez Weir
2. Perform sensitivity analysis by increasing and decreasing Manning's roughness coefficient for both the main channel and the floodplain
3. Compare hydraulic results with information from the HEC-RAS report
    a. Flow distribution between the main channel and floodplain
    b. Channel capacity of the modeled reach

c. Discharge rating curve for the Jemez Weir

4. Evaluate velocity and shear stress results near the Jemez Weir
5. Investigate and compare physical model, 1-D numerical model, and 2-D numerical fixed bed model capabilities to make recommendations for analysis of similar river structures

Jemez Weir Structure Geometry

Four rows of sheet piles confine the Jemez Weir and provide the foundation for a series of three steps. **Figure 3** displays the sloped weir crest cross section for the first row of sheet piles, whereas the remaining three sheet pile rows maintain a constant weir profile. All sheet pile rows are spaced 7.6 m (25 ft.) apart with wire-wrapped riprap between each of the sheet pile rows forming the steps. Every step maintains a constant elevation with an average 0.9 m (3 ft.) elevation drop between each step (**Figure 4** and **Figure 5)**. A 7.6 meter (25 ft.) extension comprised of 10 cm (4 in.) cobble stones was added to the structure downstream of the fourth sheet pile row to prevent localized scour. The USACE also added a row of large riprap just downstream of the cobble extension. The large riprap diameter is estimated to range between 0.9 and 1.8 m (3-6 ft.) (Coonrod et al., 2012).

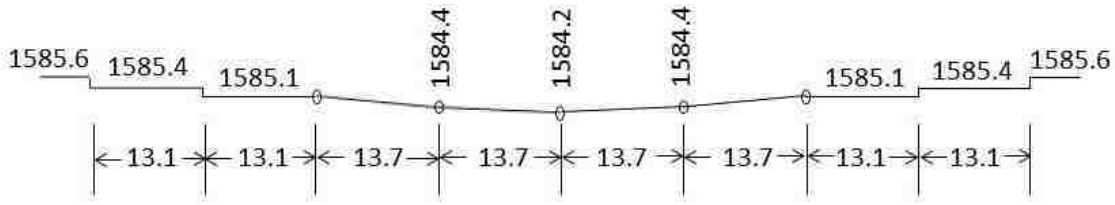

Figure 3: First row of sheet piles cross section view (all values in meters)

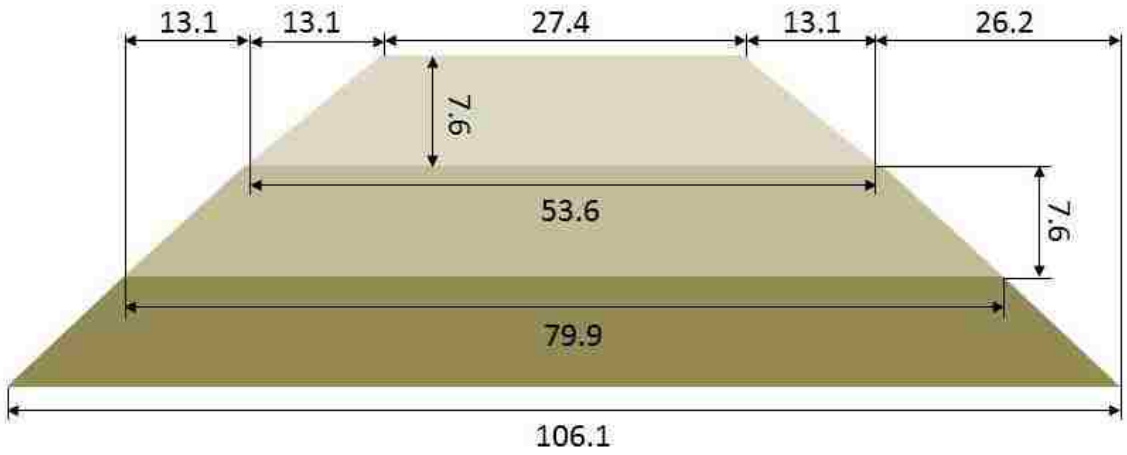

Figure 4: Jemez Weir plan view (all values in meters)

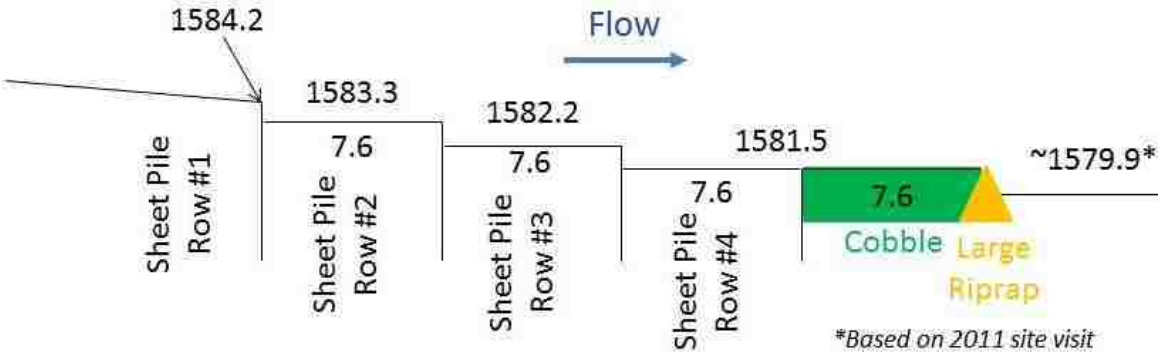

Figure 5: Profile view along the centerline (all values in meters)

Previous Research

One-Dimensional Numerical Model

The one-dimensional HEC-RAS model developed by the United States Army Corps of Engineers began 914 – 1219 m (3000 – 4000 ft.) upstream of the weir to develop inflow sediment boundary conditions. An analysis conducted by Little (2007) discovered channel discharges between 9.9 – 14.2 m^3/s (350 – 500 ft^3/s) transported a majority of the bed material. When reviewing the hydrograph data from years 1980 – 2000, Little (2007) also found that all discharge events but one, due to snowmelt, were

less than 42.5 m^3/s (1500 ft^3/s) (Little, 2007). Preliminary HEC-RAS simulations of the upstream reach revealed perched channel conditions with a bed slope of 0.23% and estimated a channel capacity between 14.2 – 28.3 m^3/s (500 – 1000 ft^3/s). Due to the one-dimensional modeling limitations, the USACE used engineering judgment to approximate flow distribution between the main channel and adjacent floodplains upstream of the weir for the perched channel. The HEC-RAS model developed by the USACE also used a weir discharge rating curve for the Jemez Weir (Maynord et al., 2012).

The USACE used a weir discharge coefficient of 2.6 for the Jemez Weir, and began the model at the downstream end of the Jemez Weir while evaluating long term bed degradation of the reach below the structure. The Yang equation was selected to model sediment transport, although the van Rijn and Acker White equations were also applicable for the Jemez River conditions. Four main scenarios were developed to estimate bed degradation downstream of the weir (Maynord et al., 2012):

1. Effective discharge of 9.9 and 14.2 m^3/s (350 and 500 ft^3/s) ran for six years without bank erosion
2. Five year record from 2005-2010 repeated five times to create a 25 year hydrograph run both with and without bank erosion
3. Sensitivity/ uncertainty analysis with 25 year hydrograph with and without bank erosion
4. 226.5 m^3/s (8000 ft^3/s) monsoon hydrograph without bank erosion

The beginning bed elevation downstream of the Jemez Weir was 1580.8 m (5186.4 ft.) for all the scenarios listed above. Effective discharge simulations resulted in

an ending bed elevation of 1576.5 and 1575.9 m (5172.4 and 5170.4 ft.) for discharges of 9.9 and 14.2 m^3/s, respectively. Ending bed elevations for 25 year hydrograph simulations with and without bank erosion were 1578.4 and 1577.9 m (5178.5 and 5176.7 ft.), respectively. The one day monsoon hydrograph resulted in a bed elevation of 1580.5 m (5185.5 ft.) (Maynord et al., 2012).

The sensitivity analysis performed by the USACE evaluated uncertainty in the equilibrium bed slope upstream of the weir and the sediment transport effects of channel widening due to bank erosion. It also addressed uncertainty of material gradation due to coarser 2003 and 2011 bed gradations when compared to the 2005 bed gradation. The ending bed elevation was 1579.5 m (5182.2 ft.) when the upstream bed slope was adjusted to 0.29% and evaluated using the 25 year hydrograph with bank erosion. When modeling for bed gradation uncertainty, the USACE used 2005 inflow sediment load, 2005 bed gradation, and an upstream bed slope of 0.29%. The 2005 bed and sediment load conditions, coupled with a 0.29% upstream bed slope, resulted in an ending bed elevation of 1579.2 m (5181.1 ft.) downstream of the Jemez Weir. To account for channel widening the USACE adjusted channel cross sections with a 50% increase at already eroded cross sections and a 100% increase at narrow cross sections resulting in an ending bed elevation of 1579.8 m (5183.2 ft.). The USACE also created another simulation with only 50% widening of narrow cross sections which resulted in an ending bed elevation of 1578.4 m (5178.5 ft.) (Maynord et al., 2012).

In addition to long term bed degradation along the reach downstream of the weir, the bed elevation is also affected by local scour. The USACE did not find a technique particular to the Jemez Weir structure to estimate local scour. However, the USACE

applied three equations developed by Bormann and Julien (1991), Laursen and Flick 1983), and Lim (1992) to bound local scour depths between 1.4 and 4.6 m (4.5 – 15 ft.)

Physical Model

The 1:30 geometric scale physical model built and tested by the University of New Mexico (UNM) used Froude number similitude to scale the prototype hydraulic properties. In spite of known similitude issues when sediment is modeled, the bed slope was not distorted. The primary aim of the model was to analyze scour patterns and relative effectiveness of counter measures used to minimize scour. Flow data from the USACE HEC-RAS report, scaled down from 105 m^3/s (3700 ft^3/s) to account for physical model ineffective flow areas shown in **Figure 6**, resulted in a flow rate of 72 m^3/s (2542 ft^3/s) for the physical model. **Figure 6** also shows the fixed upstream bed of the physical model, whereas downstream of the weir was an erodible sand bed. The fixed and erodible bed combination simulated the worst case scenario for sediment inflow through the weir structure. To eliminate bed armoring, the most uniform sand available was used for modeling (Coonrod et al., 2012).

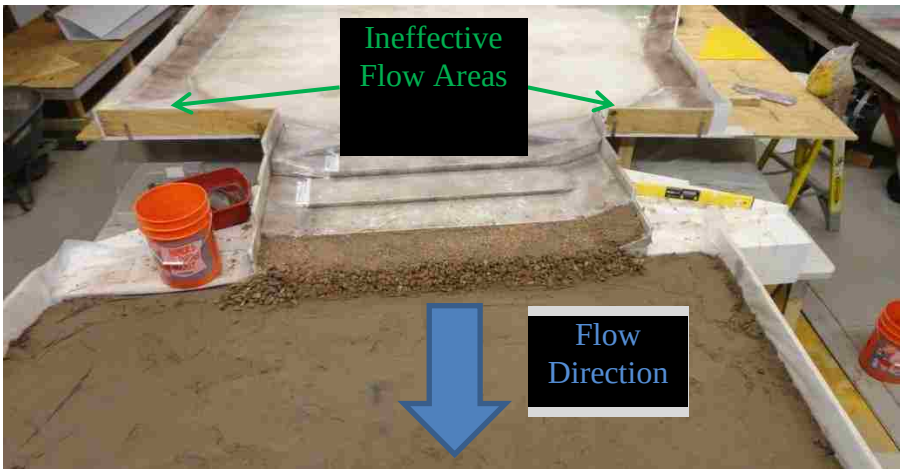

Figure 6: UNM's physical model showing ineffective flow areas

Two beginning elevations for the downstream erodible bed captured both the current prototype conditions and the worst case HEC-RAS modeling scenario at elevations 1580.8 m (5186.4 ft.) and 1577.3 m (5175 ft.), respectively. Three scenarios were modeled at each of the two starting bed elevations:

1. Current prototype configuration
2. Counter measure with additional large riprap – replace 10 cm cobble downstream of the fourth sheet pile row with 0.9-1.8 m large diameter riprap and extend the areal coverage of large riprap in the streamwise direction
3. Counter measure with additional sheet pile rows – replace 10 cm cobble with 0.9-1.8 m large riprap and add two additional sheet pile rows downstream of the last current sheet pile row

Each of the six models were video-taped and photographically documented to illustrate scour progression. A depth gage was used to measure the downstream erodible bed depth, both pre and post model runs, at 73 consistent locations. The resulting scour depth, difference between the pre and post run readings, allowed for a quantative comparison of the modeled scenarios and enabled the modelers to determine counter measure effectiveness (Coonrod et al., 2012).

Table 1: Physical model maximum scour depth results

	Physical model maximum recorded scour depth (cm)	
Beginning bed elevation (m)	1580.8	1577.3
Current prototype configuration	8.677	19.042
Counter measure with additional large riprap	2.880	8.882
Counter measure with additional sheet piles	3.228	13.465

The physical model results shown in **Table 1** reveal the counter measure with additional large riprap was most effective in reducing maximum scour depth for both of the beginning bed elevations. Maximum scour depth location is also important when considering stability of the sheet pile rows. For example, after modeling the counter measure with additional large riprap at a starting bed elevation of 1580.8 m (5186.4 ft.), the maximum model scour depth was located 42.54 cm (14.75 in.) downstream of the fourth sheet pile row. Therefore, depending on design features and soil loads imposed on the sheet pile rows, the location of maximum scour depth may be far enough downstream to have no effect on the stability of the sheet pile rows (Coonrod et al., 2012). **Figure 7** shows the counter measure with large riprap scenario post modeling. The yellow string marked with blue tape and red markers define where depth gage readings were taken.

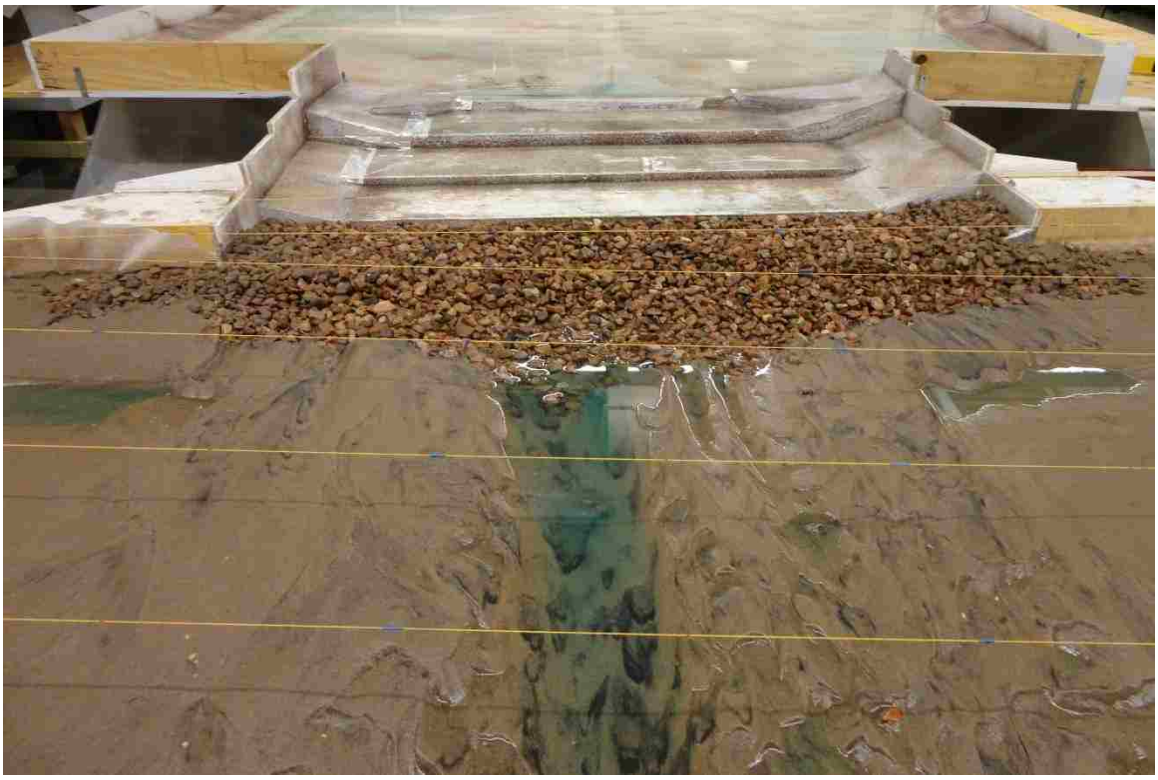

Figure 7: Counter measure with additional large rock and starting bed elevation 1580.8 m (post modeling)

Two-Dimensional Numerical Modeling

Data and Alterations

One-meter Light Detection and Ranging (LiDAR) data was utilized to generate the fixed bed modeling mesh. The LiDAR data inaccurately represented the weir steps with a fairly constant sloping surface instead of explicit, individual drops at each step transition along the Jemez Weir. Additionally, the LiDAR data did not resolve the sloped weir crest profile along the first row of sheet piles. To address these issues, four different meshes were created to represent the Jemez Weir structure:

1. Original LiDAR data
2. Original LiDAR data with a sloped weir crest profile
3. LiDAR data altered to represent weir steps
4. LiDAR data altered to represent weir steps with a sloped weir crest profile

The third mesh (LiDAR data altered to represent weir steps) was most representative of the prototype field conditions after modeling the different meshes, due to its more accurate representation of the steps. The fourth mesh added no significant modeling advantage. The third mesh was used to produce all two-dimensional modeling results for this research. Details of mesh comparison are included in the *Jemez Weir Mesh Comparison* section of the appendix.

SRH-2D

SRH-2D uses the time and depth averaged Navier Stokes Equations (known as the depth averaged St. Venant Equations) shown below to govern flow. A finite volume

approach with an implicit time scheme is used to solve the depth averaged St. Venant Equations within the program code (Lai, 2008):

$$\frac{dhU}{dt} + \frac{dhUU}{dx} + \frac{dhVU}{dy} = \frac{dhT_{xx}}{dx} + \frac{dhT_{xy}}{dy} - gh\frac{dz}{dx} - \frac{\tau_{bx}}{\rho} + D_{xx} + D_{xy}$$

$$\frac{dhV}{dt} + \frac{dhUV}{dx} + \frac{dhVV}{dy} = \frac{dhT_{xy}}{dx} + \frac{dhT_{yy}}{dy} - gh\frac{dz}{dy} - \frac{\tau_{by}}{\rho} + D_{yx} + D_{yy}$$

where t is time, x and y are horizontal Cartesian coordinates, h is water depth, U and V are depth-averaged velocities in x and y directions respectively, g is acceleration due to gravity, T_{xx}, T_{xy}, and T_{yy} are depth-averaged turbulent stresses, D_{xx}, D_{xy} , D_{yx}, and D_{yy} are terms due to depth averaging used to describe dispersion, z is water surface elevation, ρ is water density, and τ_{bx} and τ_{by} are bed shear stresses. Although the St. Venant Equations shown above include time derivatives, all model results shown below are from steady state solutions. Shear stresses are calculated using the bed shear stress equations and a roughness equation (Lai, 2008):

$$\tau_{bx} = \rho C_f U\sqrt{U^2 + V^2}$$

$$\tau_{by} = \rho C_f V\sqrt{U^2 + V^2}$$

$$C_f = \frac{gn^2}{h^{1/3}}$$

where n is Manning's roughness coefficient. A third-party mesh generation program, Aquaveo's Surface Water Modeling System (SMS), is necessary to run the SRH-2D model. Details on mesh generation are available in the SMS User Manual v11.1 (Aquaveo, 2013).

Mesh Details

The final mesh used during numerical modeling consists of nodes spaced 4.6 m (15 ft.) apart upstream and downstream of the area of concern. Quadrilateral elements were created within the channel, and floodplains were represented with triangular elements. The mesh was then refined with a decrease in node spacing from 4.6 m (15 ft.) to 1 m (3.3 ft.) as it approached the Jemez Weir. Altering the density of mesh nodes in this manner allows the modeler to find a balance between computational time, model resolution, and data accuracy.

Monitor lines were used to record average water surface elevation and total flow across the line. Monitor lines were strategically placed to address the following three objectives:

1. Quantify the flow distribution between the main channel and floodplains
2. Determine a weir discharge rating curve for the Jemez Weir
3. Quantify re-entry points of overbank flows around the Jemez Weir

Velocity vectors at each node were used to identify re-entry points of overbank flows. Monitor lines were placed along the main channel banks once flow re-entry points were identified.

Once a user creates the desired mesh the other key required inputs within SRH-2D for a fixed bed model are Manning's *n* values, and downstream boundary conditions. Initial Manning's *n* values for this research were chosen from the 1959 Open-Channel Hydraulics textbook by Chow (Chow, 1959). **Figure 8** shows material types assigned to polygons. Selected initial values for modeling are shown in **Table 2**. A water surface elevation is required for the downstream boundary condition. For each flow profile

modeled, the downstream boundary condition was adopted from the HEC-RAS model developed by the USACE. These values can be found in **Table 5** of the appendix. Discharges modeled for this research in SRH-2D range from 2.8 to 226.5 m^3/s (100 to 8000 ft^3/s).

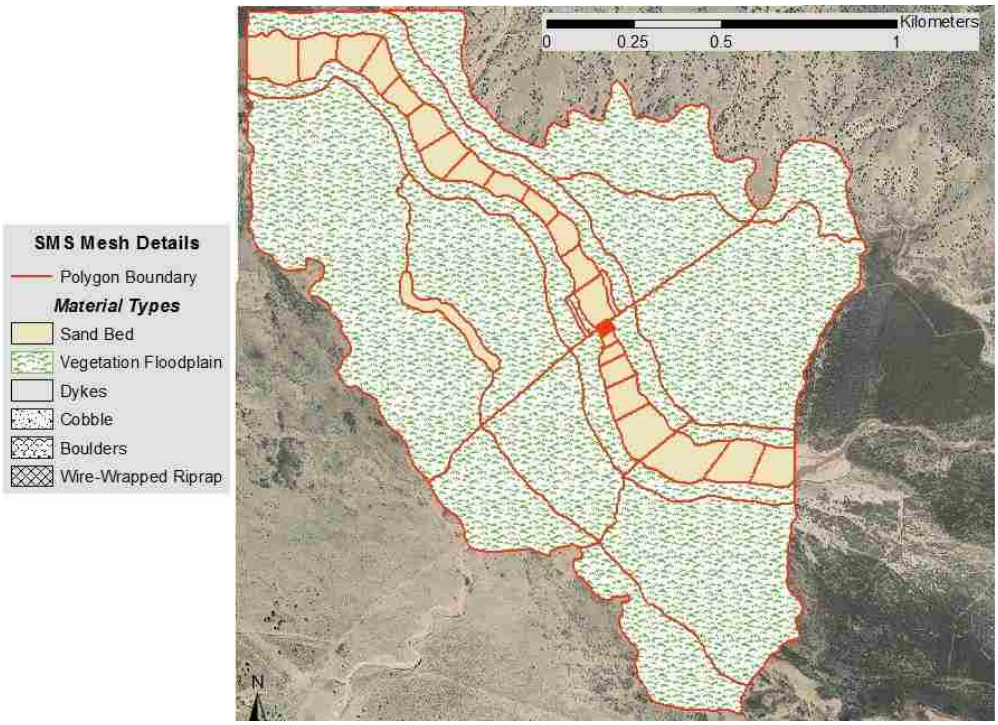

Figure 8: SMS mesh material types

Table 2: SRH-2D Initial Manning's n values

Material	Manning's *n*	Material	Manning's *n*	Material	Manning's *n*
Sand	0.030	Dikes	0.050	Large Rock	0.050
Vegetation	0.060	Cobble	0.035	Riprap Steps	0.040

Results and Discussion

Model Performance

Using the final mesh, the program ran for 200 modeling hours (7.2 runtime hours) using an Intel Core i7 – 2600 Central Processing Unit (CPU) processor with 16.0 GB of Random Access Memory (RAM). The model converged at 60 modeling hours (2.5 runtime hours). Graphic representation of data from a monitoring point placed at the downstream boundary condition helped determine model convergence time (**Figure 27** and **Figure 28** in the appendix).

Preliminary results revealed a low point in the mesh along the right river bank which allowed flow to traverse from the main channel into the right overbank. The low point was initially thought to be an error from the mesh generation stage; however, after further investigation of the LiDAR data, there was evidence of a low point in the right channel bank approximately one kilometer (0.56 miles) upstream of the weir. HEC-RAS model cross sections were then reviewed to determine if any cross sections intersected the identified low point within the main channel. **Figure 9** shows the closest cross sections (RS: 19916.4 and RS: 19555.07) are spaced just above and below the low point in the main channel. HEC-RAS likely over-predicted channel capacity in this area as a result of the cross-section spacing, resulting in an over-estimated main channel discharge further downstream.

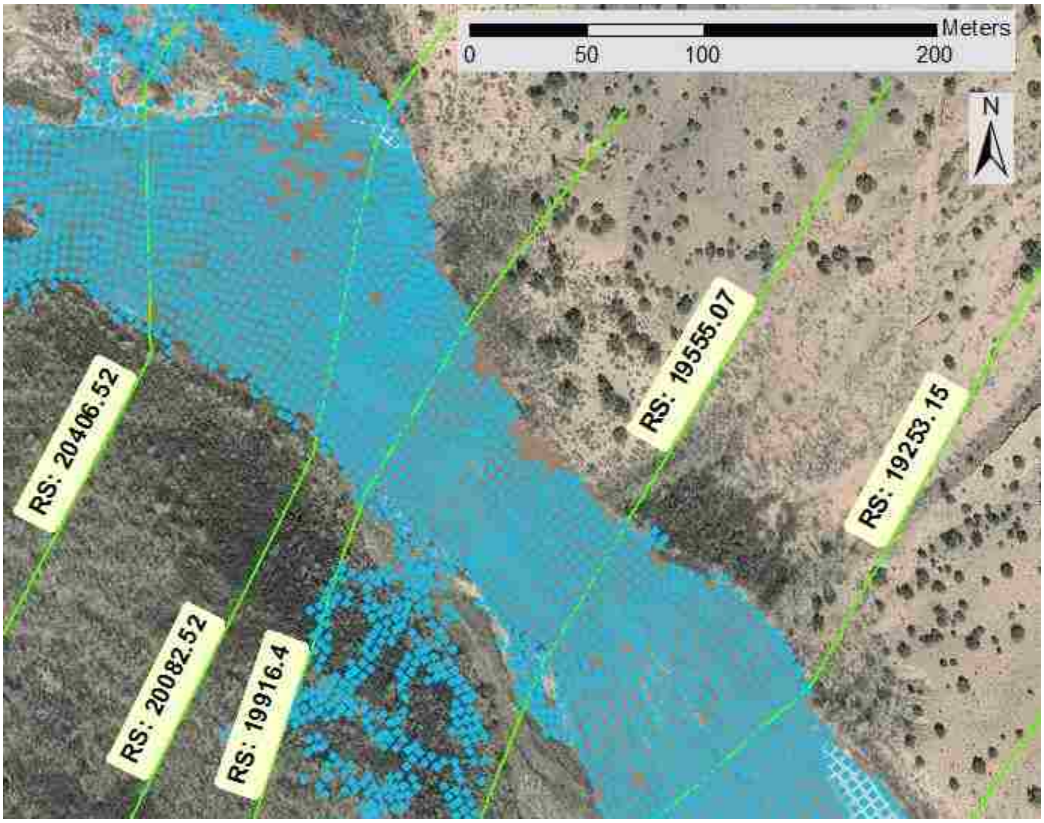

Figure 9: HEC-RAS cross sections near main channel low point

Sensitivity Analysis

To test the sensitivity of the computer model the following Manning's roughness coefficient changes were made:

1. Increase and decrease original sand bed roughness by 0.01
2. Increase and decrease original vegetation roughness by 0.01

Model discharges of 28.3 m^3/s (1000 ft^3/s) and 70.8 m^3/s (2500 ft^3/s) were selected to evaluate the sand bed and vegetation Manning's roughness coefficient sensitivities, respectively. Increasing the roughness coefficient of the sand bed increased floodplain inundation area by less than five percent approximately, and decreasing the roughness coefficient decreased floodplain inundation area by less than five percent approximately.

The orange boxes in **Figure 10** and **Figure 11** show the increase in inundation area once the Manning's roughness coefficient for the main channel was increased by 0.01.

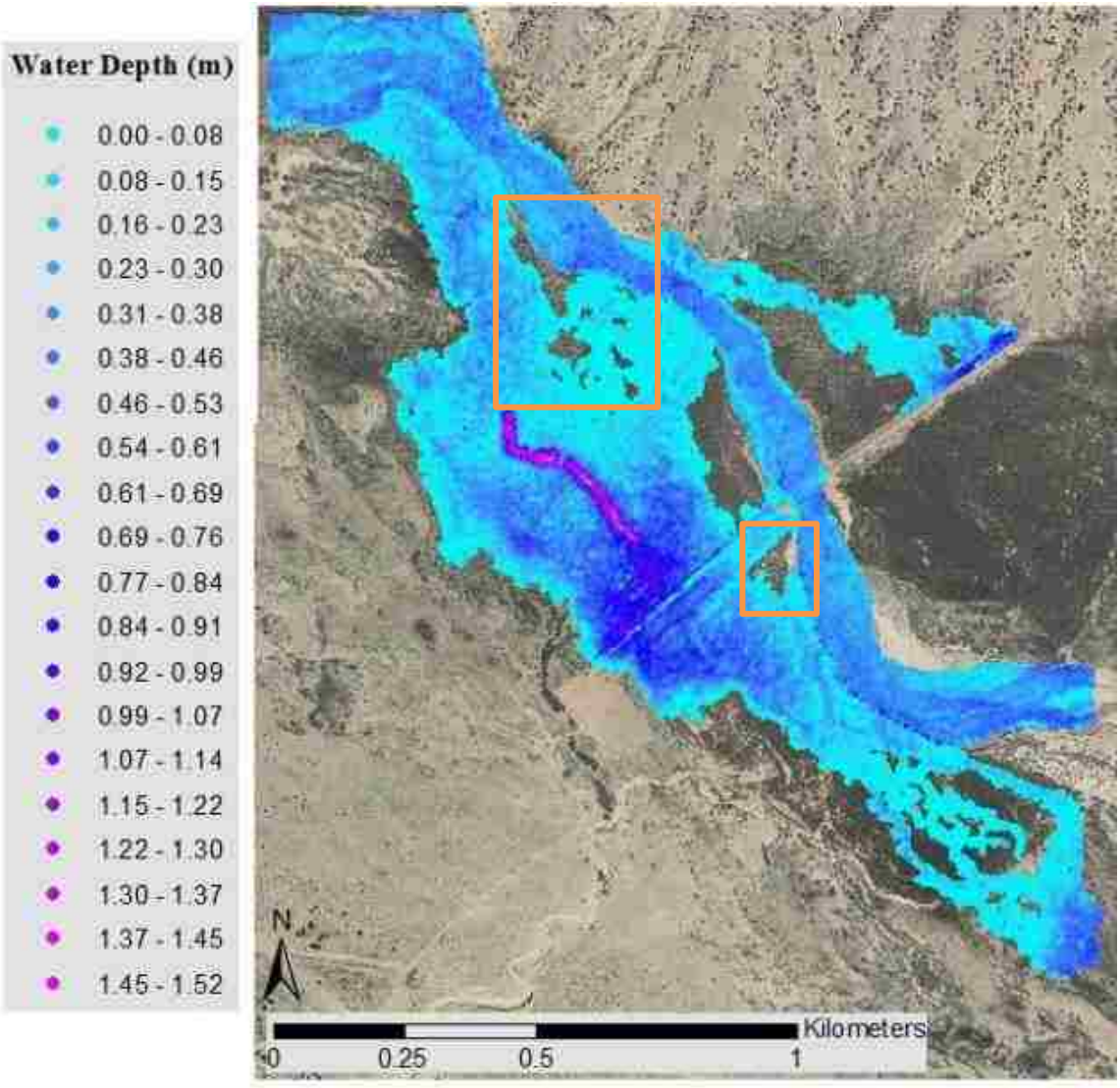

Figure 10: Water depths for 28.3 m^3/s and 0.03 Manning's *n* in the main channel

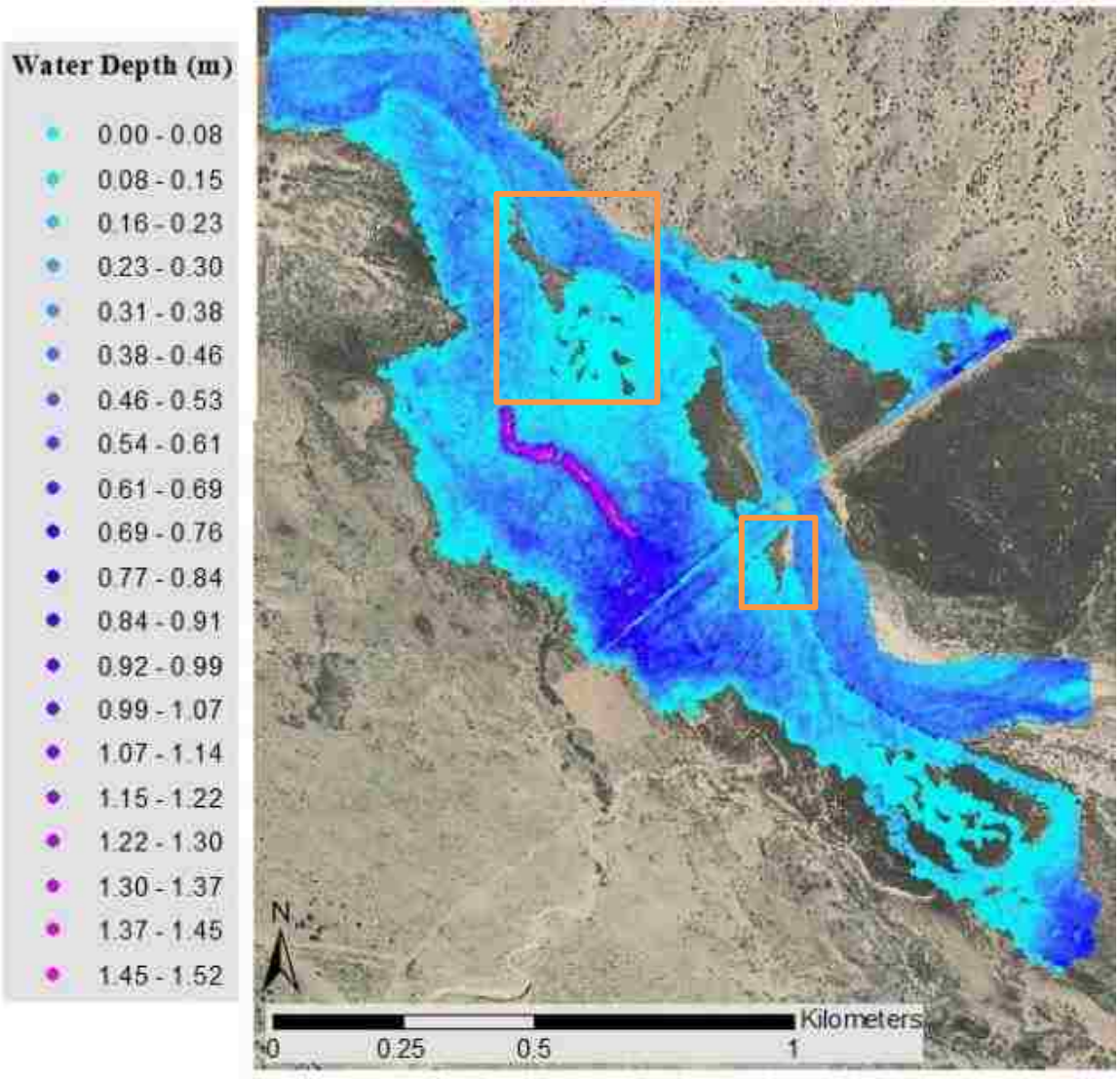

Figure 11: Water depth for 28.3 m^3/s and 0.04 Manning's *n* in the main channel

When the main channel roughness was isolated and the vegetation roughness coefficient was changed the same relationship held true, although the change was not as significant when compared to adjusting the main channel roughness values. The red circles in **Figure 12** and **Figure 13** show the small decrease in inundation area, less than five percent approximately, from a 0.01 change in the floodplain Manning's roughness coefficient.

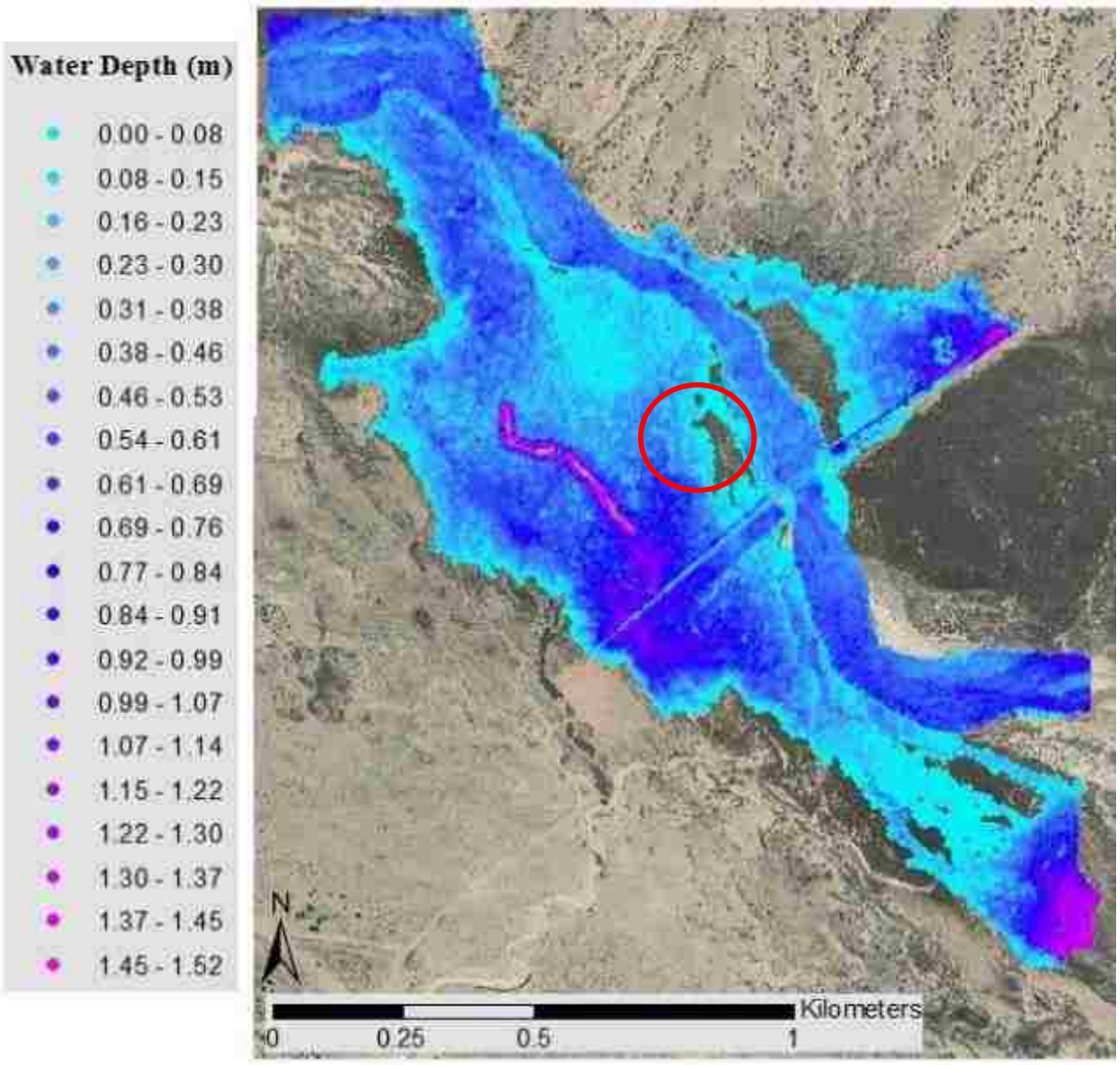

Figure 12: Water depths for 70.8 m^3/s and 0.06 Manning's *n* for the floodplain

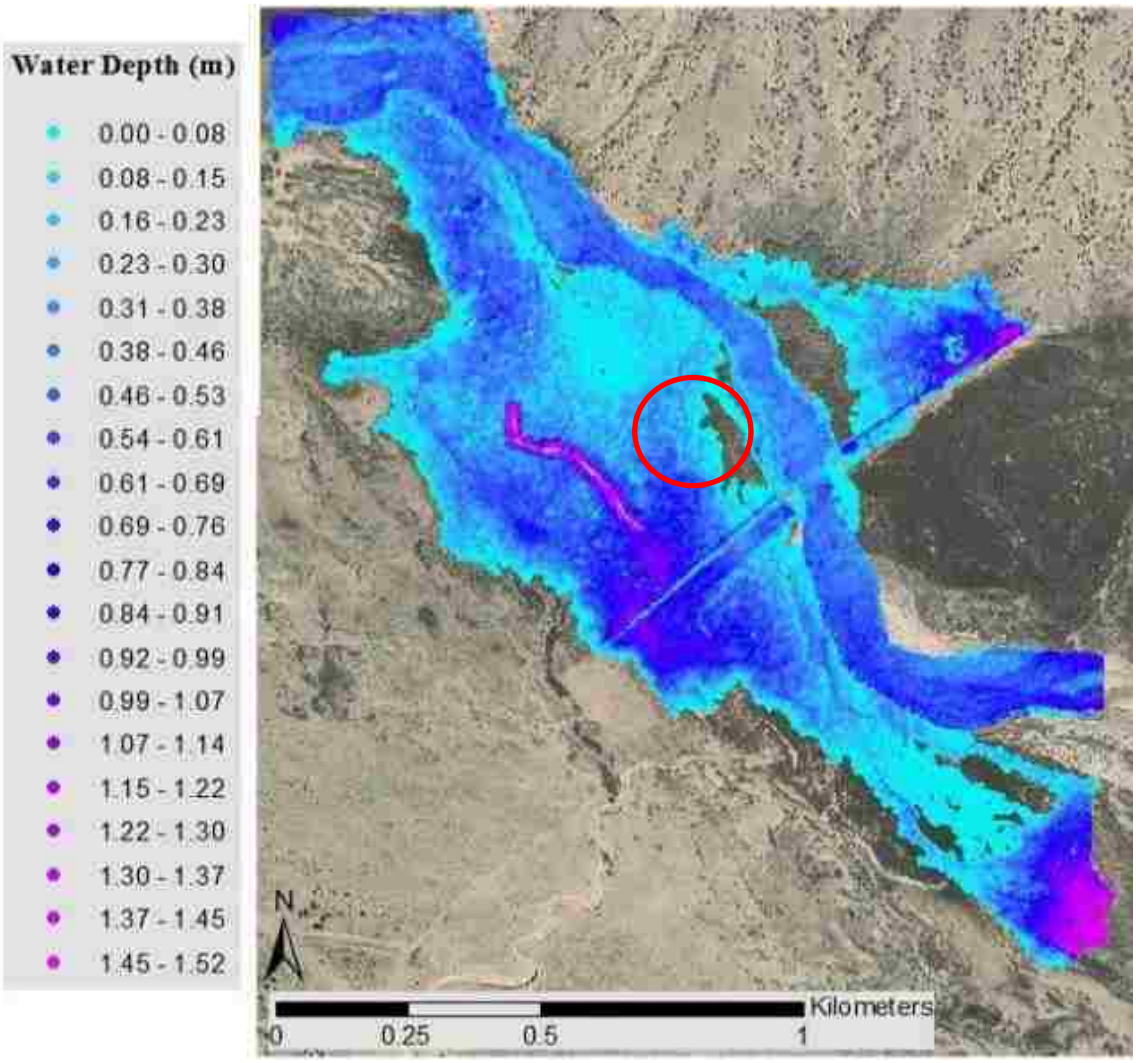

Figure 13: Water depths for 70.8 m^3/s and 0.05 Manning's *n* for the floodplain

From the figures above, the results seem relatively similar when decreasing and increasing Manning's roughness coefficient by a factor of 0.01. To perform a quantitative assessment of the sensitivity analysis, histogram plots with 12 equal interval bins were created for each scenario. A polygon near river station (RS) 16616 was created in ArcGIS to select the same nodes within the main channel for each scenario. Results of the shear stress values near river station 16616 were plotted in the histograms shown in **Figure 14** - **Figure 19**.

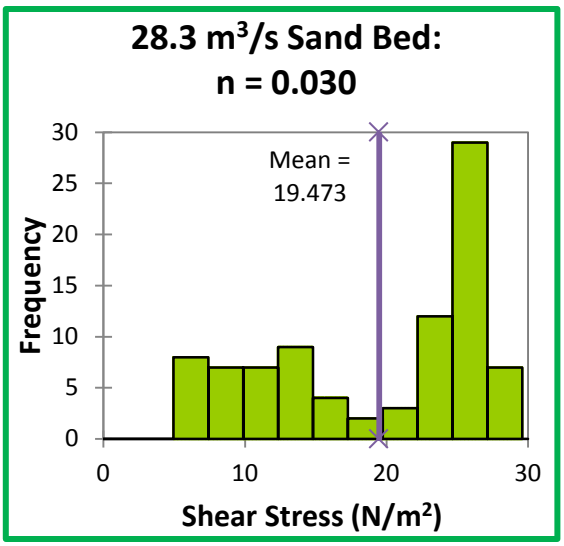

Figure 14: Shear stress histogram for 28.3 m^3/s and 0.04 Manning's *n* for the main channel

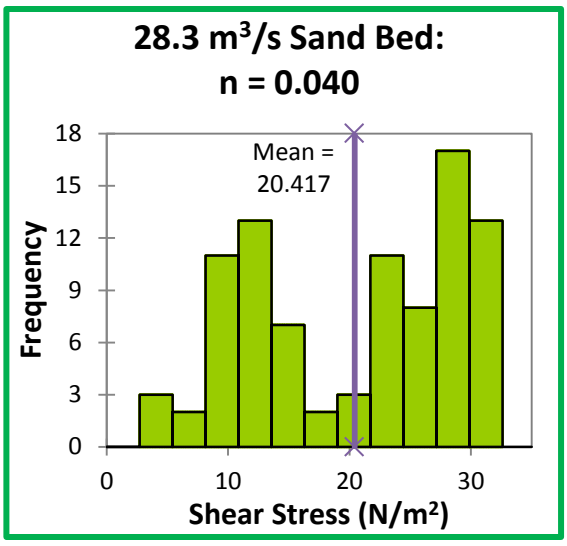

Figure 15: Shear stress histogram for 28.3 m^3/s and 0.04 Manning's *n* for the main channel

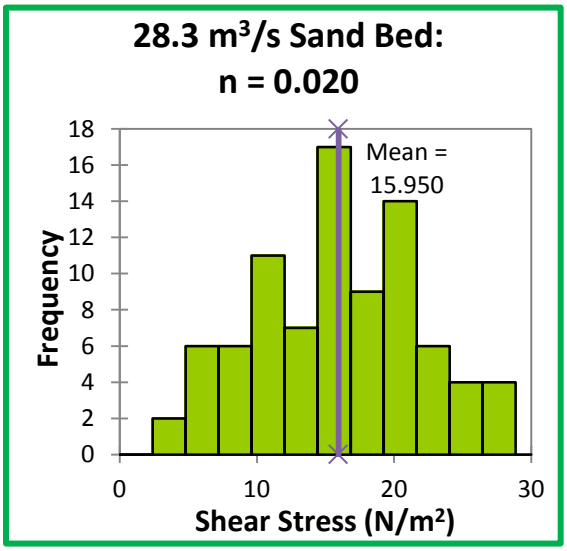

Figure 16: Shear stress histogram for 28.3 m^3/s and 0.02 Manning's *n* for the main channel

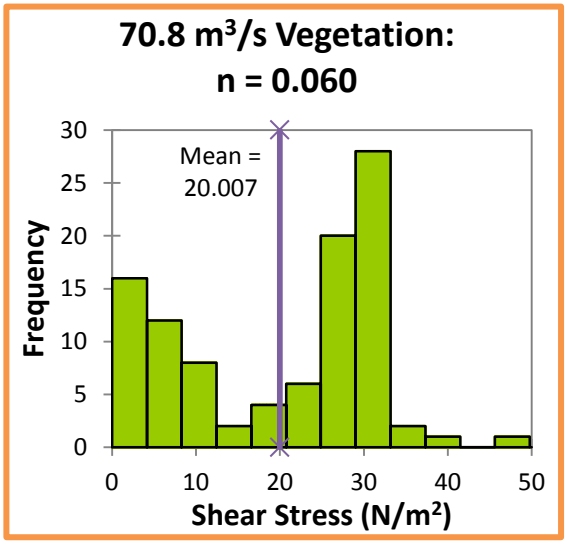

Figure 17: Shear stress histogram for 70.8 m^3/s and 0.06 Manning's *n* for the floodplain

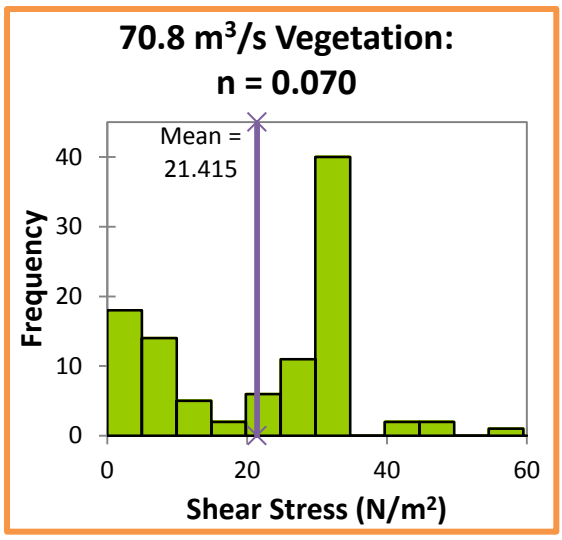

Figure 18: Shear stress histogram for 70.8 m^3/s and 0.07 Manning's *n* for the floodplain

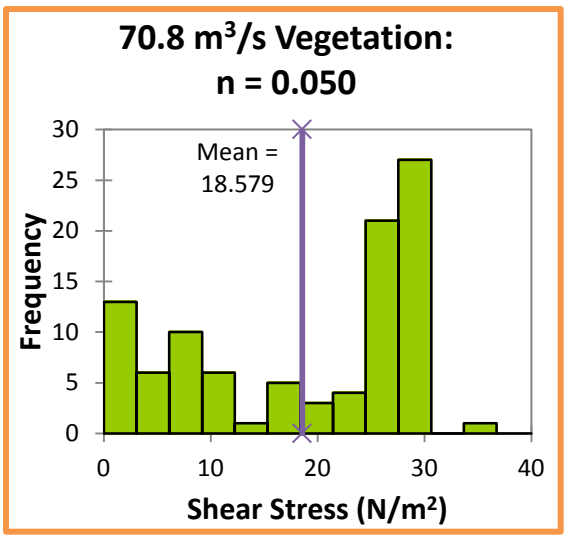

Figure 19: Shear stress histogram for 70.8 m^3/s and 0.05 Manning's *n* for the floodplain

Increasing the sand bed roughness causes the mean main channel bed shear stress at RS: 16616 to increase by 0.9 N/m^2 and results in an even distribution of shear stresses around the mean. Decreasing the sand bed roughness results in a decrease of the mean by 3.5 N/m^2 and again the results are more evenly distributed around the mean. Decreasing the vegetation roughness for the floodplain decreases the mean main channel shear stress by 1.4 N/m^2, and increasing the vegetation roughness results in an increase of the mean by 1.4 N/m^2. Adjusting the floodplain roughness value does not significantly change the main channel distribution of the shear stress results, as expected. Changing the floodplain roughness value does not affect the main channel roughness values, and the floodplain's roughness value has almost no effect on main channel velocities as a result of the limited floodplain and main channel interactions within this reach. Main channel and floodplain interaction is limited to areas upstream of the training dykes and further downstream

passed the Jemez Weir structure. Therefore, adjusting the floodplain roughness value was not expected to affect main channel shear stress distribution.

Table 3 shows a comparison of average main channel shear stress results between HEC-RAS and SRH-2D. Four consecutive cross sections downstream of the Jemez Weir were selected for comparison. Four polygons created within ArcGIS were used to select results from SRH-2D with a close proximity to the corresponding cross sections. The selected data points were then averaged to obtain a comparable value for HEC-RAS. Sensitivity to Manning's roughness coefficient for the sand bed and the vegetation were tested for discharges of 28.3 and 70.8 m^3/s, respectively. SRH-2D exhibited a dynamic relationship between floodplain and main channel shear stresses. The relationship was evident when only the vegetation roughness was changed for the higher discharge, but there was still a response within the main channel. The dynamic relationship between the floodplain and main channel shear stresses was not evident in the HEC-RAS results as shown in **Table 3**.

HEC-RAS results for river station (RS) 16616 over-predict bed shear stresses due to the solution method used in the programming code. HEC-RAS uses the average slope of the energy grade line (friction slope) between the two cross sections in question to calculate the average bed shear stress (Hydrologic Engineering Center, 2010). RS 16956 is located upstream of the Jemez Weir structure, therefore because of cross section locations, and the drastic change in elevation, HEC-RAS over-predicts shear stresses.

On the contrary, HEC-RAS shear stress results for RS 16040 and RS 15733 under-predict shear stresses because of the mild change in slope within the floodplain. Additionally, floodplain slopes downstream of the Jemez Weir slope in towards the main

channel, and floodplain flows begin to re-enter the main channel at the cross sections in question. SRH-2D is able to account for the lateral change in slope with its two-dimensional capabilities, and therefore two dimensional shear stresses are larger in value when compared to the HEC-RAS results.

Although results used in **Table 3** were obtained with the HEC-RAS geometry provided by the USACE, the reported values are not from the exact model used by the USACE to produce their final report. The HEC-RAS data provided by the USACE omitted the flow data used to produce the final report.

Table 3: Average main channel shear stress comparison at discharges of 28.3 m^3/s and 70.8 m^3/s to test sand and vegetation roughness sensitivities, respectively

	SRH-2D Shear Stress (N/m^2)				HEC-RAS Shear Stress (N/m^2)			
Scenario	RS: 16616	RS: 16369	RS: 16040	RS: 15733	RS: 16616	RS: 16369	RS: 16040	RS: 15733
Sand n = 0.02	15.6	5.8	6.8	6.3	19.2	6.2	7.2	5.8
Sand n = 0.03	19.1	6.4	7.2	7.5	40.2	8.6	8.6	8.1
Sand n = 0.04	20.4	6.8	7.1	8.3	42.1	10.1	9.6	10.5
Vegetation n = 0.05	21.3	7.7	19.5	25.2	64.6	15.8	12.9	15.3
Vegetation n = 0.06	23.8	8.2	27.1	25.5	64.6	15.8	12.9	15.3
Vegetation n = 0.07	26.0	8.7	29.5	25.9	64.2	15.8	12.9	15.3

Flow Distribution

Monitor lines placed 128 m upstream of the training dikes were utilized to develop a relationship between modeled discharge and channel section flow rates. **Table 4** shows the results of the monitor line data. Comparing modeled discharge to observed

total model flow across the monitor lines (column 1 to column 5) in **Table 4** shows a discrepancy in flow data. A small storage area located in the right overbank, where a small pool forms, explains this discrepancy. Observed model discharge through the right overbank exceeds observed model discharge in the main channel once the modeled discharge surpasses 28.3 m^3/s (1000 ft^3/s). The distribution of flow between the overbanks is skewed towards the right overbank due to the previously identified low point in **Figure 9**.

Table 4: Flow distribution results for SRH-2D model at all modeled discharges

Modeled Discharge (m^3/s)	Flow Distribution (m^3/s)			
	Left Overbank	Main Channel	Right Overbank	Total
5.7	0.0	5.6	0.0	5.6
8.5	0.0	8.1	0.0	8.1
11.3	0.0	10.4	0.6	10.9
14.2	0.0	12.2	1.0	13.2
17.0	0.0	13.6	2.4	16.0
19.8	0.0	14.8	4.8	19.7
22.7	0.1	15.8	6.6	22.5
25.5	0.2	16.7	8.5	25.4
28.3	0.3	17.4	10.5	28.2
42.5	0.5	20.4	21.4	42.4
56.6	0.7	22.8	32.8	56.4
70.8	1.0	25.0	44.4	70.4
85.0	1.4	27.0	56.2	84.5
113.3	2.3	30.3	80.4	113.0
141.6	3.5	33.8	104.3	141.5
169.9	4.6	38.3	127.0	169.9
198.2	5.7	43.8	148.7	198.2
226.5	7.0	49.9	169.6	226.5

The HEC-RAS model used by the USACE to determine long term bed degradation in the reach below the Jemez Weir began at the downstream end of the weir. This required the development of a discharge rating curve created in HEC-RAS using a

weir discharge coefficient of 2.6 for a broad crested weir (Maynord et al., 2012). **Figure 20** shows the developed flow distribution schematic at a discharge of 226.5 m^3/s. When compared to the results in SRH-2D, the flow distribution used by the USACE for a river discharge of 226.5 m^3/s more than doubled the main channel discharge from 49.9 m^3/s to 104.8 m^3/s (1762 ft^3/s to 3700 ft^3/s).

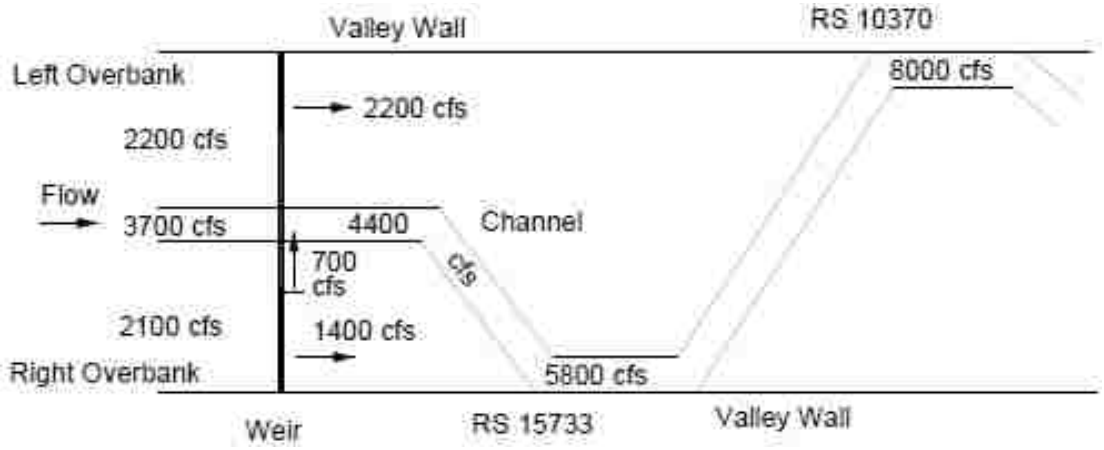

Figure 20: Flow distribution at the weir for 226.5 m^3/s (8000 ft^3/s) (USACE, 2010)

The decrease in main channel discharge identified using SRH-2D would likely impact local scour conditions just downstream of the Jemez Weir through a reduction in total affected area of local scour. A reduction in flow rate through the center portion of the weir would decrease velocities and therefore, decrease the bed shear stresses. The discharge rating curve developed by the USACE and the discharge rating curve, for modeled flow rate, developed using the two-dimensional model results for the Jemez Weir are both shown in **Figure 21**.

It is uncertain how the change in main channel discharge would impact the long term bed degradation due to flow re-entry points downstream of the Jemez Weir. Model results showed 43.7 m^3/s of the 169.6 m^3/s (approximately 25%) in the right overbank re-

entered the main channel within a distance of roughly 120 m (400 ft.) downstream of the Jemez Weir. The schematic developed by the USACE assumes 19.8 m^3/s (exactly 33%) of the flow in the right overbank would re-enter the main channel just downstream of the Jemez Weir. The change in long term bed degradation would likely be small, if any, because the remaining 67% (75 % for the SRH-2D model) of flows from the right overbank re-enter the main channel approximately 270 m (880 ft.) downstream from the Jemez Weir (Maynord et al., 2012).

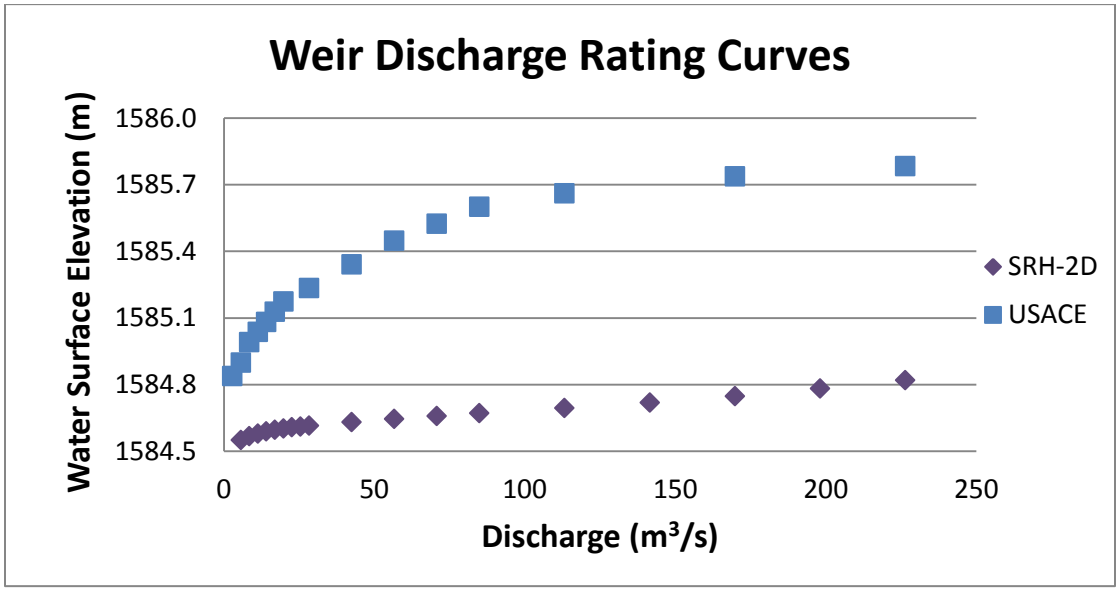

Figure 21: SRH-2D and USACE HEC-RAS (2010) weir discharge rating curve comparison

Velocity Data

The Maximum Permissible Velocity (MPV) method is based on the assumption that a channel bed will not erode if the maximum permissible velocity exceeds the average velocity along a channel cross-section. Data from the USACE reveals a majority of the Jemez River channel bed is comprised of medium sands (Maynord et al., 2012). Applying the MPV method to the Jemez River channel bed bounds the maximum

permissible velocity between 0.6 and 1.2 m/s (2 and 4 ft./s), for a fine and coarse sand bed respectively (Akan, 2006; United States Army Corps of Engineers, 1994). **Figure 22** displays the model results for each node and uses the median value of 0.91 m/s (3ft./s) to differentiate between areas of high velocity (medium to dark blue) and acceptable velocity (light blue). SRH-2D reports a depth averaged velocity both in the x and y direction as well as a velocity magnitude for each node. For the purpose of this investigation velocity magnitudes are displayed and analyzed.

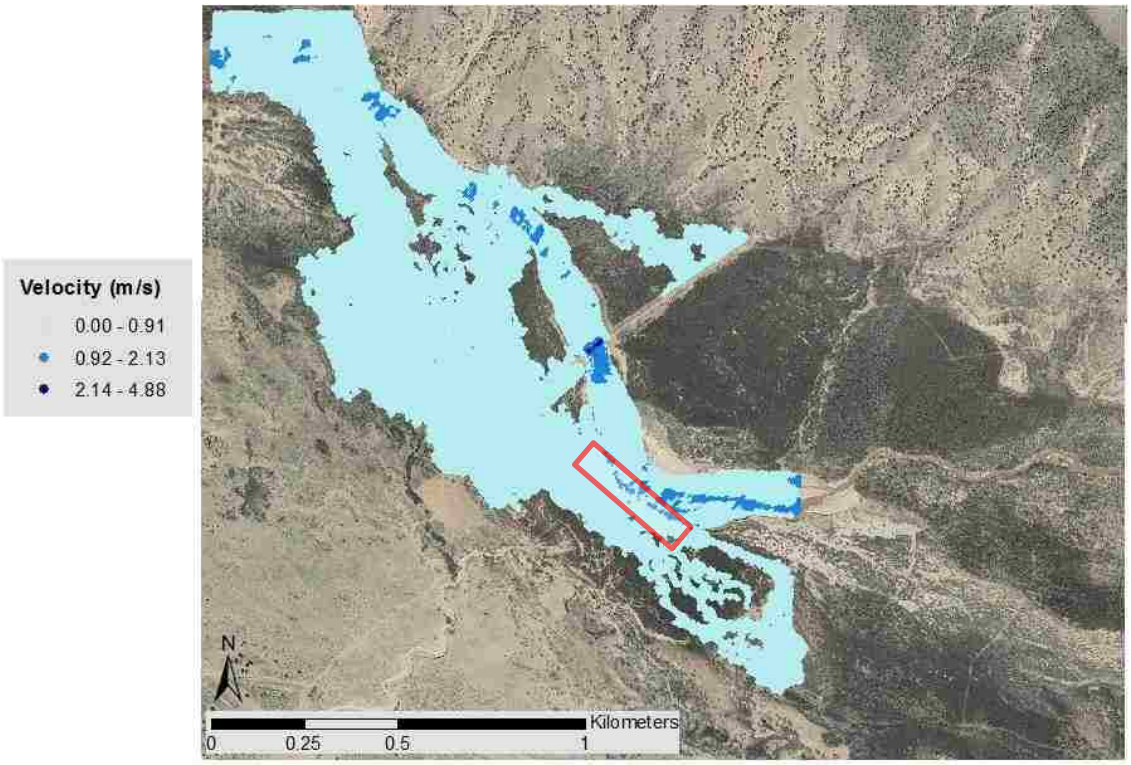

Figure 22: SRH-2D velocity results for 28.3 m^3/s modeled discharge

Velocity results for all modeled discharges below 42.5 m^3/s (1500 ft^3/s) display similar results, with a majority of the Jemez River main channel bed remaining below the maximum permissible velocity. Once modeled discharge met or exceeded 42.5 m^3/s, a majority of the main channel bed also exceeded the maximum permissible velocity for a

medium to coarse sand bed material. The high velocity areas downstream of the Jemez Weir outlined by the red rectangle are due to overbank flows re-entering the main channel through a near vertical bank face. Excluding these areas, and applying the maximum permissible velocity theory would imply a majority of the channel bed would be safe from erosion for discharges below 42.5 m^3/s and subject to erosion for discharges equal to and greater than 42.5 m^3/s. However, when focusing on the area surrounding the Jemez Weir results show bed erosion can be expected in areas where the model velocities exceed the maximum permissible velocity for a medium sand bed.

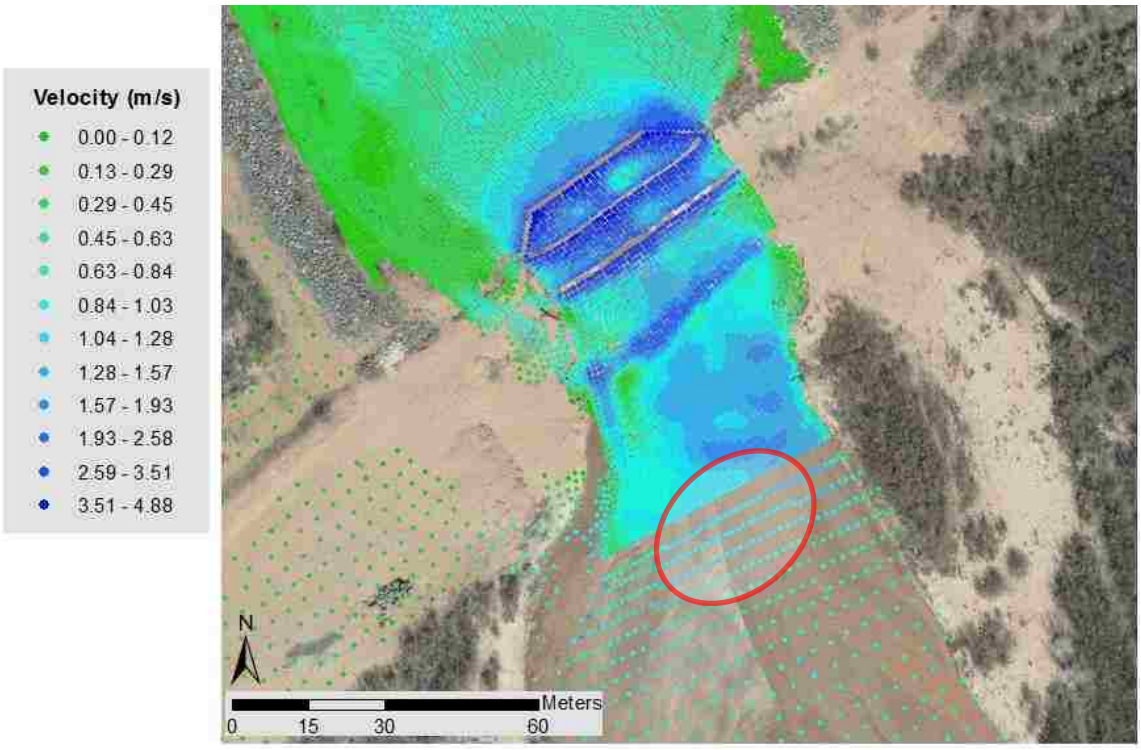

Figure 23: Velocity results near the Jemez Weir for 28.3 m^3/s modeled discharge

Figure 23 shows a blow up view of the same results around the Jemez Weir from **Figure 22** with a slight change in color scheme. In **Figure 23**, shades of green are used to represent velocities below 0.91 m/s and shades of blue represent velocities which exceed 0.91 m/s. The highest velocities are reported near the transition areas between each of the

weir steps and downstream of the large diameter riprap for discharges lower than 226.5 m^3/s (8000 ft^3/s). High velocities were expected in areas where significant changes in bed elevation are present due to the transfer from potential energy to kinetic energy. Areas downstream of the large diameter rock where erosion is likely to occur are identified with a red oval in **Figure 23**.

Erosion is unlikely to occur along the Jemez Weir steps due to the use of wire-wrapped riprap, and would only occur after failure of the wire-wrap material. Transport of the cobble stone extension and the large diameter rock are also unlikely, where the maximum permissible velocity for 10 cm cobble is approximately 2.2 m/s (7.2 ft./s) and that of the large diameter rock exceeds 3.0 m/s (10 ft./s) (United States Army Corps of Engineers, 1994). Applying the same MPV concept for material transport downstream of the large diameter riprap would require placement of 15 cm cobble to prevent erosion. Velocities in this region do not exceed 2.6 m/s (8.5 ft./s). However, when accounting for impact scour it is unsure if the 15 cm cobble downstream of the large diameter rock would remain immobilized. Impact scour is likely to occur downstream of the large diameter rock due to the 1.6 meter drop in elevation from the large rock to the channel bed. Impact scour is only mentioned as a potential method of material transport and is not investigated in this research.

Shear Stress Data

SRH-2D reports shear stress data for each node within the modeled mesh. Chow's (1959) mean shear stress equation can be utilized to estimate the average maximum bed shear stress expected in the channel:

$$\tau_O = \gamma R S_O$$

where τ_O is mean bed shear stress, γ is the specific weight of water, R is the hydraulic radius (sometimes estimated as depth in wide channels), and S_O is the bed slope. The computed shear stress from Chow's equation can then be used to analyze modeling results. The channel depth was substituted for the hydraulic radius to estimate the maximum mean bed shear stress. Solving Manning's Equation for a 96 meter (315 ft.) wide rectangular channel with a discharge of 226.5 m^3/s (8000 ft^3/s), a Manning's roughness coefficient of 0.032, and a 0.23% bed slope results in a water depth of 1.33 m (4.36 ft.):

$$Q = \frac{k}{n} A R^{2/3} S_O^{1/2}$$

where Q is discharge, k is a unit correction factor, n is Manning's Roughness Coefficient, and A is cross-sectional area.

A channel width of 96 m was chosen to replicate the average channel width reported by the USACE for the Jemez River (Maynord et al., 2012). A rectangular channel was chosen to simplify calculations. Chow's equation can then be solved using a water depth of 1.2 m (rounded to the nearest whole integer in U.S. units) and a 0.23% bed slope resulting in 28.7 N/m^2 (0.599 $lbs./ft^2$) as the maximum average shear stress. **Figure 24** displays the model results for each node with 28.7 N/m^2 differentiating between areas of high shear stress (yellow and red) and low shear stress (green). The area outlined in red identifies shear stresses due to flow re-entry through near vertical bank faces.

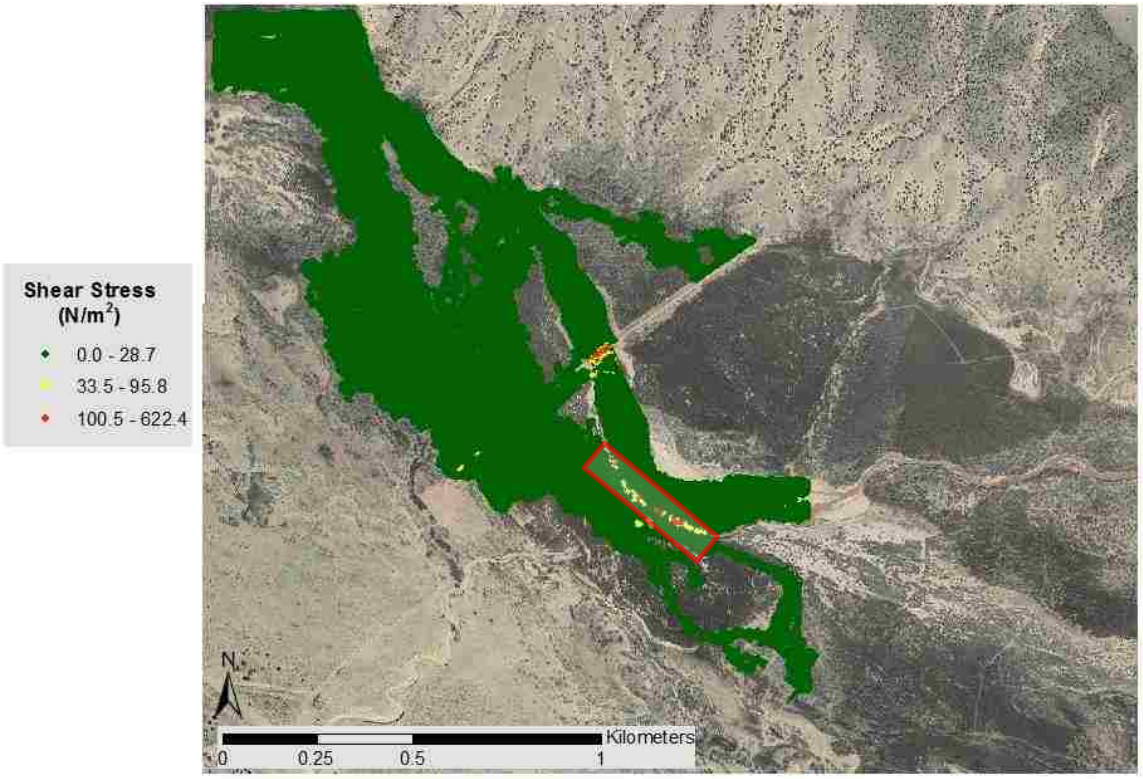

Figure 24: SHR-2D shear stress results for 28.3 m^3/s modeled discharge

Shear stress results were similar for all modeled flow rates. High shear stress areas for discharges lower than 85 m^3/s (3000 ft^3/s) were limited to zones around the Jemez Weir, areas of flow re-entry into the main channel downstream of the structure, and small isolated regions in the floodplain. Once the modeled discharge rate exceeded 85 m^3/s some areas within the main channel began to display high shear stress values.

Figure 25 identifies the most prevalent locations of high channel shear stresses for the larger discharge rates modeled. The transparent rectangle identifies the location of high shear stresses near the channel low point illustrated in **Figure 9**. High channel bed shear stresses near the channel low point were consistently present for modeled discharges above 85 m^3/s. The transparent oval locates high shear stresses near the

channel bend downstream of the Jemez Weir which were consistently present for discharges above 85 m^3/s.

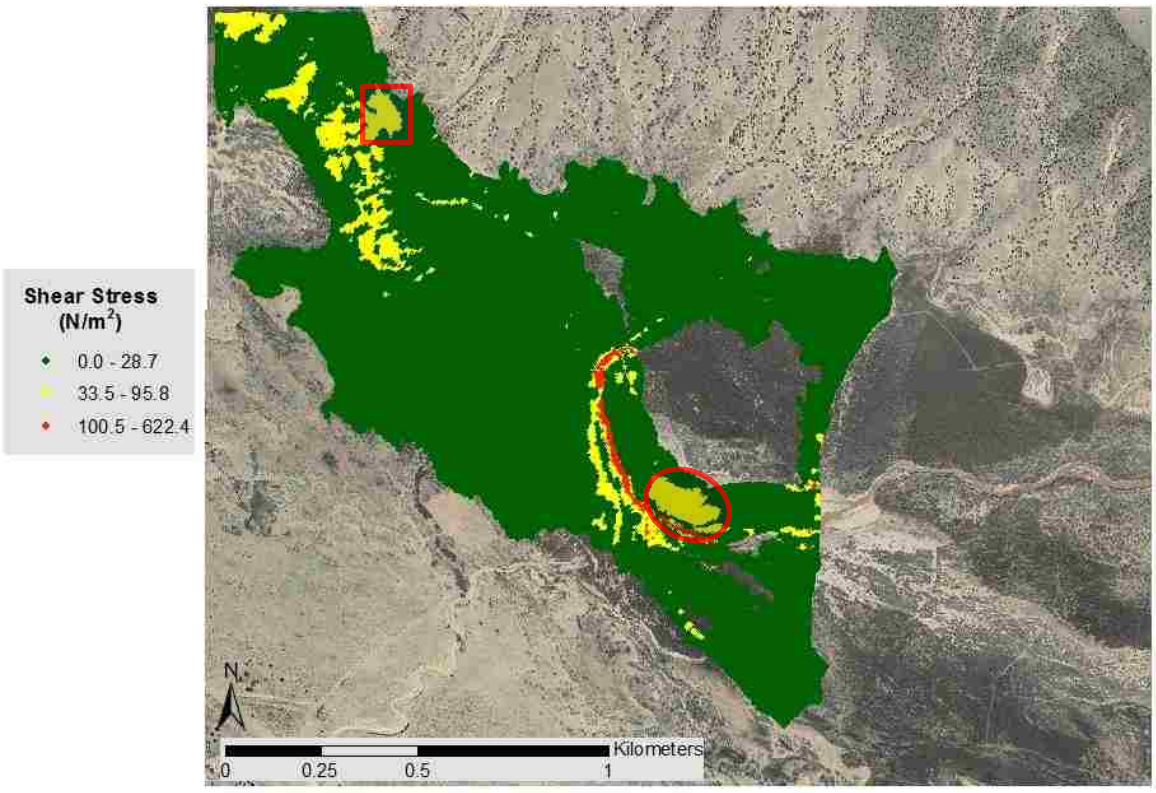

Figure 25: SRH-2D shear stress results for 226.5 m^3/s modeled discharge

When focusing on the area surrounding the Jemez Weir the highest shear stress values were located near the transition regions between each weir step, and just downstream of the large diameter rock. The red outlined area downstream of the large diameter rock in **Figure 26** also displayed high shear stress values which were concurrent with the velocity results. Shields parameter can be used to determine the particle size necessary to prevent erosion downstream of the large diameter rock.

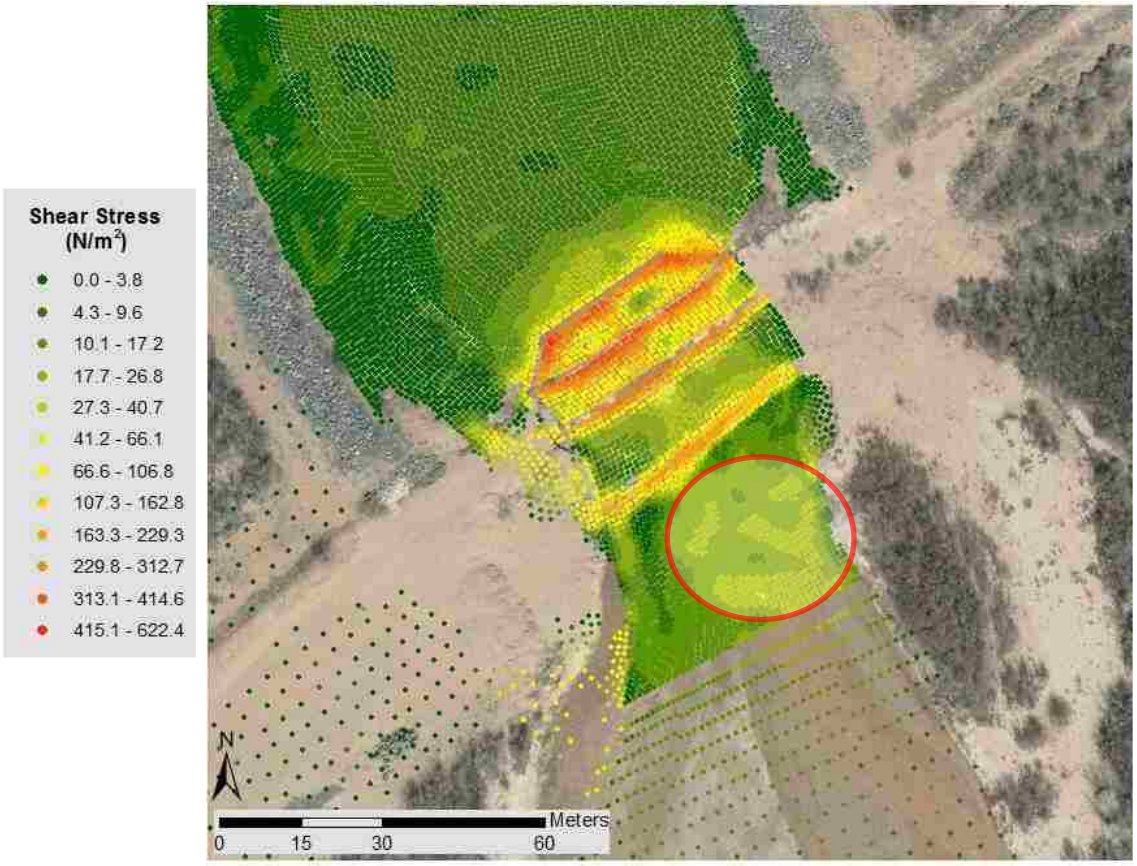

Figure 26: Shear stress results near the Jemez Weir for 28.3 m^3/s modeled discharge

Shields parameter is a dimensionless value often used to represent the boundary between static conditions and incipient motion for a specified particle size (Garcia, 2008).To obtain the particle size both Shields Parameter and Shields Rouse Parameter equations need to be solved iteratively until a common solution for Shield's parameter is acquired (Guo, 2002; Shields, 1936):

$$\tau_{*1} = \frac{\tau_c}{Rgd}$$

$$\tau_{*2} = \frac{0.23}{d^*} + 0.054\left[1 - e^{\left(\frac{-d^{*0.85}}{23}\right)}\right]$$

$$d^* = \frac{d}{1000}\left[\frac{Rg}{\nu}\right]^{1/3}$$

where τ_c is the critical bed shear stress, R is the submerged specific gravity of the sediment, g is gravity, d is sediment diameter in mm, ν is the fluid kinematic viscosity, τ_{*1} and τ_{*2} are Shields parameter as developed by A. Shields and J. Guo, respectively. Although both equations are empirically derived, Shields expresses the parameter as a function of critical shear stress whereas Guo expresses the parameter as a function of sediment diameter.

Using R = 1.65 and τ_c = 40.7 N/m^2 results in a common Shields parameter of 0.034 and a particle diameter of 73.45 mm. Work done by Gessler (1970) and Neill & Yalin (1969) recommend multiplying the Shields parameter by a factor of two when applying the Shields parameter to coarse particles used for engineering purposes. Multiplying the Shields parameter by two effectively doubles the sediment diameter resulting in a particle diameter of 147 mm. The 147 mm particle size calculated using the Shields Parameter compares well with the 15 cm cobble estimated using the maximum permissible velocity method. However, impact scour is also neglected when using the Shields Parameter to describe particle motion.

Discussion

SRH-2D, a two-dimensional fixed bed model, was utilized to model detailed hydraulics for a 2.5 kilometer stretch of the Jemez River near the Jemez Weir. The objective of the model was to describe in detail Jemez River hydraulics near the Jemez Weir. Secondary objectives were as follows: increase understanding of flow distribution patterns between main channel and floodplain, compare hydraulic results to a HEC-RAS

model, compare flow patterns to physical model, and evaluate shear stress and velocity distributions downstream of the Jemez Weir. During model development Aquaveo's SMS program was used to create four meshes to represent the Jemez Weir. The mesh used to obtain research results was created from original LiDAR data with alterations to represent the individual weir steps. Initial modeling with the final mesh revealed a low point in the right channel bank that allowed flow to traverse from the main channel to the right overbank.

Two-dimensional fixed bed model results were different from HEC-RAS as a result of the identified low point in the right channel bank. As previously discussed, the small scale details would have little to no effect on the reach scale bed change due to floodplain flow re-entry points approximately 120 m and 270 m (400 and 880 ft.) downstream of the Jemez Weir. However, when considering the study area of the physical model, the physical model data results were obtained using a higher discharge rate for the Jemez Weir. SRH-2D provided more detail regarding floodplain and main channel interaction around the Jemez Weir, including points of flow exit from, and re-entry to the main channel. The two-dimensional model also quantified shear stresses immediately downstream of the weir structure, and results were used to make design recommendations using both Shield's Parameter and the Maximum Permissible Velocity method.

UNM's physical model provided insights into counter measure effectiveness and successfully demonstrated failure of the cobble and large riprap extensions. The two-dimensional fixed bed model was unable to provide insight regarding counter measure effectiveness. The USACE's HEC-RAS model was essential in defining boundary

conditions for both the physical and two-dimensional fixed bed model. The long term bed change for the reach downstream of the Jemez Weir was successfully evaluated using HEC-RAS.

Conclusion

The HEC-RAS one-dimensional numerical model was essential in evaluating the long term bed change of the reach downstream of the Jemez Weir. Understanding bed adjustments at this scope allows for proper mitigation measures at the Jemez Weir to address the predicted changes in reach scale bed degradation. Flow data from the one-dimensional model was critical in the development of the physical model to define the modeled flow rate, and in the development of the two-dimensional numerical model to define the downstream boundary condition. Drawbacks of the one-dimensional model became apparent when the two-dimensional model results showed a low point in the main channel, which affected flow distribution between the main channel and floodplains. One-dimensional models require many assumptions including the accurate representation of a river using selected cross section data, and neglecting of some orthogonal and vertical velocity components.

UNM's physical model was successful in demonstrating failure of the cobble and large riprap extensions, and evaluating counter measure effectiveness. However, measured scour results from the physical model do not translate to the prototype due to similitude issues. Froude similitude ensures the ratio of inertial forces to gravitational forces is similar between the model and prototype. Reynolds number similitude ensures the ratio of inertial forces to viscous forces is similar between the model and prototype

(Munson, Young, Okiishi, & Huebsch, 2009). When modeling a mobile bed, viscous forces are present and must be accounted for through the use of a distorted model. Distorted physical models ensure Froude similitude criteria are met, while adjusting the model slope, sediment size, and sediment properties to also achieve Reynolds number similitude (Ho, 2006).

Utilizing a two-dimensional fixed bed numerical model was effective in describing flow distribution between the main channel and floodplains, identifying points of flow re-entry from the floodplains, and quantifying shear stresses and velocities around the Jemez Weir. However, modeling the same reach, approximately two kilometers in length, would take significantly longer and require precise sediment boundary conditions for a mobile bed model. Therefore, using a one-dimensional numerical sediment transport model is more efficient for the five kilometer reach downstream of the weir. The two-dimensional fixed bed numerical model also lacks the ability to test counter measures, which could only be represented through a change in the surface Manning's roughness coefficient.

The results of this study can inform hydraulic modeling studies in similar settings because of the different modeling techniques employed to address specific questions. Through the three different modeling approaches employed to define Jemez Weir hydraulics, researchers are provided with a range of tools that can be utilized to obtain specific results. Therefore, future case studies can use this study's results to guide modeling technique and help formulate a research method to answer a specific question.

References

Akan, A. O. (2006). *Open Channel Hydraulics* (1st ed., pp. 159–163). Burlington, MA: Butterworth-Heinemann.

Aquaveo. (2013). SMS User Manual (v11.1). Retrieved from http://smsdocs.aquaveo.com/SMS_User_Manual_v11.1.pdf

Bormann, N. E., & Julien, P. Y. (1991). Scour Downstream of Grade-Control Structures. *Journal of Hydraulic Engineering*, *117*(5), 579–594. doi:10.1061/(ASCE)0733-9429(1991)117:5(579)

Chow, V. Te. (1959). *Open-Channel Hydraulics*. New York: McGraw-Hill.

Coonrod, J., Saint-Lot, E. K., & Gillihan, T. (2012). *Physical Modeling of Scour Patterns Near the Jemez Weir* (pp. 1–39).

Garcia, M. (Ed.). (2008). *Sedimentation Engineering (Manual 110) Processes, Measurements, Modeling, and Practice* (110th ed., pp. 44–55).

Gessler, J. (1970). Self-Stabilizing Tendencies of Sediment Mixtures with Large Range of Grain Sizes. *Journal of Waterway and Harbor Division, ASCE*, *96*(2), 235–249.

Guo, J. (2002). Hunter Rouse and Shields Diagram. In *Proceeding Proc., 13th IAHR-APD, Advances in Hydraulics and Water Engineering* (pp. 1096–1098). Singapore, Vol 2.

Ho, J. (2006). *Hydraulic Modeling Study To Determine Diversion Structure Impacts: Rio Grande At Albuquerque, New Mexico / by Jungseok Ho* (pp. 27–40).

Hoffmans, G. J. C. M., & Pilarczyk, K. W. (1995). Local Scour Downstream of Hydraulic Structures. *Journal of Hydraulic Engineering*, *121*(4), 326–340. doi:10.1061/(ASCE)0733-9429(1995)121:4(326)

Hydrologic Engineering Center. (2010). *HEC-RAS 4.1 Hydraulic Reference Manual* (pp. 18–35). Davis, California.

Jemez Watershed Group. (2005). *Jemez Watershed Restoration Action Strategy (WRAS)* (pp. 2–9).

Lai, Y. (2008). SRH-2D version 2: Theory and User's Manual. *Sedimentation and River Hydraulics–Two-Dimensional …*. Denver, CO: US Bureau of Reclamation, Technical Service Center.

Laursen, E. M., & Flick, M. W. (1983). *Scour at Sill Structures*.

Lim, S.-Y. (1992). Discussion of " Scour Downstream of Grade Control Structures " by Noel E. Borman and Pierre Y. Julien (May, 1991, Vol. 117, No. 5). *Journal of Hydraulic Engineering*, *118*(7), 1070–1072. doi:10.1061/(ASCE)0733-9429(1992)118:7(1070.2)

Little, C. (2007). *Effective Discharge Analysis, Jemez Canyon Dam Sediment Bypass*.

Lv, X., Zou, Q., & Reeve, D. (2011). Numerical Simulation of Overflow at Vertical Weirs Using a Hybrid Level Set/VOF Method. *Advances in Water Resources*, *34*(10), 1320–1334. doi:10.1016/j.advwatres.2011.06.009

Maynord, S. T., Floyd, I. E., Heath, R. E., & Little, C. D. (2012). *Channel Degradation Downstream of Jemez Weir, Jemez River, New Mexico* (pp. 1–119).

Munson, B. R., Young, D. F., Okiishi, T. H., & Huebsch, W. W. (2009). *Fundamentals of Fluid Mechanics*. *Fundamentals of Fluid Mechanics* (Sixth., pp. 346–350). Don Fowley.

Neill, C. R., & Yalin, M. S. (1969). Qualitative Definition of Beginning of Bed Movement. *Journal of the Hydraulics Division, ASCE*, *95*(1), 585–587.

Piotrowski, J. A. (2010). *Development of a High-Resolution Two-Dinmensional Urban/Rural Flood Simulation*. University of Iowa. Retrieved from http://ir.uiowa.edu/etd/574

Savage, B. M., & Johnson, M. C. (2001). Flow Over Ogee Spillway: Physical and Numerical Model Case Study. *Journal of Hydraulic Engineering*, *127*(8), 640–649. doi:10.1061/(ASCE)0733-9429(2001)127:8(640)

Shields, A. (1936). Anwendung der Aehnlichkeitsmechanik und der Turbulenzforschung auf die Geschiebebewegung. *Mitt Preuss Versuchsanstalt fur Wasserbau und Schiffbau*, *26*.

U.S. Geological Survey. (2013). *Water Resources Data for the United States, Water Year 2012: Geological Survey Water-Data Report WDR-US-2012, Site 08324000* (pp. 1–3). Retrieved from http://wdr.water.usgs.gov/wy2012/pdfs/08324000.2012.pdf

United States Army Corps of Engineers. (1994). Engineering and Design - Hydraulic Design of Flood Control Channels. In *Engineering and Design*. United States Army Corps of Engineers.

Appendices

Appendix A: Mesh and SRH-2D Model Development

ArcGIS

1. 9 post processed LiDAR datasets and one ecw file provided by the Army Corps of Engineers
2. LiDAR DEM's were all opened together
3. Mosaic tool in ArcGIS under the Raster Dataset folder was used to create one dataset with all of the LiDAR points named *lidarraster*
4. SMS would not import a raster DEM dataset (lidarr*aster*)
5. An attempt was made to convert the raster dataset into an ASCII file (lidarascii) and imported but again SMS rejected the file
6. The newly mosaicked dataset was converted into floating points utilizing the ArcGIS Raster to Float tool in the From Raster folder under Conversion Tools, the new file was named *lidarfloat*

SMS Mesh Generation Procedure

1. Floating points file (*lidarfloat*.hdr) was opened in SMS
    a. Choose the scatter dataset option
2. Upload the ecw file to help create mesh
3. Using the map module create arcs which delineate areas of interest (i.e. banks, main channel, vegetation)
4. Under the Feature Objects tab select clean (this ensures all arcs intersect)

5. Select all arcs then choose the Feature Objects tab and then select redistribute vertices. In the spacing option input the desired spacing for vertices (units will be same as project units)
6. To create more dense polygons in areas of concern, arcs surrounding the area of interest can be selected and vertex spacing redefined to create more vertices and finer grid sizes
    a. Spacing of 15 feet used for all areas outside the area of interest
    b. Spacing of 3.3 feet (~ 1 meter) used for area of interest
7. In the Project Explorer window right click the default coverage and change the type to generic 2D mesh
8. Select all arcs and under the Feature Objects tab select build polygons
9. Under the Edit tab select Materials Data and add the names of materials needed for the mesh
10. Select each polygon and assign the appropriate mesh type, bathymetry type, and material; then preview the mesh for each polygon to ensure a stable mesh is created
    a. Main channel mesh was patched (quadrilateral grids created), used scatter set for bathymetry type and method of interpolation and extrapolation used inverse distance weighted method
    b. Banks, dykes, and vegetation were all paved (triangular grids created), used scatter set for bathymetry type and method of interpolation and extrapolation used inverse distance weighted method
11. SMS uses the equation to interpolate points for mesh creation:

$$w_i = \frac{\left[\frac{R - h_i}{R h_i}\right]^2}{\sum_{j=1}^{n}\left[\frac{R - h_j}{R h_j}\right]^2}$$

Where h_i is the distance from the interpolation point to scatter point i, R is the distance from the interpolation point to the most distant scatter point, and n is the total number of scatter points.

12. Select all polygons once all materials, bathymetry, and mesh types have been assigned to each polygon and under the Feature Objects tab select the Map->2D Mesh option to create your mesh then select the linear option
13. In the Mesh Module click on create nodestrings option and begin to create nodestrings for inlet and exit boundary conditions as well as internal monitoring nodestrings. These will be used by SRH-2D to assign inlet and outlet boundary conditions and to store model run data for the monitor lines (internal monitoring nodestrings)

SRH-2D

1. Download SRH-2D v2.2 from the United States Bureau of Reclamation website
2. Copy the batch files (both the preprocessor and processor) into the folder where the SMS file is saved and edit the path for the batch file to find the SRH-2D executable
3. Run the srhpre (partial interface mode was used for all simulations) batch file and use the SRH-2D manual v.2.0 Chapter 4 for direction inputting commands in the partial interface mode
4. Once preprocessor opens up enter 2 for Part-Interface, 1 for Interactive, a CASE NAME and Simulation Description

8000 CFS Trial Run 1 Input Commands

1. FLOW
2. 4
3. 1535752.3 1605832.02 1539065.77 1603324.67 1539129.16 1603212.3 1540515.99 1602008.18
4. STEADY
5. 0.0 10 8
6. PARA
7. 0.7
8. DRY
9. FOOT
10. Mesh.2dm sms
11. 2
12. 6
13. 0.030
14. 0.060
15. 0.050
16. 0.035
17. 0.050
18. 0.040
19. 0
20. INLET-Q
21. 8000 EN

22. EXIT-H
23. 5183.4 EN (based on rectangular channel with 0.23% slope, 8000 cfs, 0.032 manning's n, and bottom width 315 ft RESULT y = 4.36 ft rounded to 4.5 ft and added to bottom minimum elevation of 5178.86 ft)
24. MONITOR
25. MONITOR
26. MONITOR
27. MONITOR
28. MONITOR
29. (Leave blank by pressing Enter)
30. XMDF EN
31. (Select default by pressing Enter)
32. 1 (Successful message displayed)

5. After the preprocessor runs select the srh2d batch file and enter the name of your data file (CASE NAME) and press enter
6. Use SMS to upload the model outputs and perform data analysis/ interpretation by opening your original mesh file and the opening the CASENAME_XMDF.h5 file

SRH-2D Trial Run 1 Results

1. Model results look good and outflow boundary conditions are similar to results from HEC-RAS river station 13826.617 trial run with 8000 cfs
    a. Average water surface elevation at the most downstream monitor line for trial 1 was ~5184.5 ft compared to the HEC-RAS value of 5184 which was located near the downstream boundary of the mesh

b. These values are relatively close and it was determined the downstream boundary condition set in the pre-processor was representative of prototype conditions

2. Floodplain boundary for Mesh #1 did not encompass enough area to model prototype conditions
    a. Current mesh will be modified to encompass prototype floodplain
3. The proper steps to expand existing mesh were taken in SMS using the procedures listed in the SMS Mesh Generation Procedure section
    a. Generating a mesh using the inverse distance weighted scheme for scatter interpolation was computationally challenging for the computer and resulted in abnormal wait times (approximately 48 hours for less than 1/4 of the mesh)
        i. Meshed area was 0.161 percent of total area
    b. SMS representatives advised utilizing the linear interpolation scheme for the new mesh
    c. For consistency the first mesh bathymetry was changed to linear interpolation and SRH-2D was launched using the same input commands as for Trial Run 1 and re-named the output files to Trial Run 3
4. After the mesh was adjusted the same input commands used in the 8000 CFS Trial 1 Input Commands section were used within the pre-processor commands to create a new data file named 8000 CFS Trial 2

8000 CFS Trial Run 2 Input Commands

1. FLOW

2. 4
3. 1535752.3 1605832.02 1539065.77 1603324.67 1539129.16 1603212.3 1540515.99 1602008.18
4. STEADY
5. 0.0 10 12
6. PARA
7. 0.7
8. DRY
9. FOOT
10. Mesh5.2dm sms
11. 2
12. 6
13. 0.030
14. 0.060
15. 0.050
16. 0.035
17. 0.050
18. 0.040
19. 0
20. INLET-Q
21. 8000 EN
22. EXIT-H

23. 5183.4 EN (based on rectangular channel with 0.23% slope, 8000 cfs, 0.032 manning's n, and bottom width 315 ft RESULT y = 4.36 ft rounded to 4.5 ft and added to bottom minimum elevation of 5178.86 ft)
24. MONITOR
25. MONITOR
26. MONITOR
27. MONITOR
28. MONITOR
29. (Leave blank by pressing Enter)
30. XMDF EN
31. (Select default by pressing Enter)
32. 1 (Successful message displayed)

SRH-2D Trial Run 2 Results

1. Model results look good and outflow boundary conditions are similar to results from HEC-RAS river station 13826.617 trial run with 8000 cfs
    a. Average water surface elevation at the most downstream monitor line for trial 2 was ~5183.5 ft compared to the HEC-RAS value of 5184 which was located near the downstream boundary of the mesh
    b. These values are relatively close and it was determined the downstream boundary condition set in the pre-processor was representative of prototype conditions
2. Floodplain boundary for MESH #5 did encompass enough area to model prototype conditions

Modeling Decisions

- After modeling Mesh5 for 200 hours (7 CPU hours) it was determined the model reached equilibrium after 60 hours (if linear with CPU hours 1.75 hours)

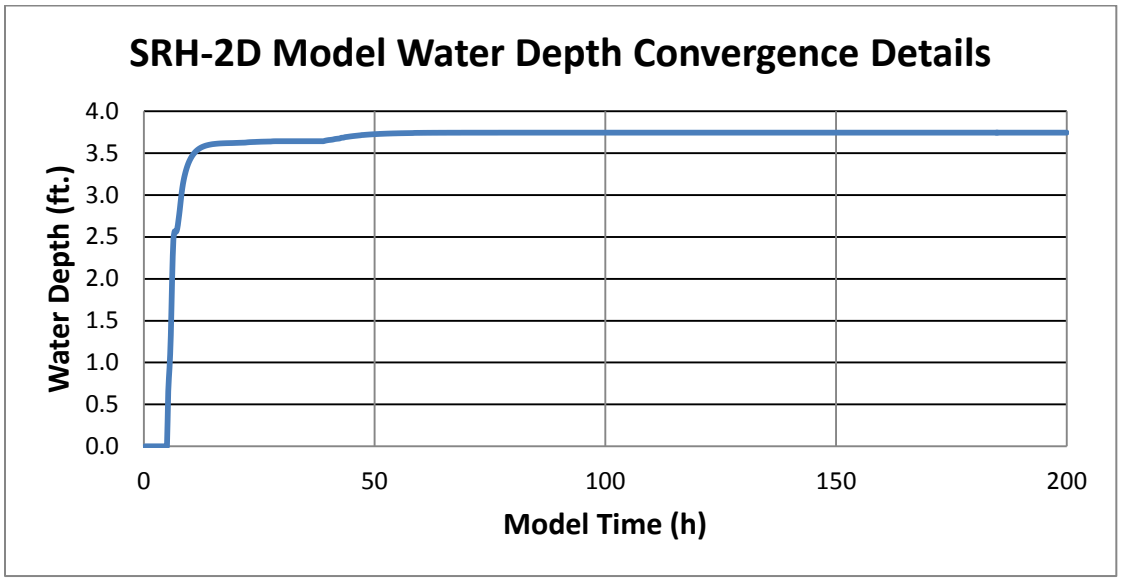

Figure 27: SRH-2D water depth convergence graph

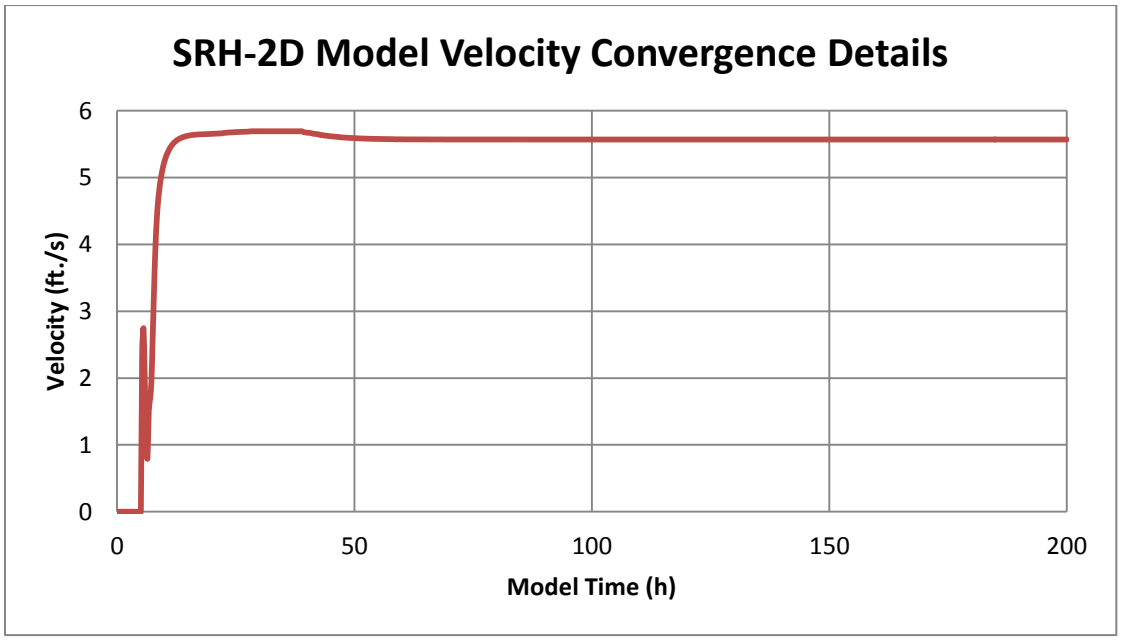

Figure 28: SRH-2D velocity convergence graph

- HEC-RAS will be utilized to populate downstream boundary conditions for future SRH-2D runs

Table 5: Downstream boundary conditions from HEC-RAS

Modeled Discharge (m^3/s)	Downstream Water Surface Elevation (m)	Modeled Discharge (ft^3/s)	Downstream Water Surface Elevation (ft.)
1.42	1578.48	50	5178.74
2.83	1578.51	100	5178.85
5.66	1578.57	200	5179.03
8.50	1578.62	300	5179.19
11.33	1578.68	400	5179.38
14.16	1578.73	500	5179.57
16.99	1578.78	600	5179.74
19.82	1578.78	700	5179.73
22.65	1578.91	800	5180.14
25.49	1578.96	900	5180.33
28.32	1579.04	1000	5180.57
42.48	1579.25	1500	5181.28
56.63	1579.38	2000	5181.70
70.79	1579.48	2500	5182.03
84.95	1579.57	3000	5182.31
113.27	1579.71	4000	5182.76
141.58	1579.82	5000	5183.13
169.90	1579.92	6000	5183.47
198.22	1580.01	7000	5183.77
226.53	1580.09	8000	5184.03

- To obtain weir discharge coefficient the following discharge were ran in SRH-2D
    - 50-1000 cfs with 100 cfs increments
    - 1000-3000 cfs with 500 cfs increments
    - 3000-8000 cfs using 1000 cfs increments

The program did not converge when river discharge was less than 5.7 m^3/s (200 ft^3/s) in the Jemez River. This was thought to be due to inaccurate exit boundary water surface elevations from the HEC-RAS model, program code instability at low flow rates, or the model time step being too large for the modeling discharge rates. This issue was not resolved, nor further investigated because a sufficient dataset was acquired from modeling the remaining discharge rates.

Jemez Weir Mesh Comparison

Four meshes created

- Lidar without sloped weir crest profile
- Lidar with sloped weir crest profile
- Hard Steps without sloped weir crest profile
- Hard Steps with sloped weir crest profile

- After looking at shear stress distributions it was determined the Hard Steps without sloped weir crest profile would be used as the Modeling Mesh
  - Adding the sloped weir crest profile only added minimal inundation area just downstream on the left side of the weir
  - Adding in hard steps created different distributions in shear stresses which more accurately represented prototype conditions

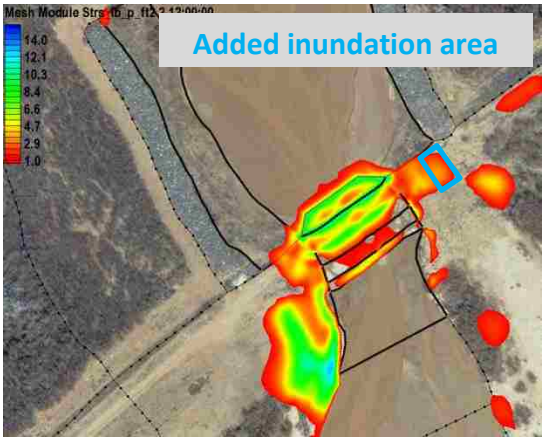

Figure 29: SRH-2D mesh – Hard steps with weir crest

Figure 30: SRH-2D mesh – Hard steps no weir crest

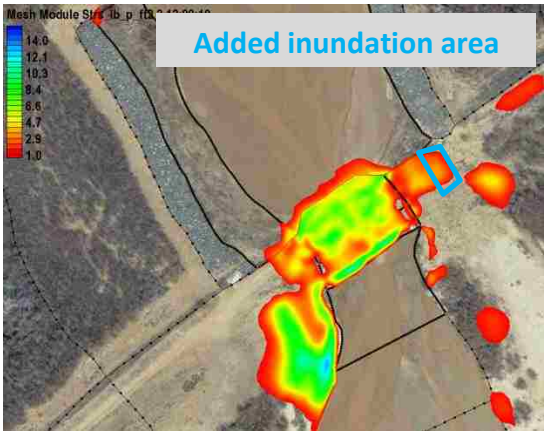

Figure 31: SRH-2D mesh – LiDAR with weir crest

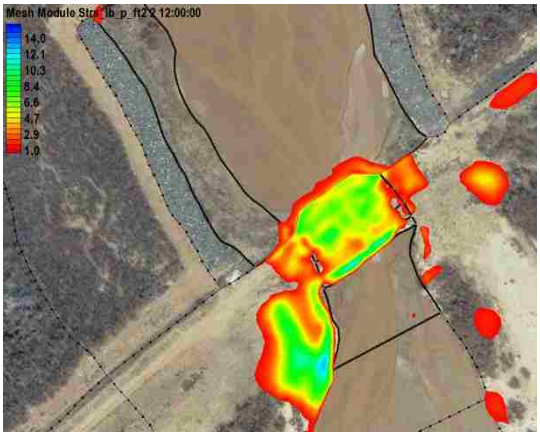

Figure 32: SRH-2D mesh – LiDAR no weir crest

Modeling Inputs for final mesh

1. 2
2. 1
3. 50cfs (Name of model run)
4. (Description of run)
5. FLOW
6. 2
7. 1535752.3 1605832.02 1540515.99 1602008.18

8. STEADY
9. 0 10 60
10. PARA
11. 0.7
12. DRY
13. FOOT
14. Mesh9.2dm sms
15. 2
16. 6
17. 0.030
18. 0.060
19. 0.050
20. 0.035
21. 0.050
22. 0.040
23. 0
24. INLET-Q
25. 50 EN (Varies depending on flow rate modeled)
26. EXIT-H
27. 5178.74 EN (Varies depending on flow rate modeled)
28. MONITOR
29. MONITOR
30. MONITOR

31. MONITOR
32. MONITOR
33. MONITOR
34. MONITOR
35. MONITOR
36. MONITOR
37. MONITOR
38. MONITOR
39. MONITOR
40. MONITOR
41. MONITOR
42. (Leave blank by pressing Enter)
43. SRHN EN
44. (Select default by pressing Enter)
45. 1 (Successful message displayed)

- For each run the same SIF file generated was used with only 2 changes*
    - Changing the discharge (INLET-Q) and the exit boundary water surface elevation (EXIT-H) according to the next run
    - Two meshes were created and used in final runs:
        1. Mesh9 was used for all flows $\geq$ 2000 ft^3/s
            - Had a wider distribution of flow across upstream inlet
        2. Mesh10 was used for all flows $\leq$ 1500 ft^3/s

        - Limited distribution of flow to within channel banks across upstream inlet

- Manning's n sensitivity test
    - Main channel – increase and decrease manning's n by 0.01
        1. Chose 1000 cfs because more than 50% of flow remained within the channel banks at all main channel monitoring lines
    - Floodplains – increase and decrease manning's n by 0.01
        1. Chose 2500 cfs because more than 50% of discharge was distributed over left and right overbanks at all main channel monitoring lines

LiDAR Data Details

To develop accurate cross-sectional data for HEC-RAS the United States Army Corps of Engineers (USACE) collected one meter LiDAR data of the Jemez River. This data was collected on March 13th, 2010 with a mean daily discharge of 0.39 m^3/s (14 ft^3/s) in the channel (Maynord et al., 2012). The low discharge covered only a small percentage of the main channel which allowed for accurate representation of the river bed as well as the channel floodplains. Post data collection the USACE noticed the LiDAR data resulted in sloped bank faces where channel banks were in fact vertical. This inaccuracy was considered acceptable because only a small portion of the channel area was affected and channel depths are low (Maynord et al., 2012).

Appendix B: Modeling Results

Sensitivity Analysis Results

The following figures represent shear stress histograms for specified Manning's roughness coefficients near four HEC-RAS cross sections for modeled discharges of 28.3 and 70.8 m^3/s (1000 and 2500 ft^3/s).

28.3 m^3/s Sand Bed n = 0.02

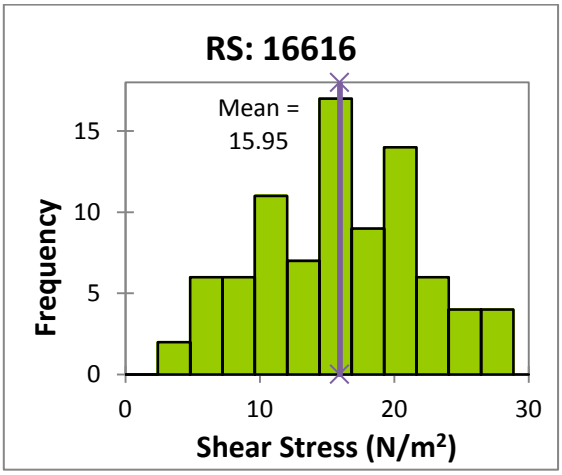

Figure 33: Shear stress histogram at river station: 16616 for 28.3 m^3/s and 0.02 Manning's *n* for the main channel

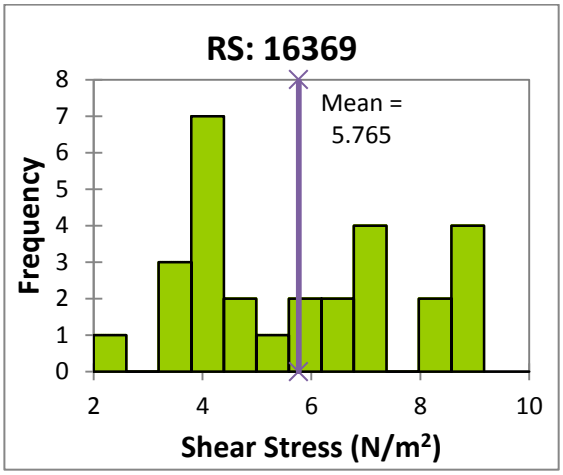

Figure 34: Shear stress histogram at river station: 16369 for 28.3 m^3/s and 0.02 Manning's *n* for the main channel

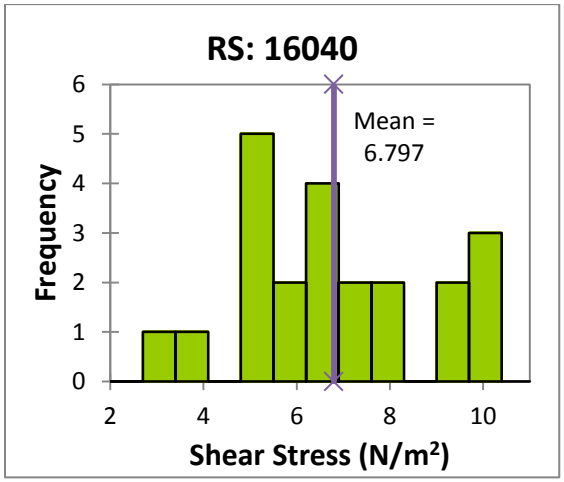

Figure 35: Shear stress histogram at river station: 16040 for 28.3 m^3/s and 0.02 Manning's *n* for the main channel

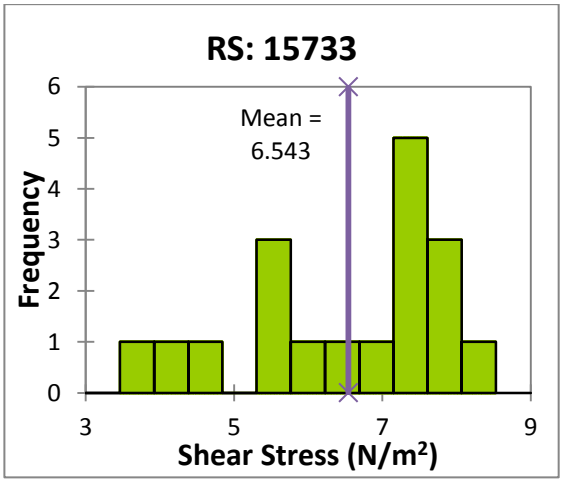

Figure 36: Shear stress histogram at river station: 15733 for 28.3 m^3/s and 0.02 Manning's *n* for the main channel

28.3 m^3/s Sand Bed n = 0.03

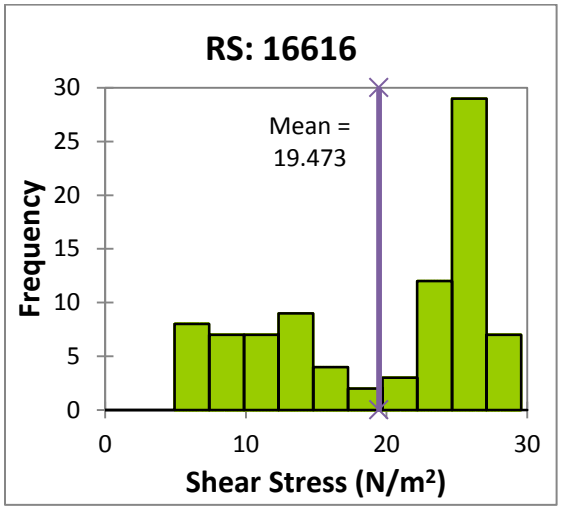

Figure 37: Shear stress histogram at river station: 16616 for 28.3 m^3/s and 0.03 Manning's *n* for the main channel

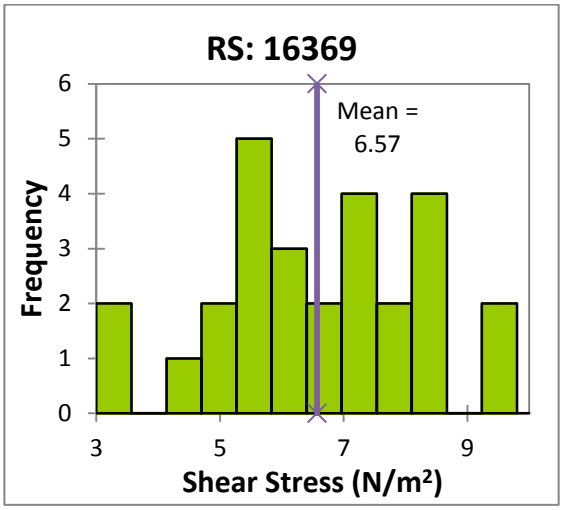

Figure 38: Shear stress histogram at river station: 16369 for 28.3 m^3/s and 0.03 Manning's *n* for the main channel

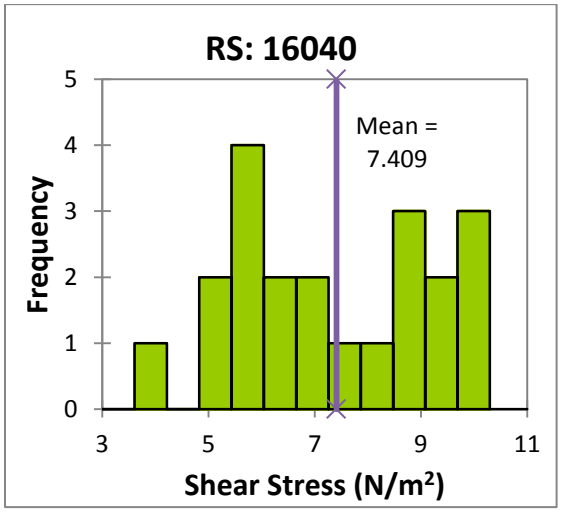

Figure 39: Shear stress histogram at river station: 16040 for 28.3 m^3/s and 0.03 Manning's *n* for the main channel

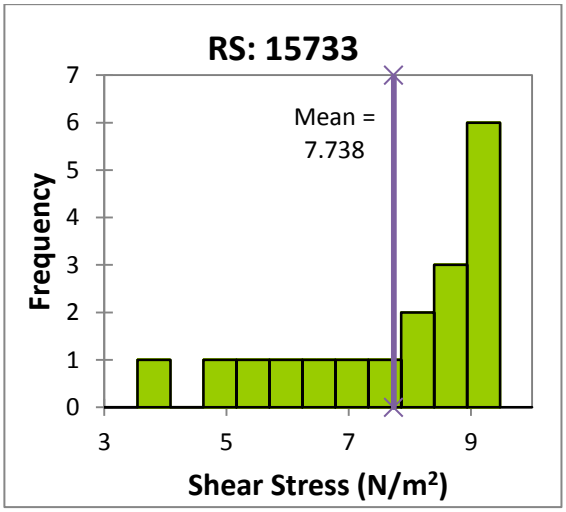

Figure 40: Shear stress histogram at river station: 15733 for 28.3 m^3/s and 0.03 Manning's *n* for the main channel

28.3 m^3/s Sand Bed n = 0.04

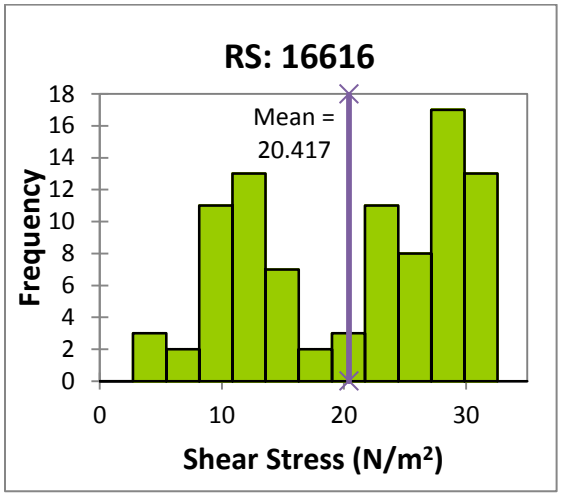

Figure 41: Shear stress histogram at river station: 16616 for 28.3 m^3/s and 0.04 Manning's *n* for the main channel

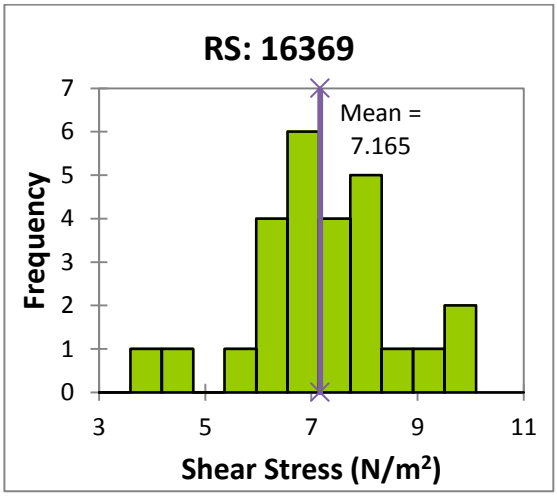

Figure 42: Shear stress histogram at river station: 16369 for 28.3 m^3/s and 0.04 Manning's *n* for the main channel

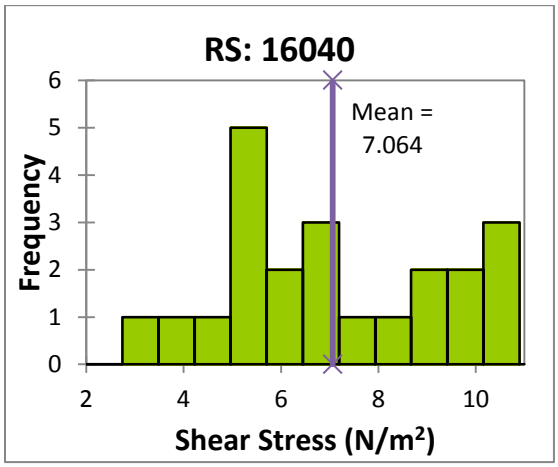

Figure 43: Shear stress histogram at river station: 16040 for 28.3 m^3/s and 0.04 Manning's *n* for the main channel

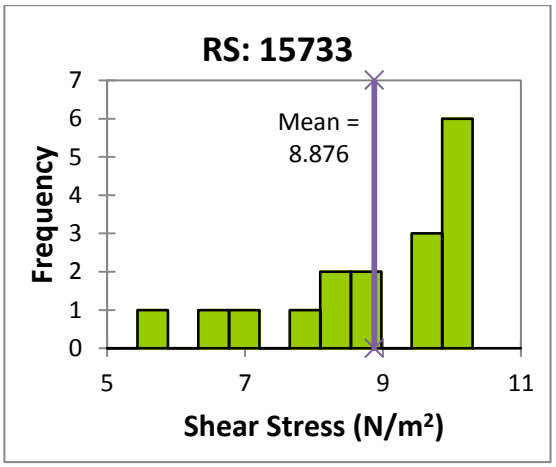

Figure 44: Shear stress histogram at river station: 15733 for 28.3 m^3/s and 0.04 Manning's *n* for the main channel

70.8 m^3/s Vegetation n = 0.05

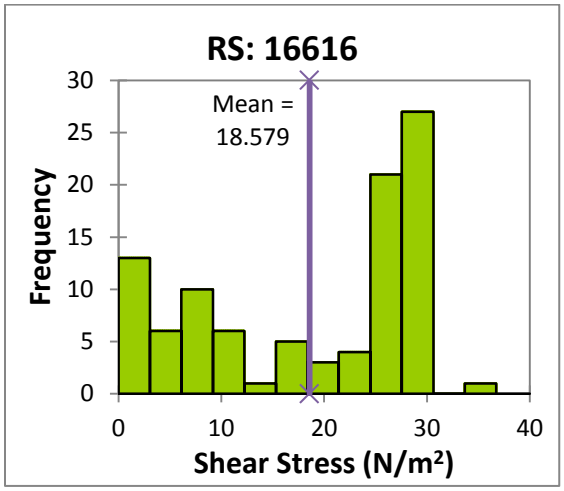

Figure 45: Shear stress histogram at river station: 16616 for 70.8 m^3/s and 0.05 Manning's *n* for the floodplain

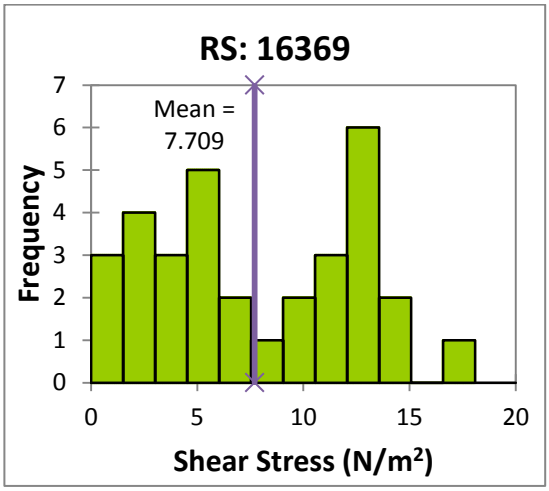

Figure 46: Shear stress histogram at river station: 16369 for 70.8 m^3/s and 0.05 Manning's *n* for the floodplain

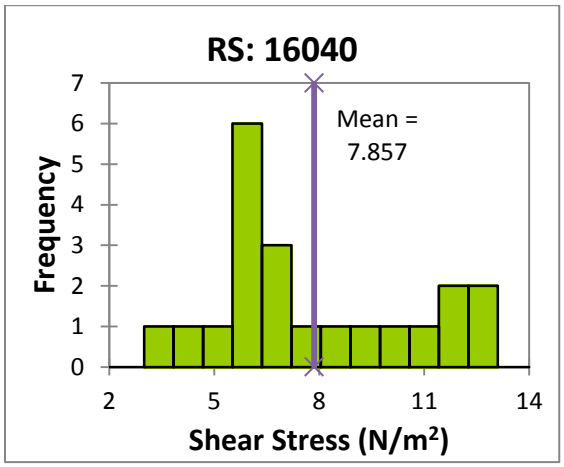

Figure 47: Shear stress histogram at river station: 16040 for 70.8 m^3/s and 0.05 Manning's *n* for the floodplain

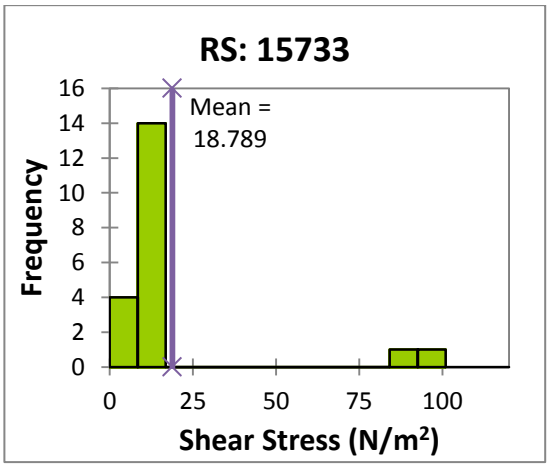

Figure 48: Shear stress histogram at river station: 15733 for 70.8 m^3/s and 0.05 Manning's *n* for the floodplain

70.8 m^3/s Vegetation n = 0.06

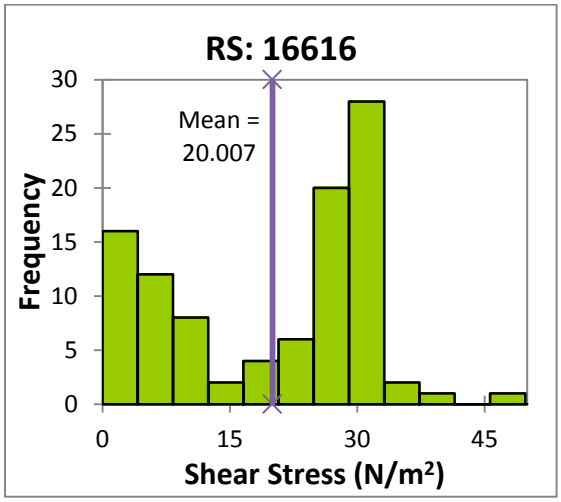

Figure 49: Shear stress histogram at river station: 16616 for 70.8 m^3/s and 0.06 Manning's *n* for the floodplain

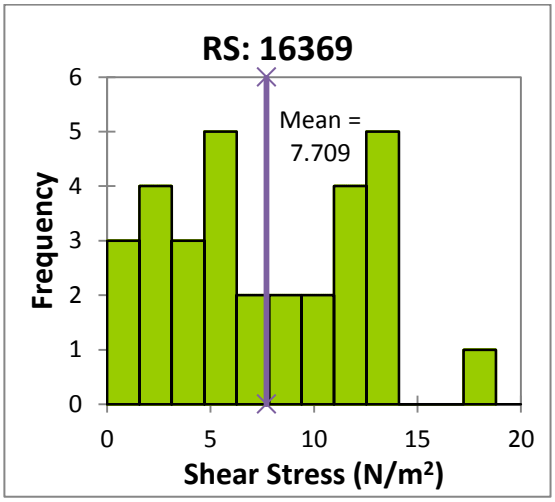

Figure 50: Shear stress histogram at river station: 16369 for 70.8 m^3/s and 0.06 Manning's *n* for the floodplain

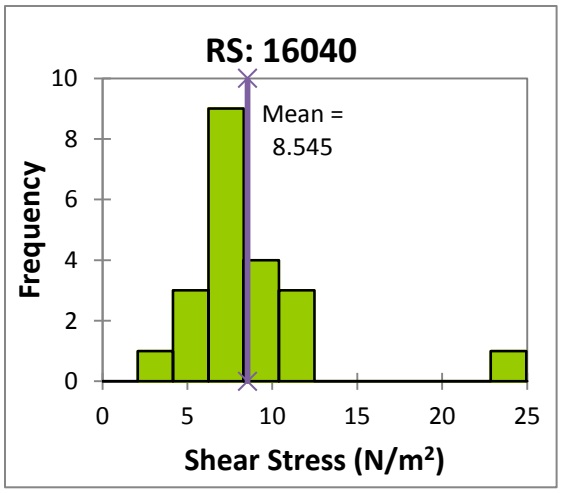

Figure 51: Shear stress histogram at river station: 16040 for 70.8 m^3/s and 0.06 Manning's *n* for the floodplain

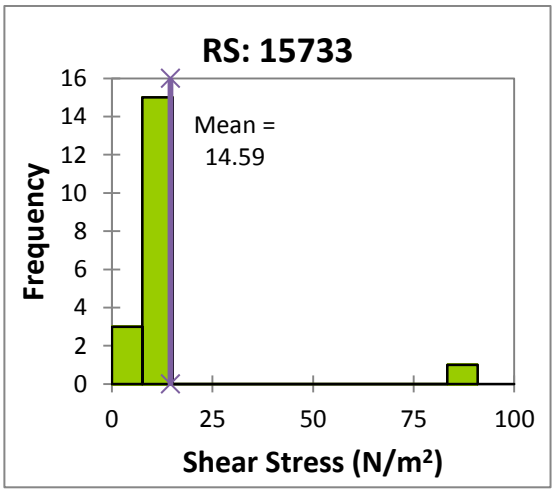

Figure 52: Shear stress histogram at river station: 15733 for 70.8 m^3/s and 0.06 Manning's *n* for the floodplain

70.8 m^3/s Vegetation n = 0.07

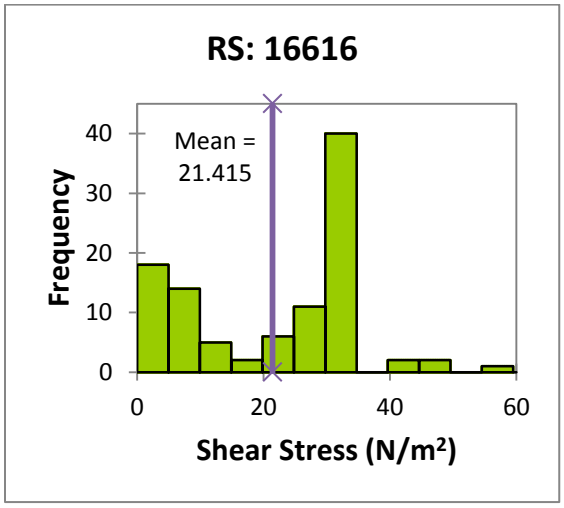

Figure 53: Shear stress histogram at river station: 16616 for 70.8 m^3/s and 0.07 Manning's *n* for the floodplain

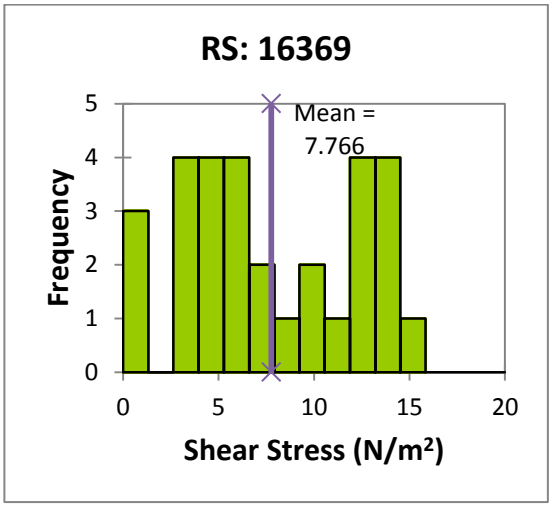

Figure 54: Shear stress histogram at river station: 16369 for 70.8 m^3/s and 0.07 Manning's *n* for the floodplain

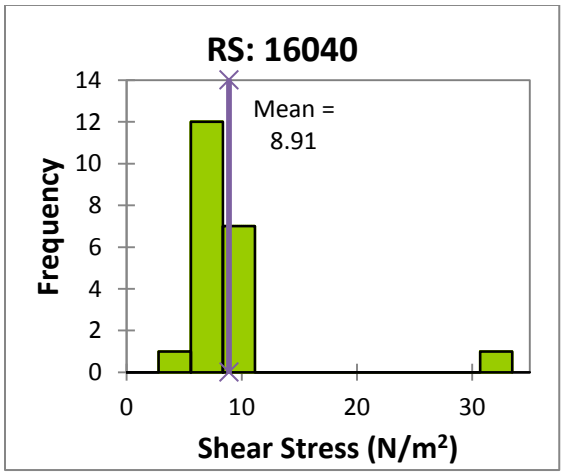

Figure 55: Shear stress histogram at river station: 16040 for 70.8 m^3/s and 0.07 Manning's *n* for the floodplain

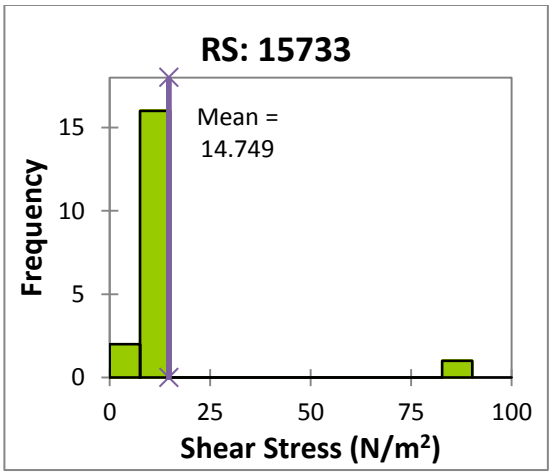

Figure 56: Shear stress histogram at river station: 15733 for 70.8 m^3/s and 0.07 Manning's *n* for the floodplain

Water Depth Results

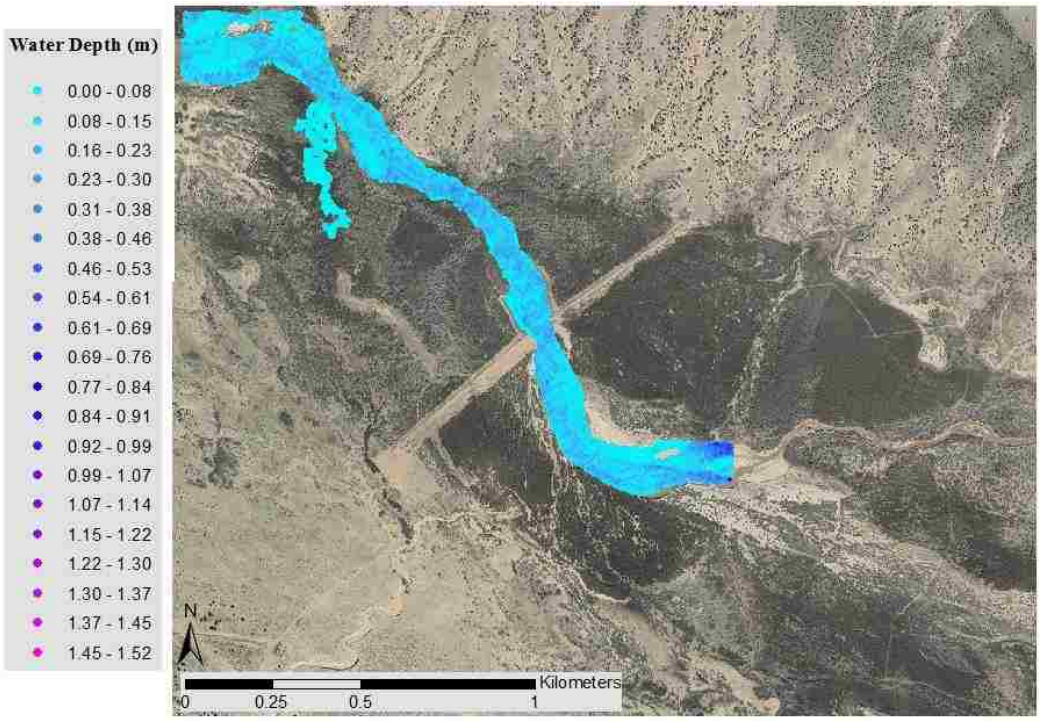

Figure 57: SRH-2D water depth results at 5.7 m^3/s modeled discharge

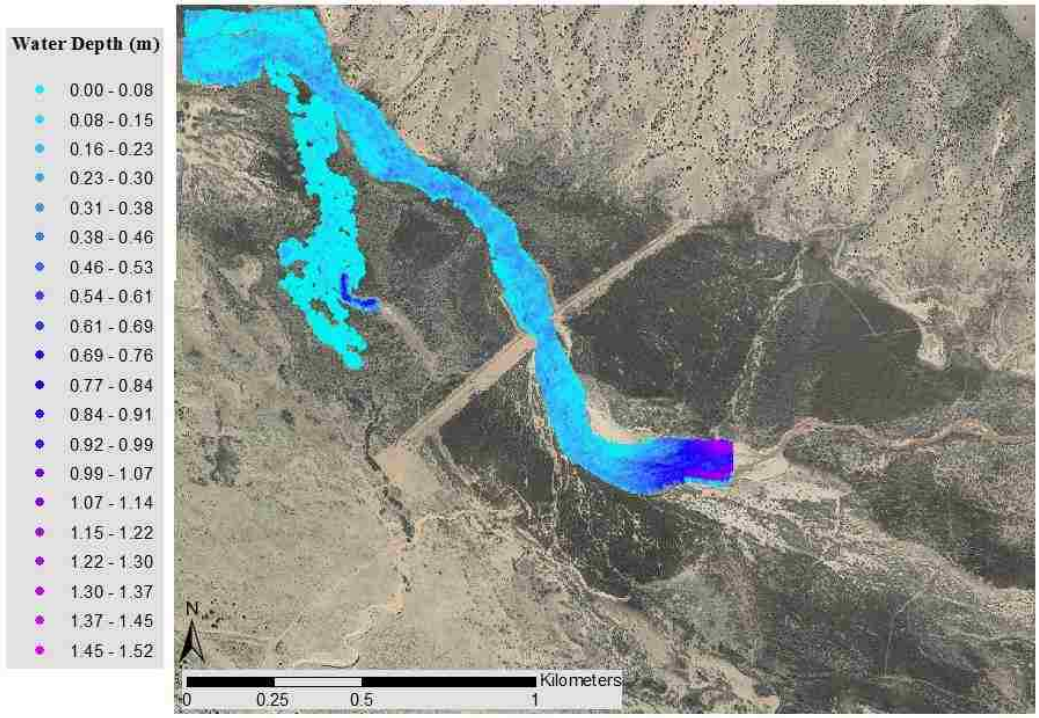

Figure 58: SRH-2D water depth results at 8.5 m^3/s modeled discharge

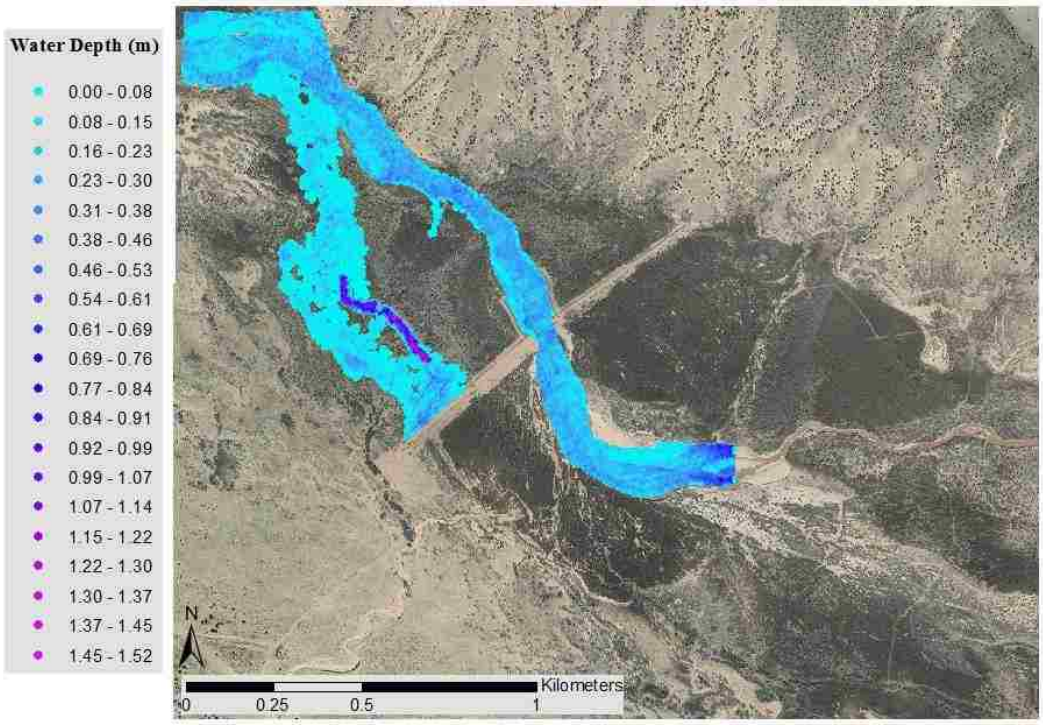

Figure 59: SRH-2D water depth results at 11.3 m^3/s modeled discharge

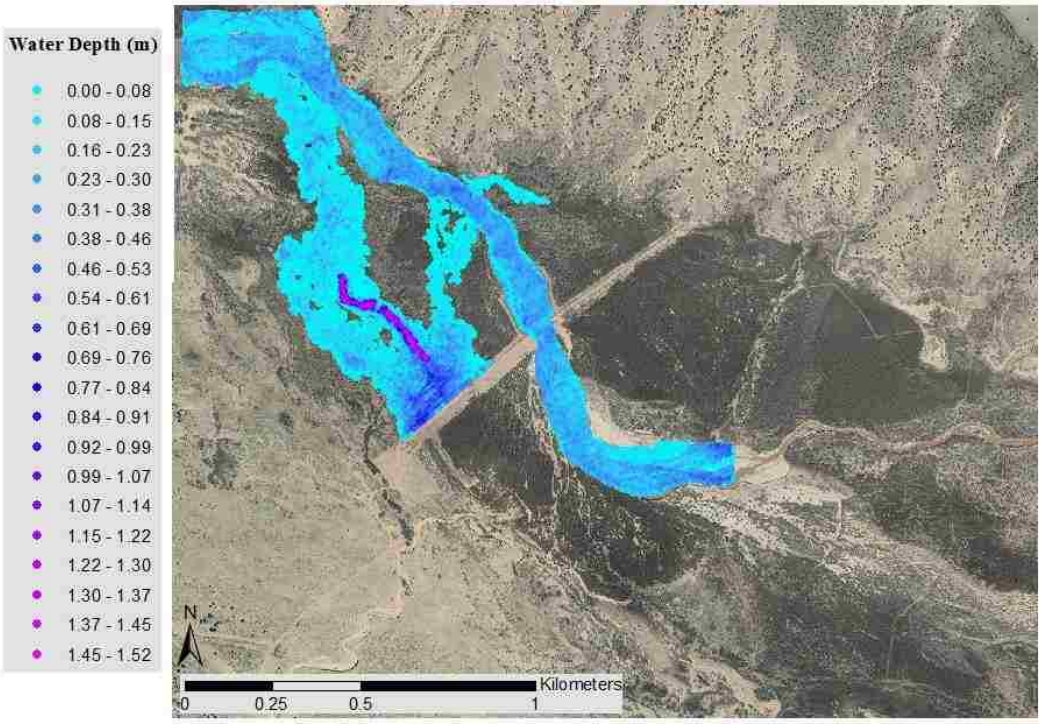

Figure 60: SRH-2D water depth results at 14.2 m^3/s modeled discharge

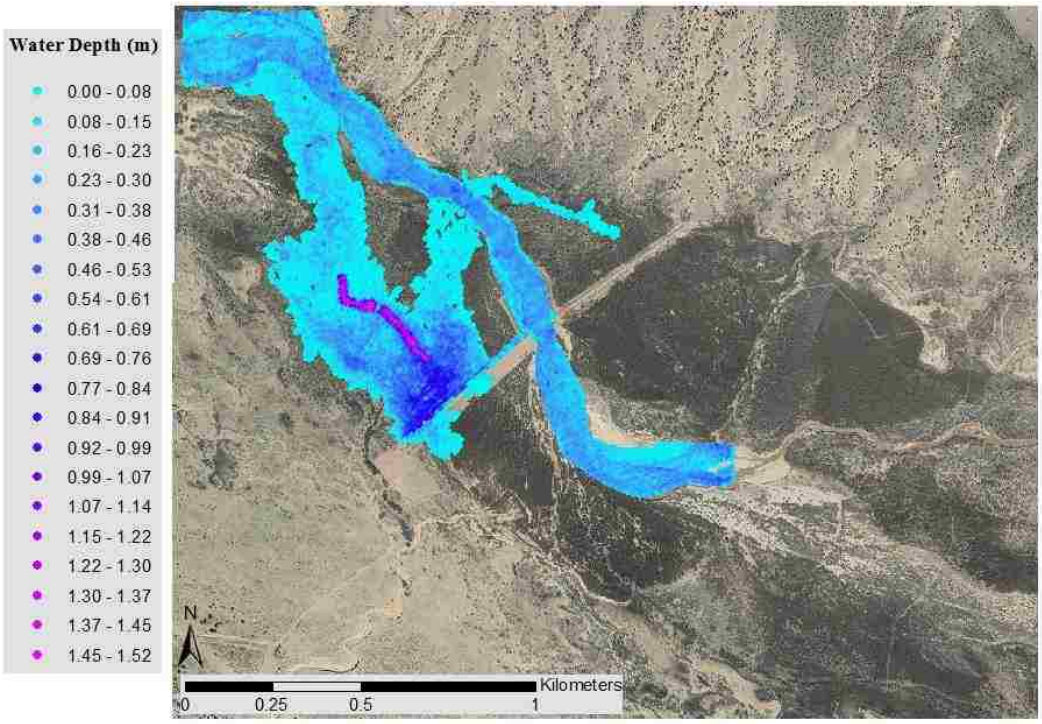

Figure 61: SRH-2D water depth results at 17.0 m^3/s modeled discharge

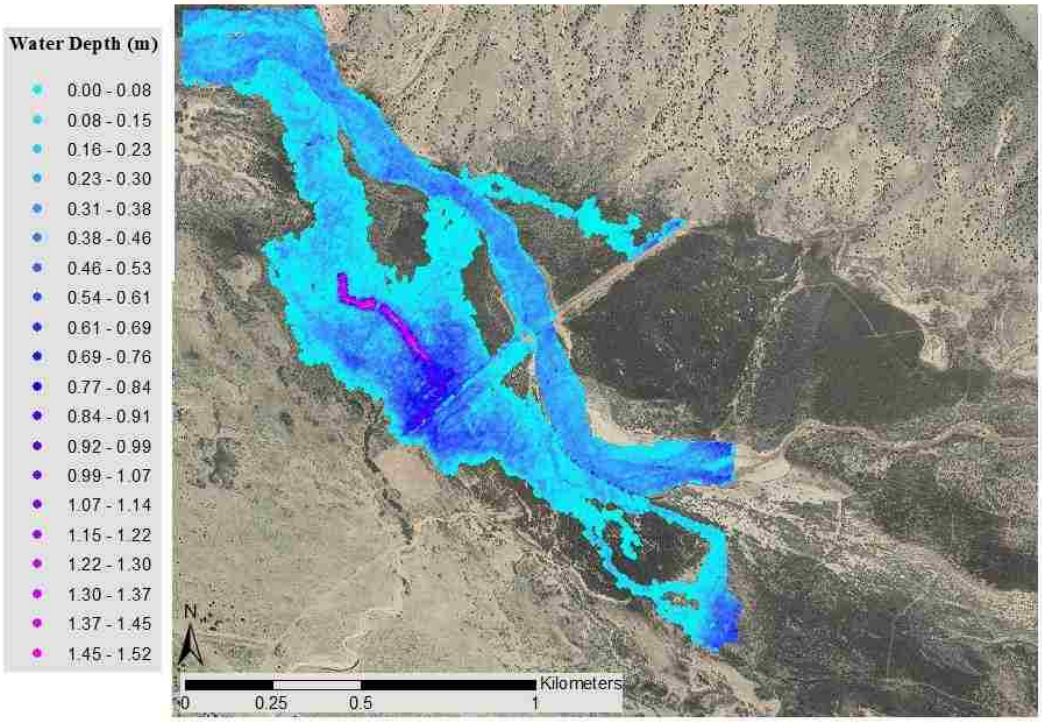

Figure 62: SRH-2D water depth results at 19.8 m^3/s modeled discharge

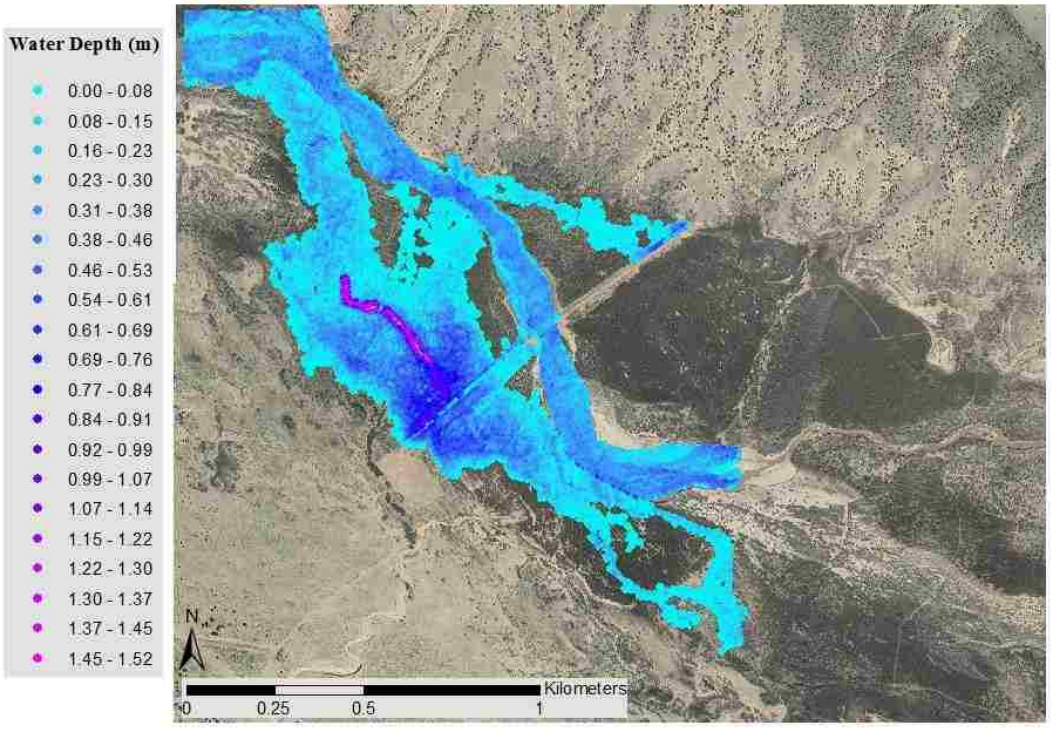

Figure 63: SRH-2D water depth results at 22.7 m^3/s modeled discharge

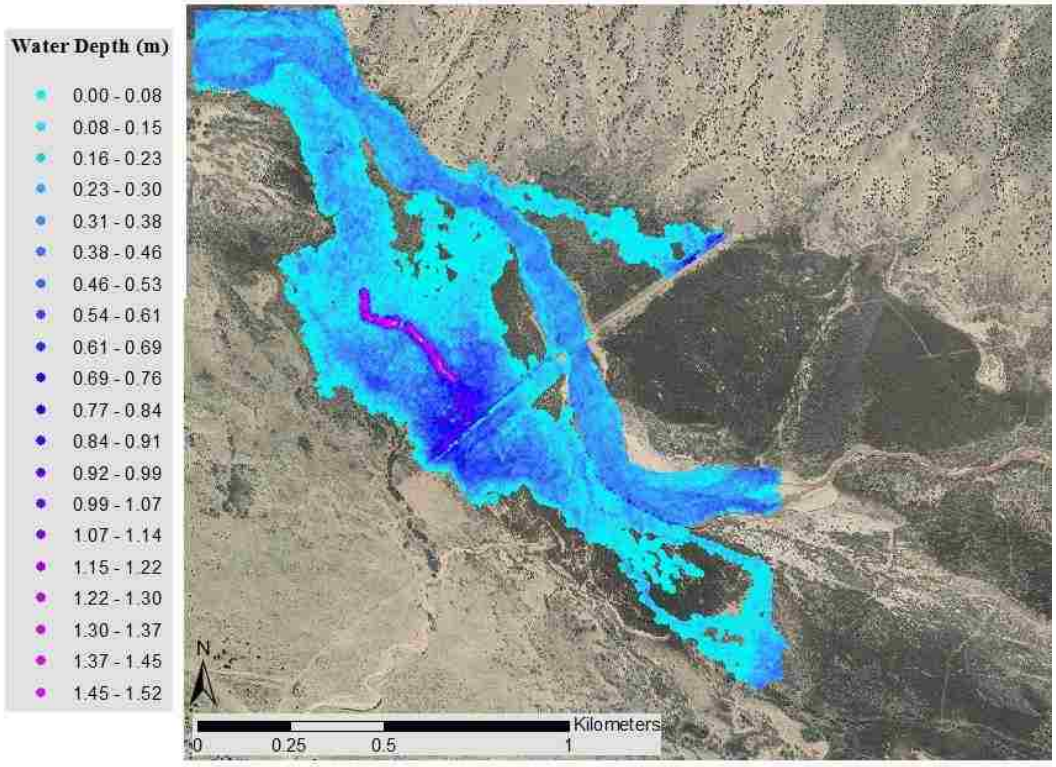

Figure 64: SRH-2D water depth results at 25.5 m^3/s modeled discharge

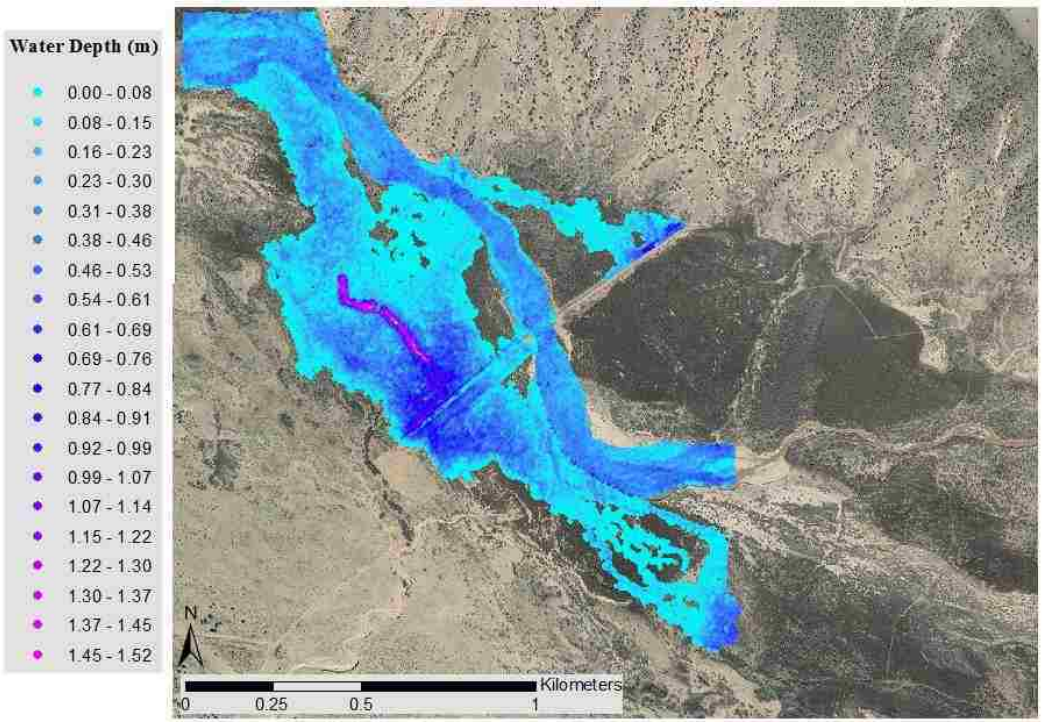

Figure 65: SRH-2D water depth results at 28.3 m^3/s modeled discharge

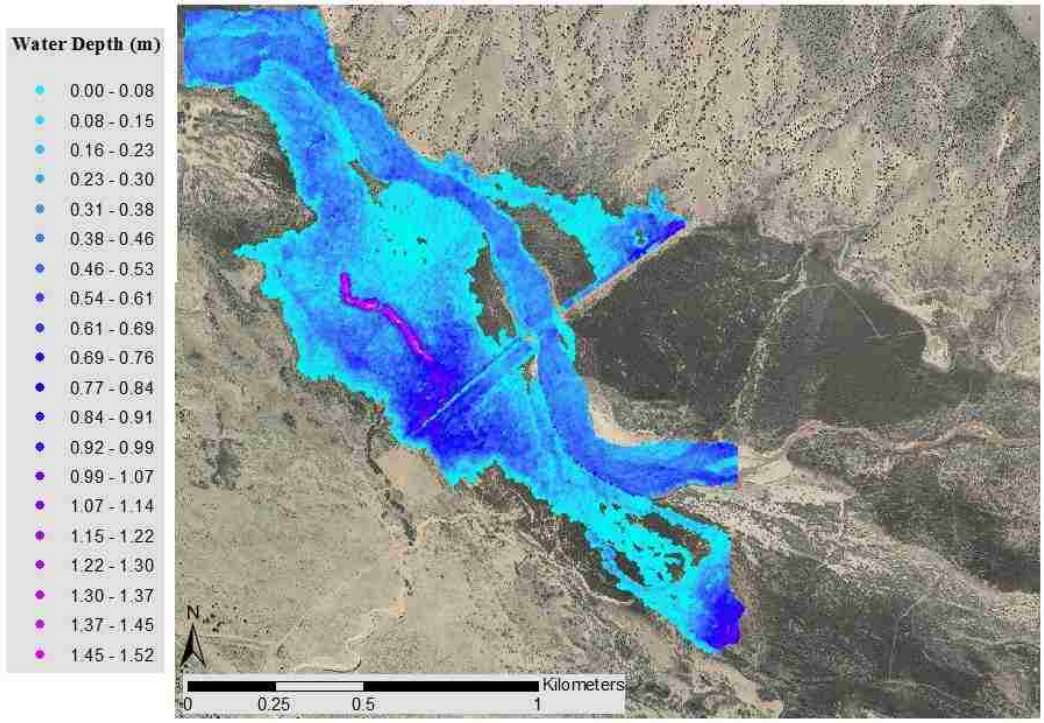

Figure 66: SRH-2D water depth results at 42.5 m^3/s modeled discharge

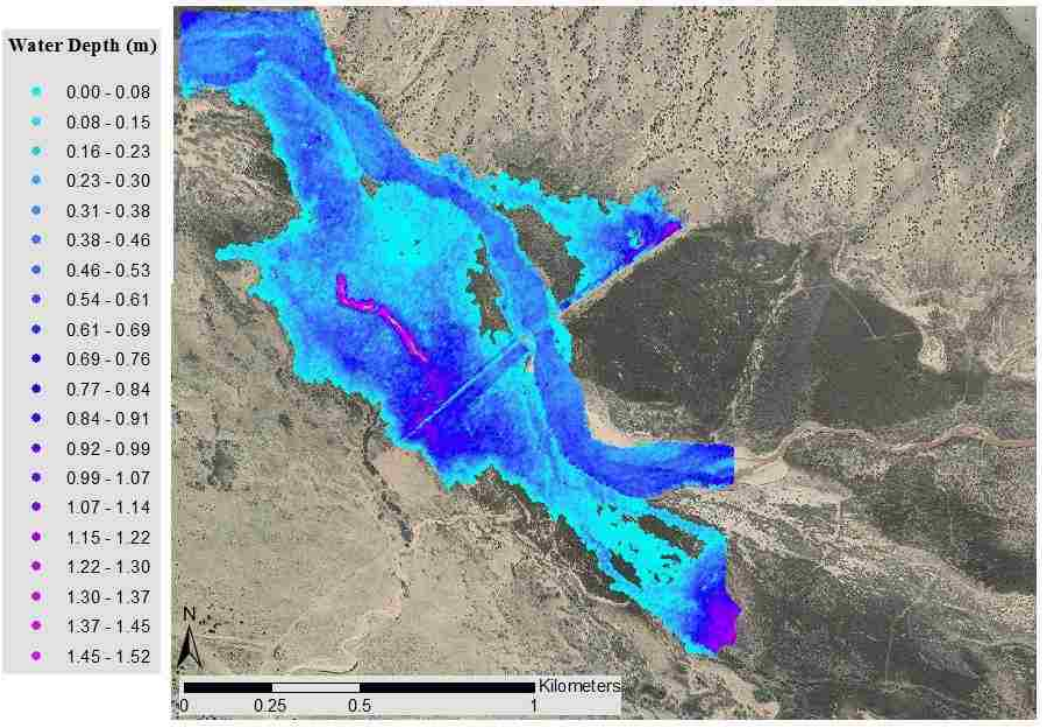

Figure 67: SRH-2D water depth results at 56.6 m^3/s modeled discharge

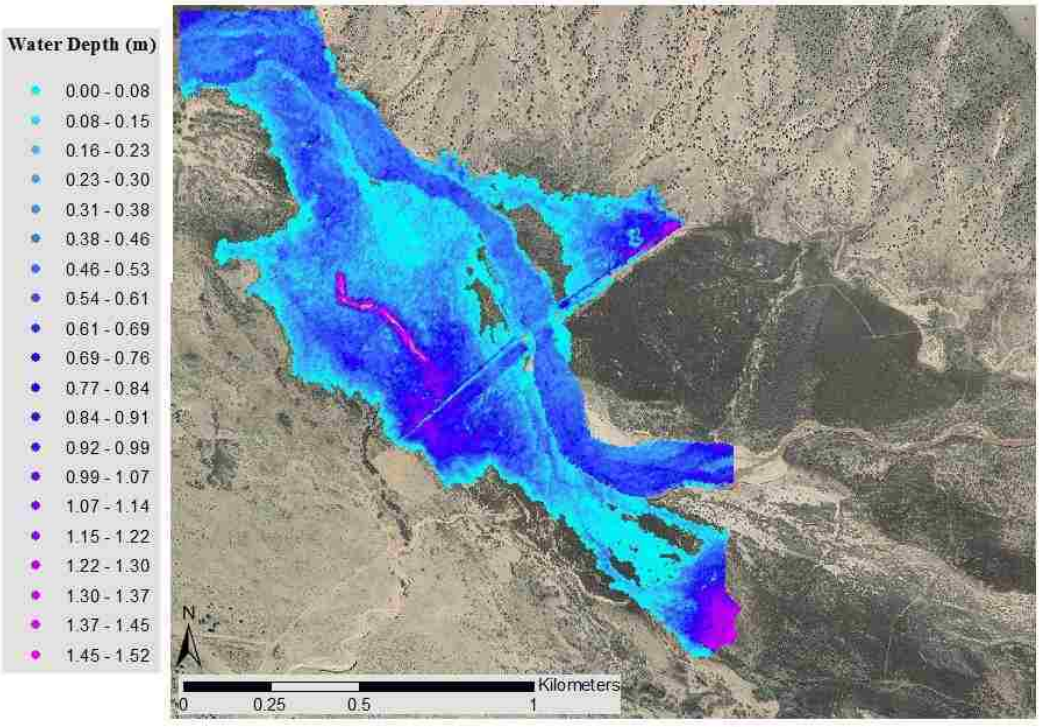

Figure 68: SRH-2D water depth results at 70.8 m^3/s modeled discharge

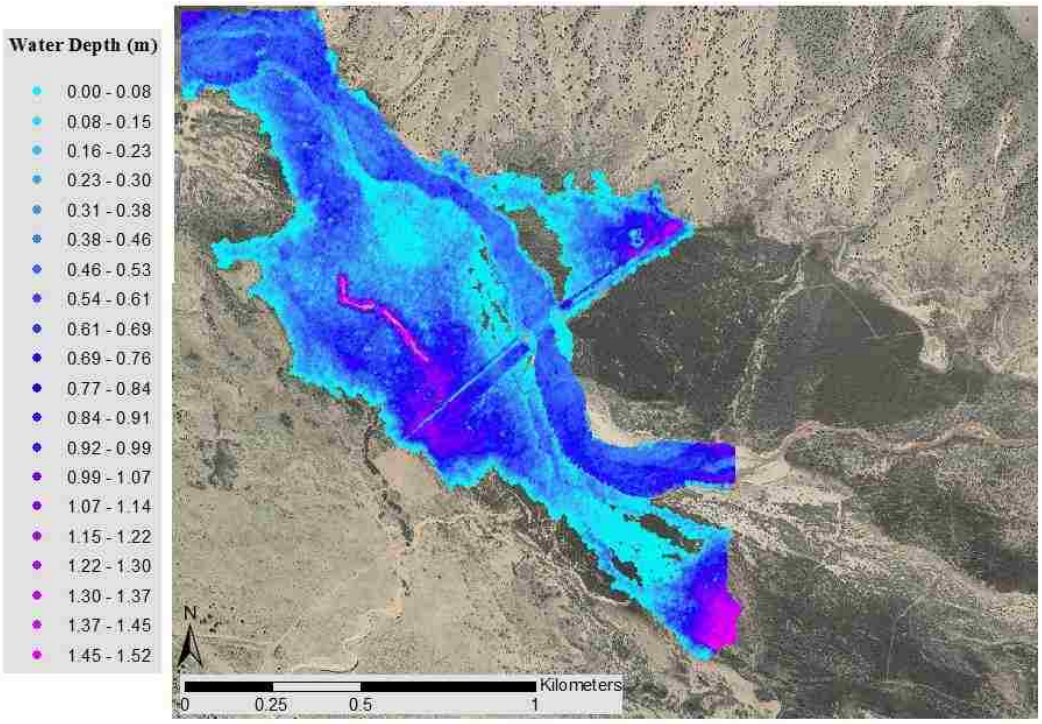

Figure 69: SRH-2D water depth results at 85.0 m^3/s modeled discharge

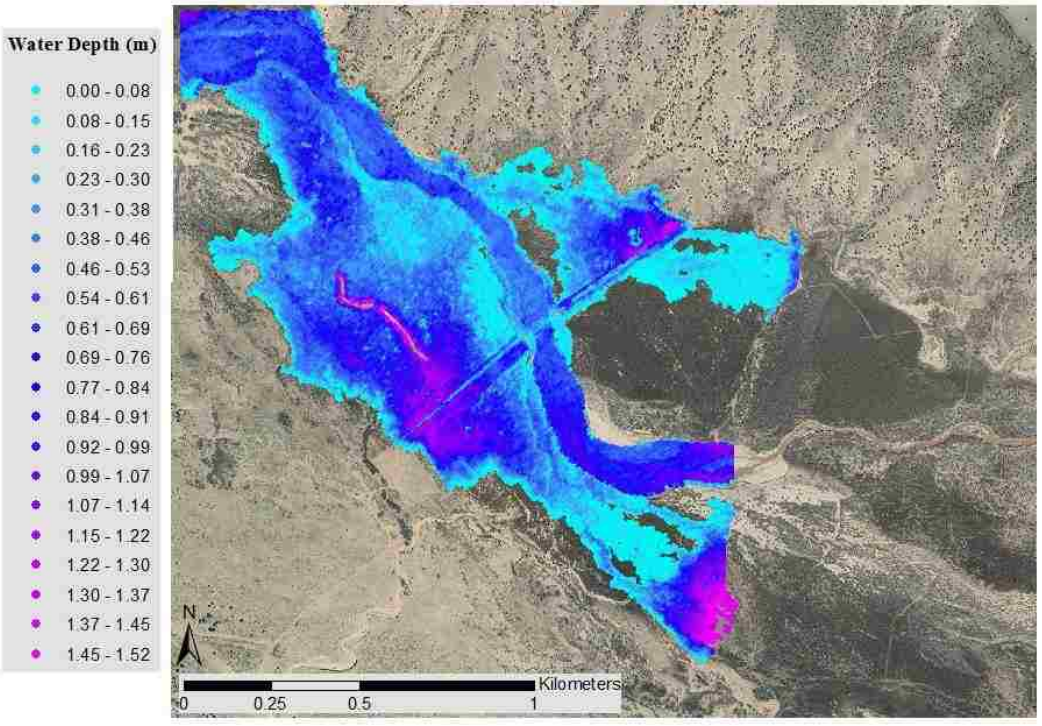

Figure 70: SRH-2D water depth results at 113.3 m^3/s modeled discharge

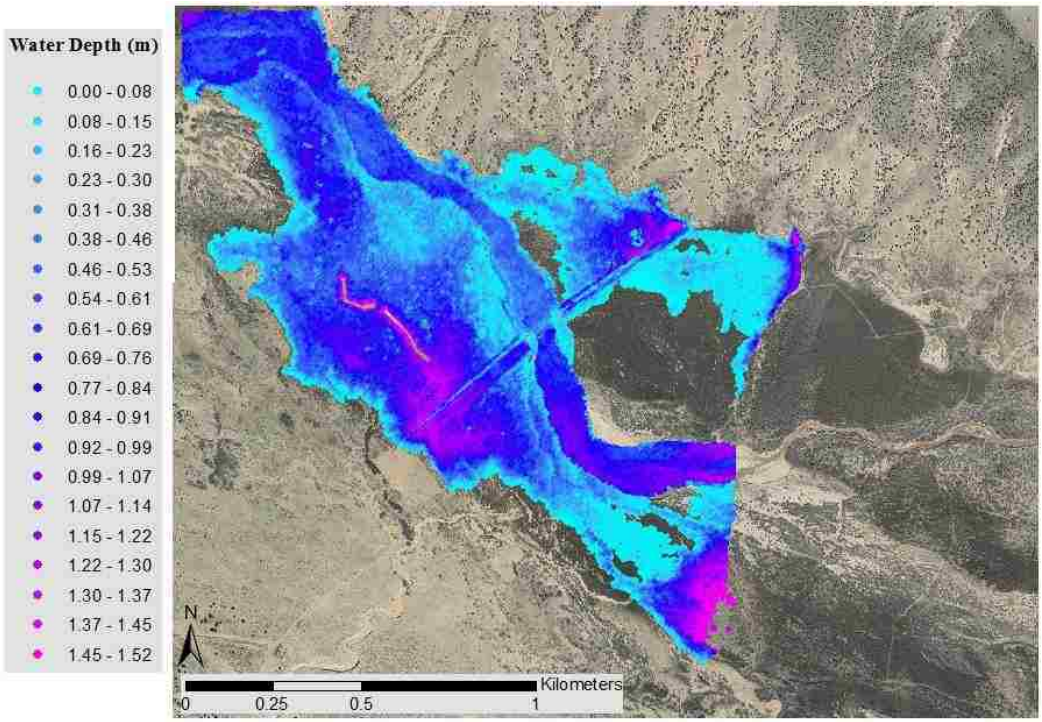

Figure 71: SRH-2D water depth results at 141.6 m^3/s modeled discharge

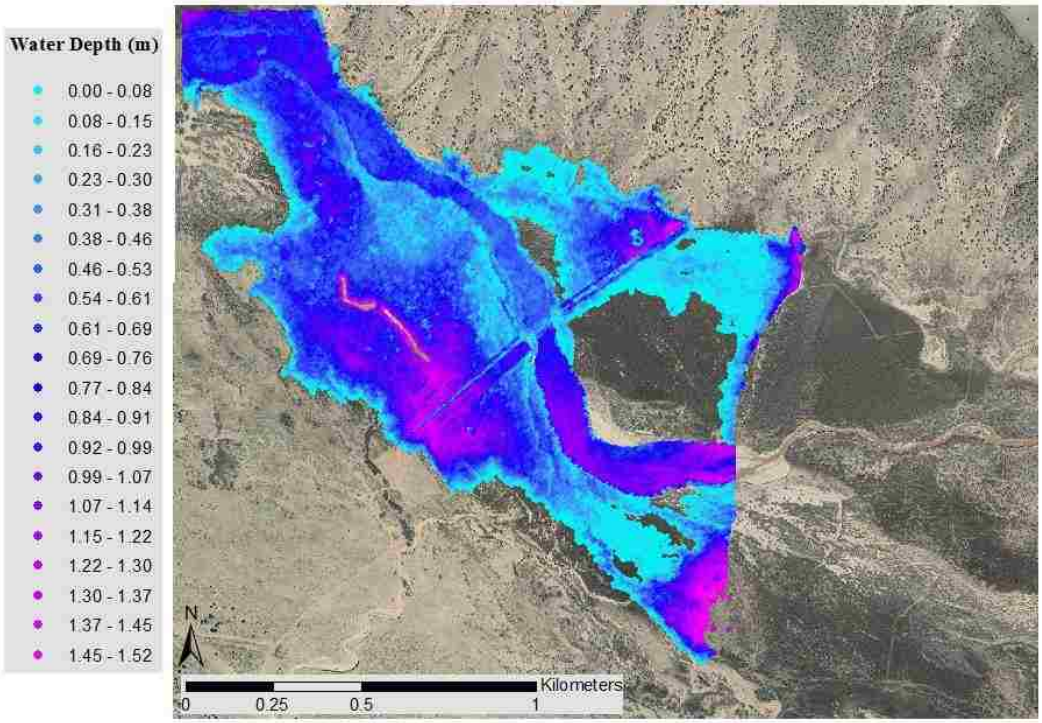

Figure 72: SRH-2D water depth results at 169.9 m^3/s modeled discharge

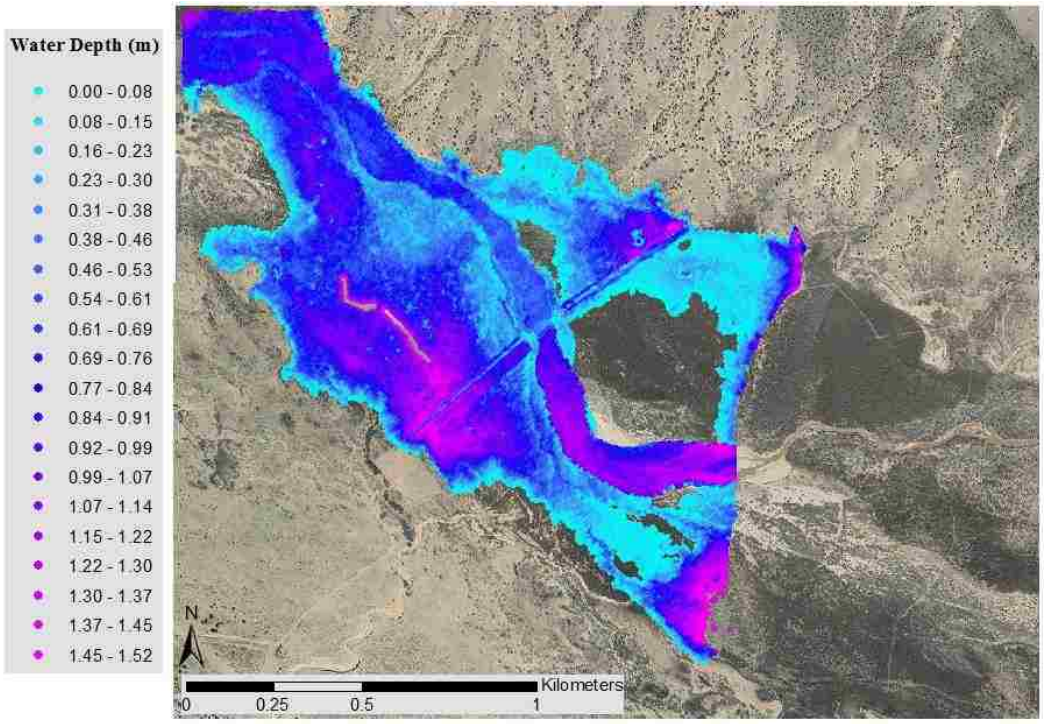

Figure 73: SRH-2D water depth results at 198.2 m^3/s modeled discharge

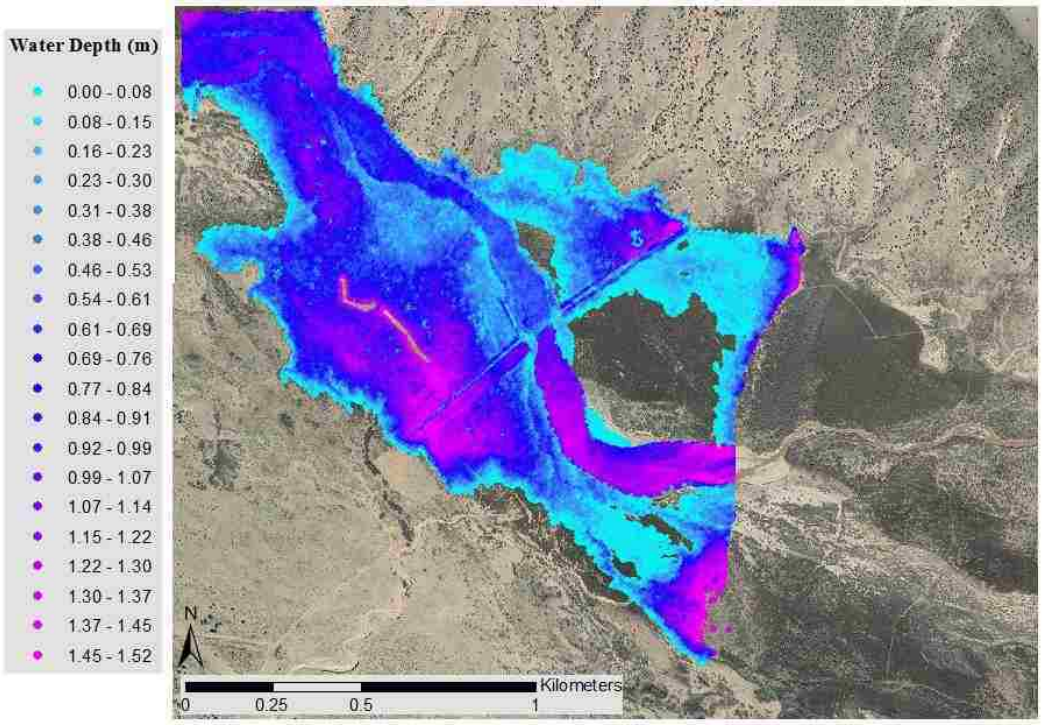

Figure 74: SRH-2D water depth results at 226.5 m^3/s modeled discharge

Velocity Results

Figure 75: SRH-2D velocity results at 5.7 m^3/s modeled discharge

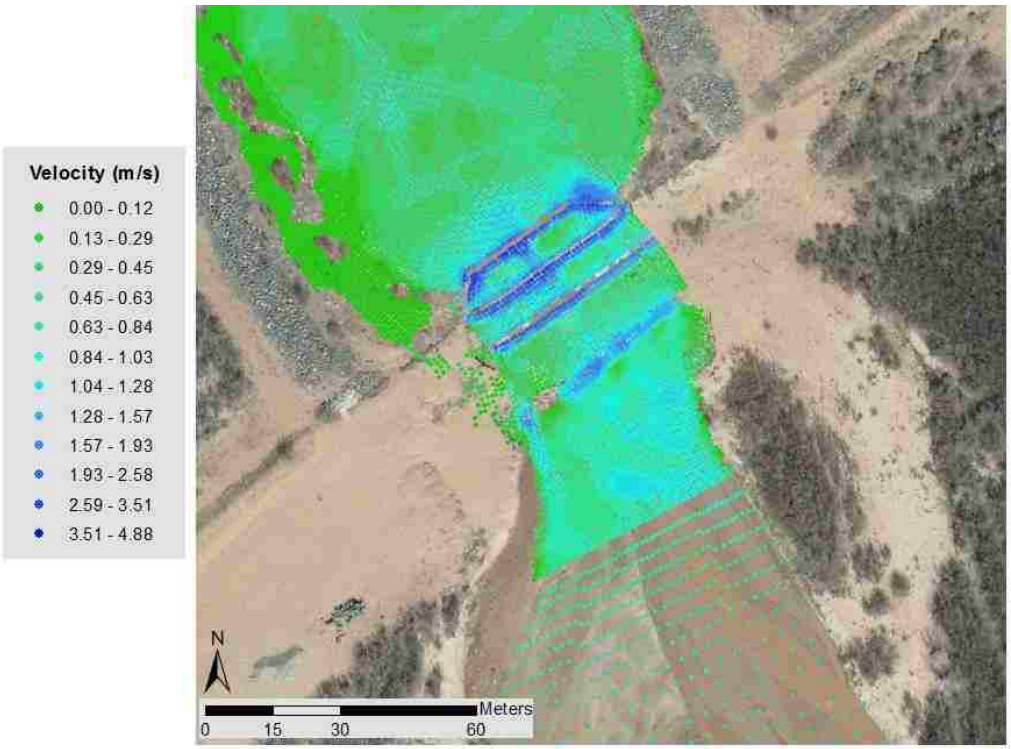

Figure 76: Jemez Weir velocity results at 5.7 m^3/s modeled discharge

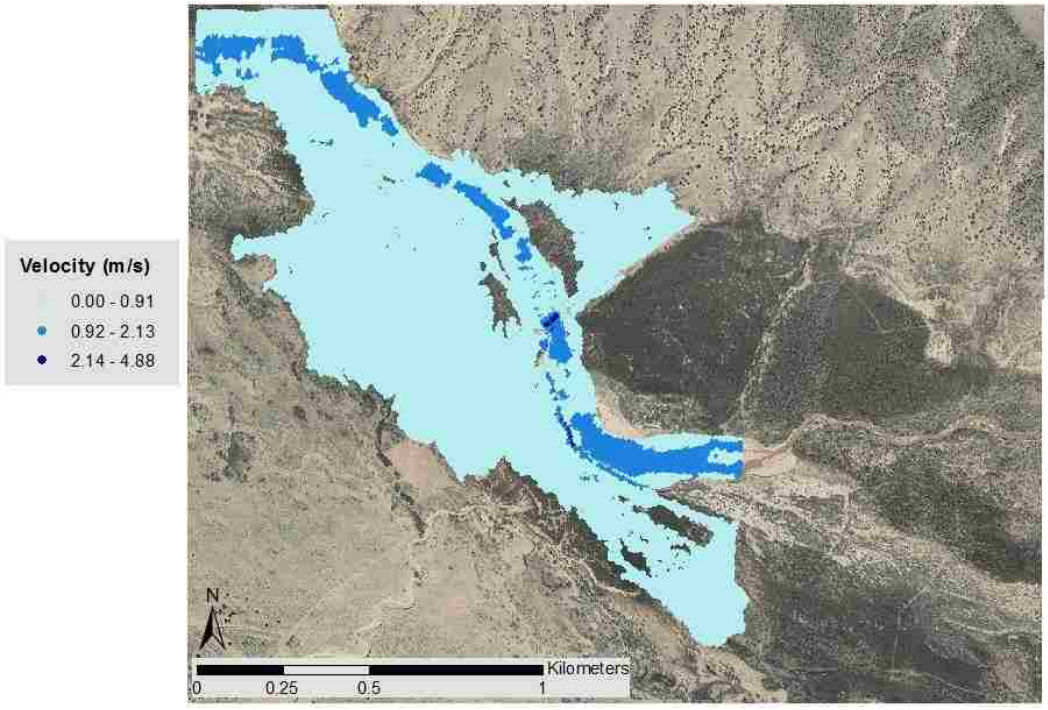

Figure 77: SRH-2D velocity results at 70.8 m^3/s modeled discharge

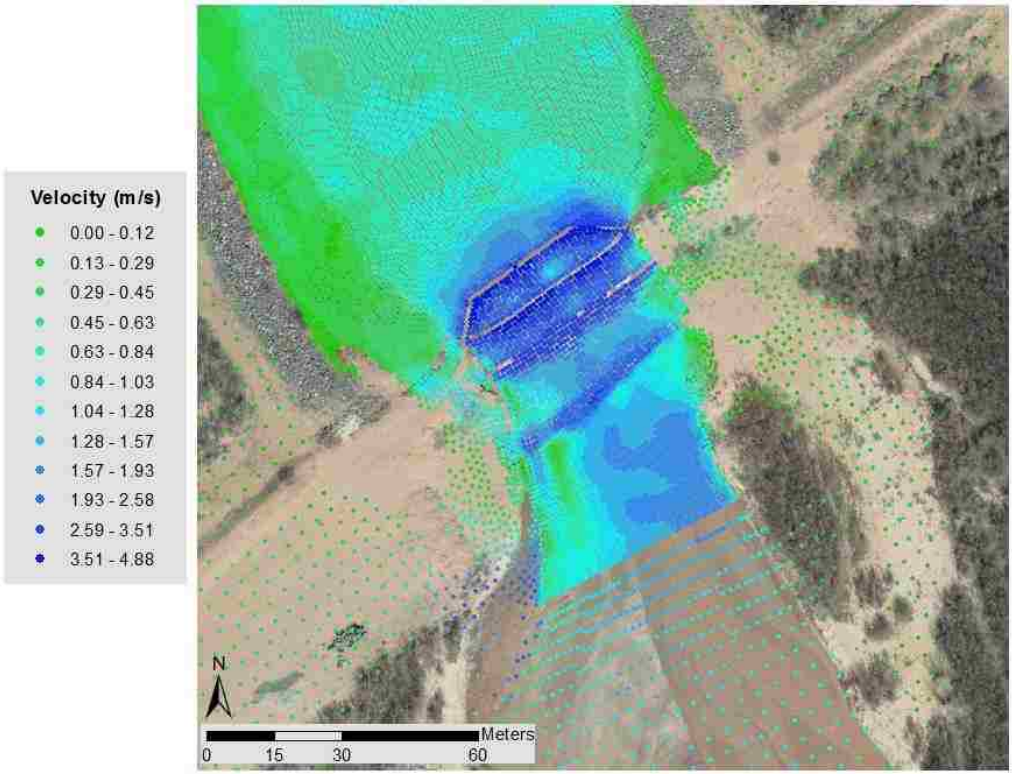

Figure 78: Jemez Weir velocity results at 70.8 m^3/s modeled discharge

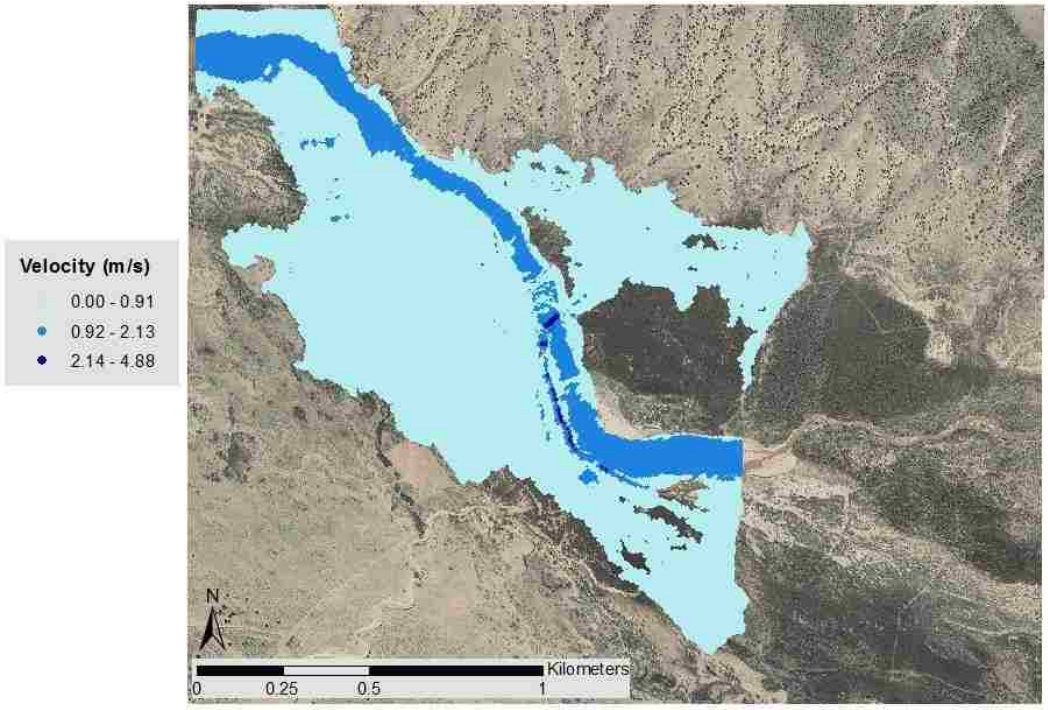

Figure 79: SRH-2D velocity results at 141.6 m^3/s modeled discharge

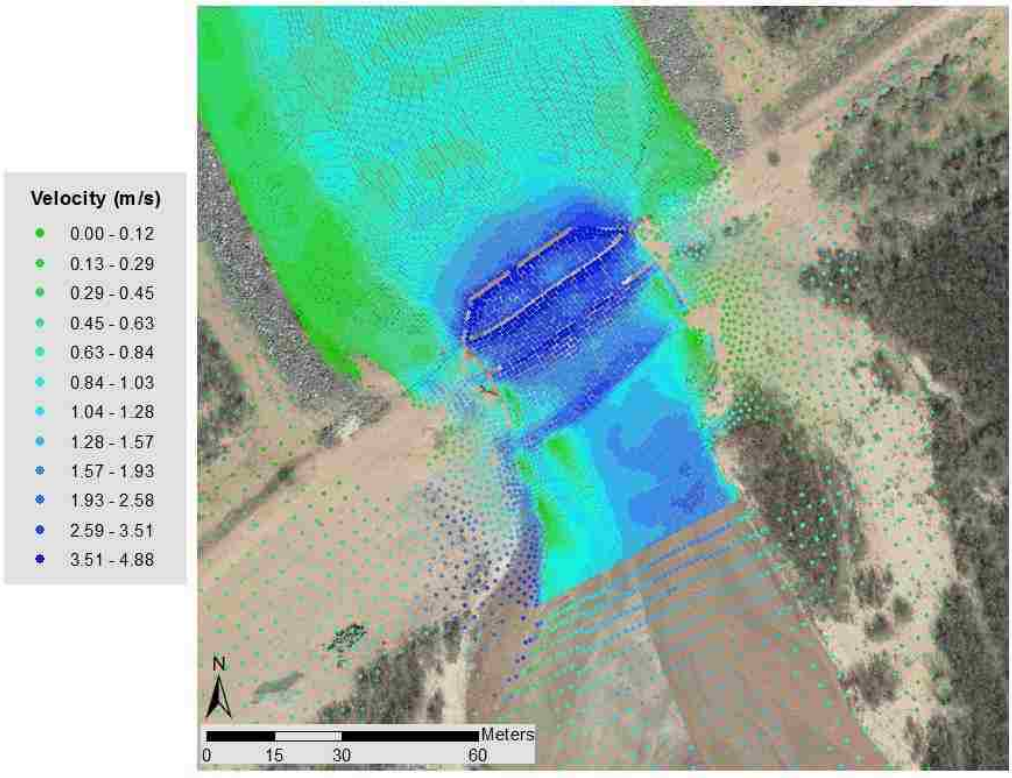

Figure 80: Jemez Weir velocity results at 141.6 m^3/s modeled discharge

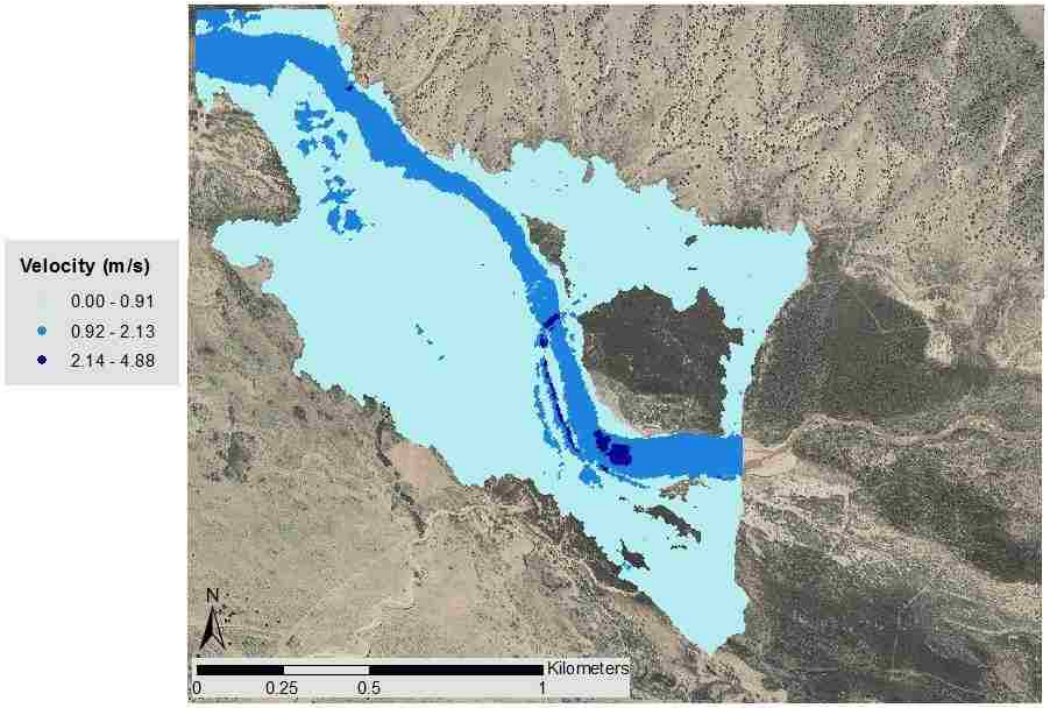

Figure 81: SRH-2D velocity results at 226.5 m^3/s modeled discharge

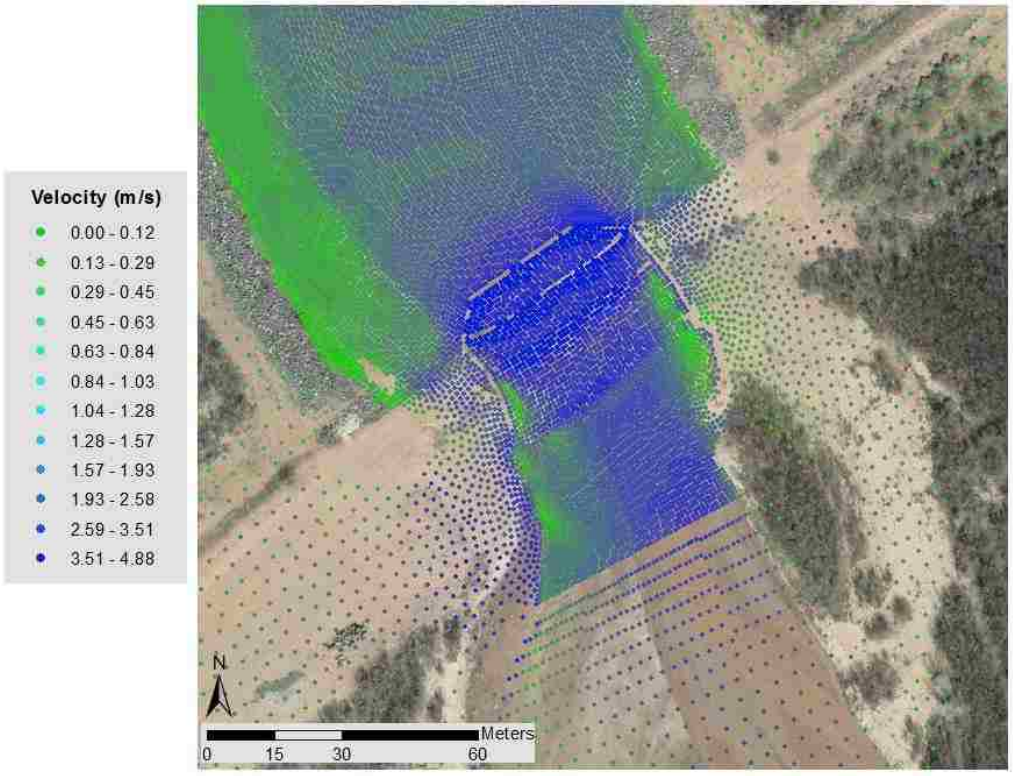

Figure 82: Jemez Weir velocity results at 226.5 m^3/s modeled discharge

Shear Stress Results

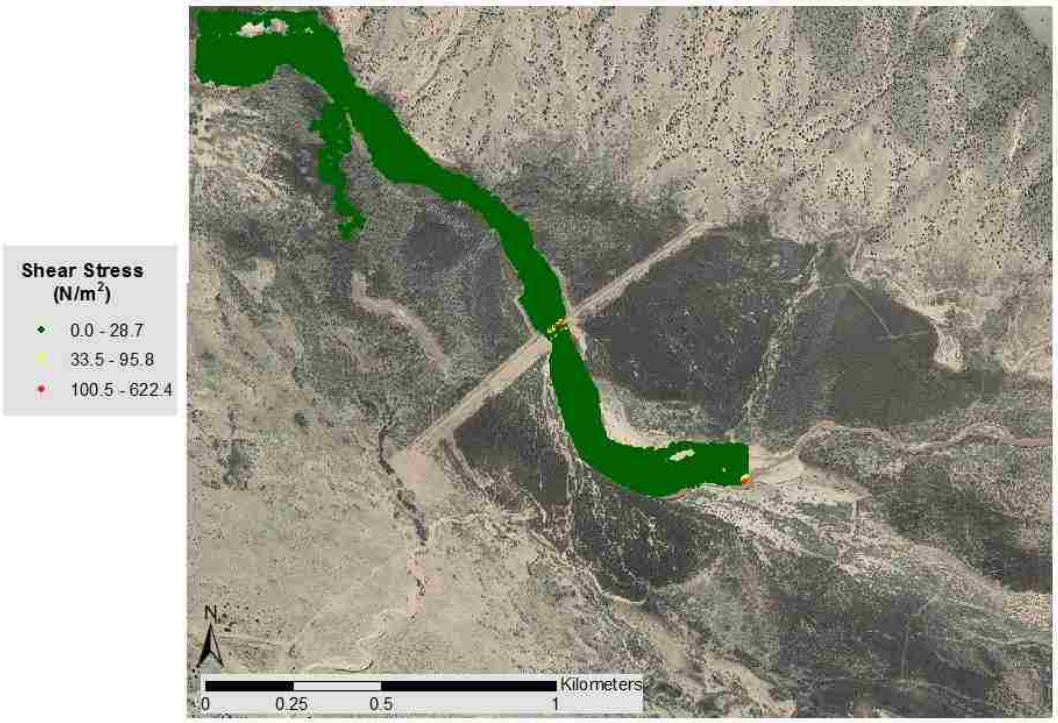

Figure 83: SRH-2D shear stress results at 5.7 m^3/s modeled discharge

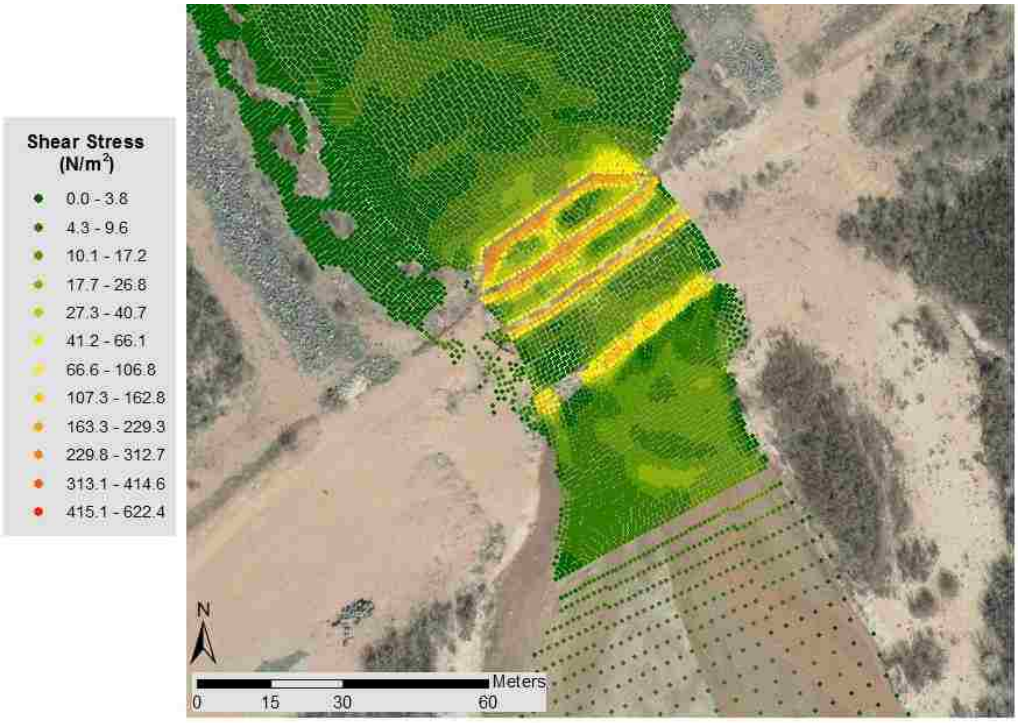

Figure 84: Jemez Weir shear stress results at 5.7 m^3/s modeled discharge

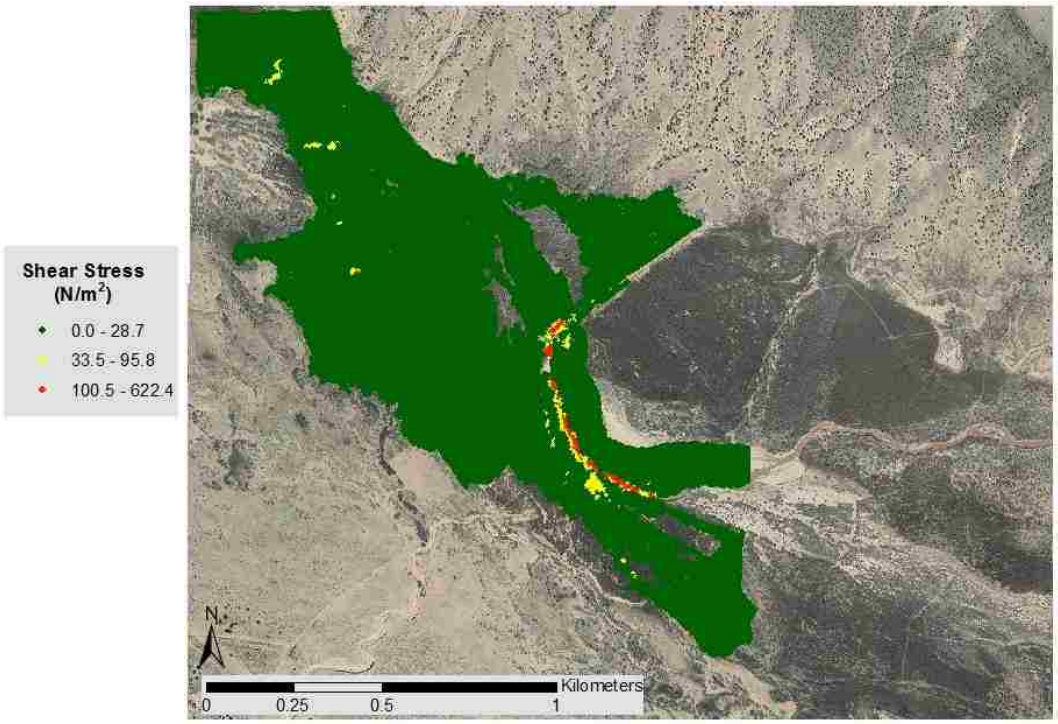

Figure 85: SRH-2D shear stress results at 70.8 m^3/s modeled discharge

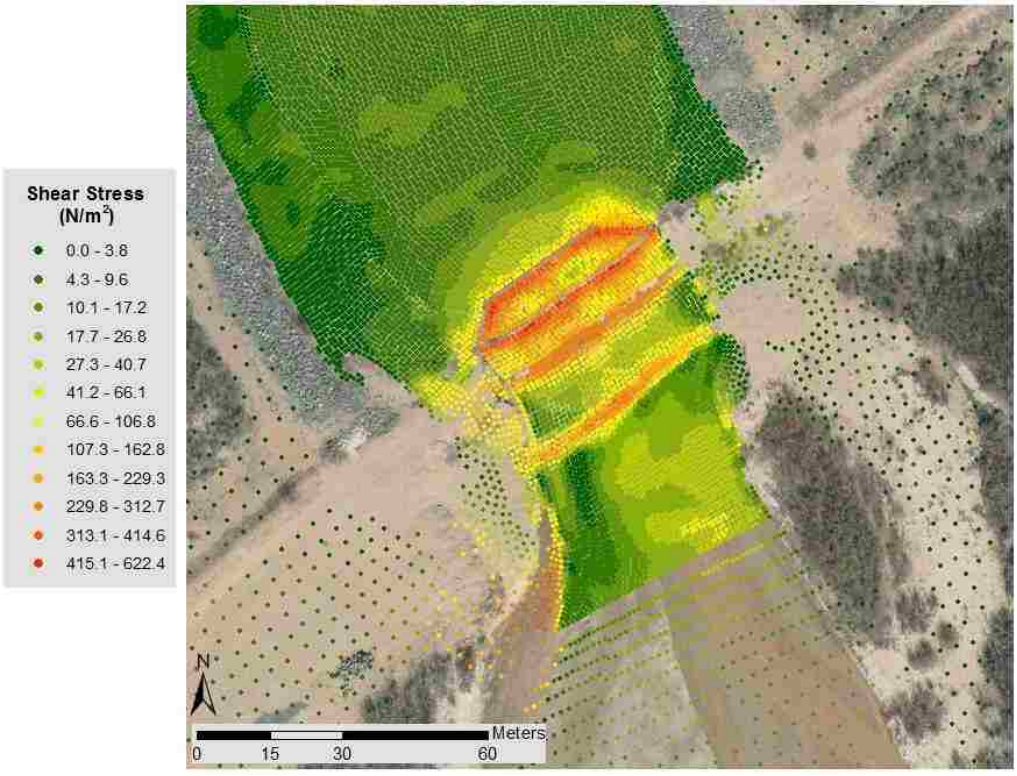

Figure 86: Jemez Weir shear stress results at 70.8 m^3/s modeled discharge

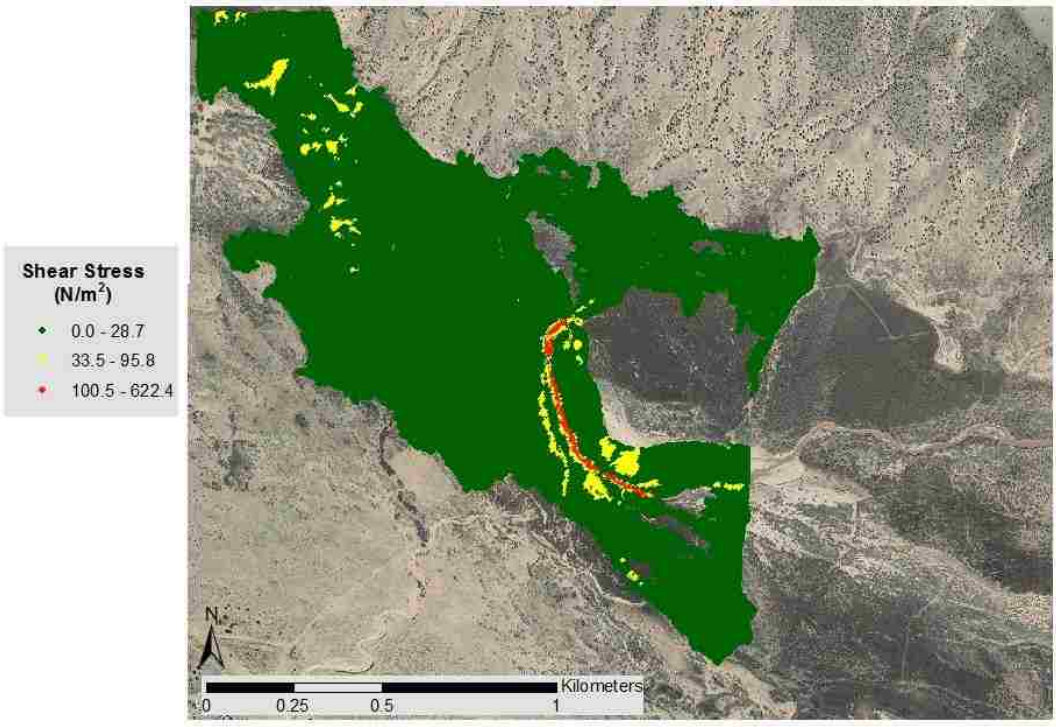

Figure 87: SRH-2D shear stress results at 141.6 m^3/s modeled discharge

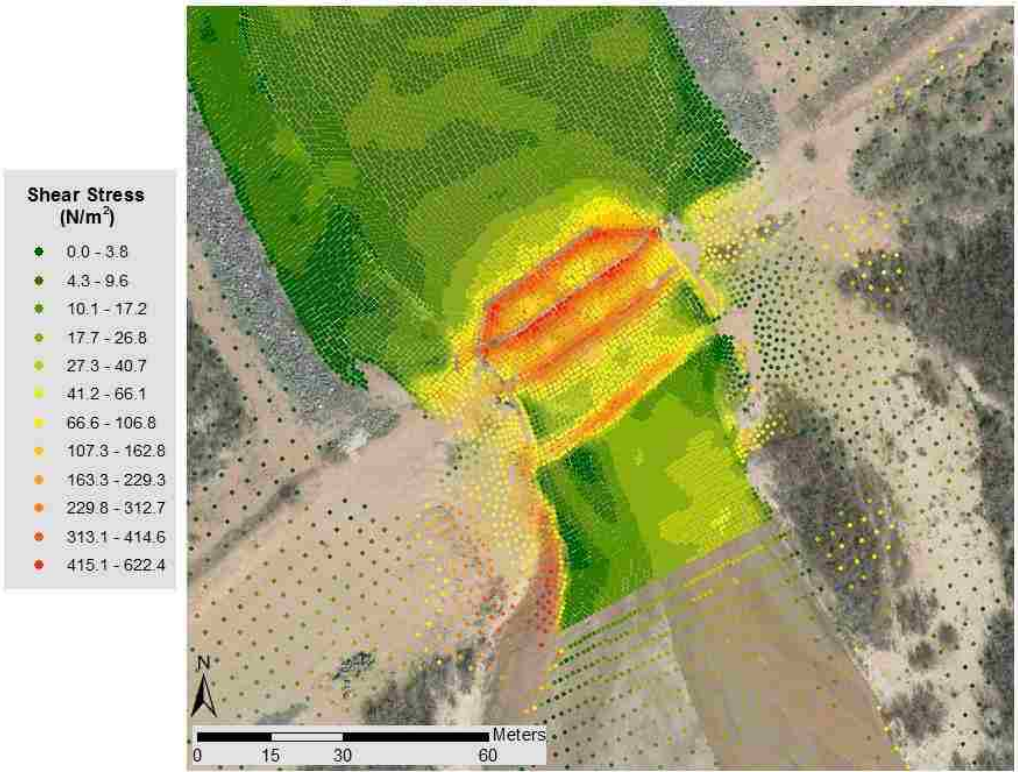

Figure 88: Jemez Weir shear stress results at 141.6 m^3/s modeled discharge

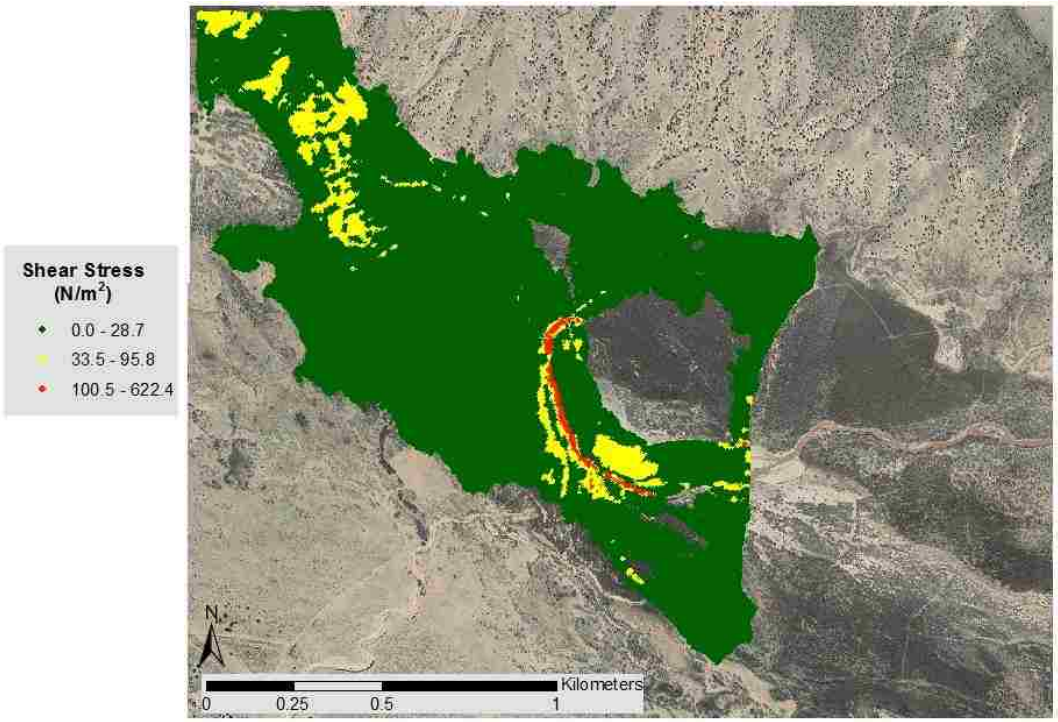

Figure 89: SRH-2D shear stress results at 226.5 m^3/s modeled discharge

Figure 90: Jemez Weir shear stress results at 226.5 m^3/s modeled discharge